Available on CMS information server

CMS AN -2010/242

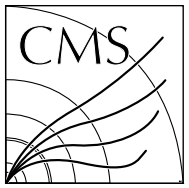

The Compact Muon Solenoid Experiment

Analysis Note

The content of this note is intended for CMS internal use and distribution only

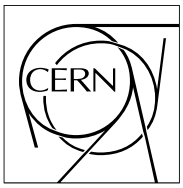

09 August 2010 (v6, 25 November 2010)

Search for a missing energy signature from New Physics in di-jet and multi-jet events

R. Bainbridge, B. Betchart, O. Buchmueller, H. Flaecher, E. Laird, B. Mathias, T. Rommerskirchen, P. Sphicas, M. Stoye, T. Whyntie

Abstract

We present a search for a missing energy signature in di-jet and multi-jet events based on a data sample of approximately 35 pb^{-}1 at 7 TeV centre-of-mass energy. The presented search makes use of a kinematic variable, α_T, to discriminate against the dominant background from QCD events. At present, our findings are in good agreement with Standard Model expectations. We compare our results with expectations from selected SUSY benchmark points and interpret them in the context of the Constrained Minimal SuperSymmetric Model.

CMS Draft Analysis Note

2010/11/25
Head Id: 22017
Archive Id: 19233:23159M
Archive Date: 2010/11/17
Archive Tag: trunk

Search for a missing energy signature from New Physics in di-jet and multi-jet events

R. Bainbridge[1], B. Betchart[2], O. Buchmüller[1], H. Flächer[2], E. Laird[3], B. Mathias[1], T. Rommerskirchen[4], P. Sphicas[4], M. Stoye[4], and T. Whyntie[1]

[1] Imperial College, London, UK
[2] University of Rochester, Rochester, NY, USA
[3] Princeton University, Princeton, NJ, USA
[4] CERN, Geneva, Switzerland

Abstract

We present a search for multi-jet events with missing energy based on 35 pb^{-1} of $\sqrt{s} = 7$ TeV LHC collision data. The presented search makes use of a kinematic variable, α_T, to discriminate against the dominant background from QCD events. At present, our findings are in good agreement with Standard Model expectations. We compare our results with expectations from selected SUSY benchmark points and interpret them in the context of the Constrained Minimal SuperSymmetric Model.

Contents

1 Introduction

In this note we present a search for a missing energy signature in dijet and multijet events based on 35 pb^{-1} of LHC data recorded in 2010 at a centre-of-mass energy of $\sqrt{s} = 7\,\text{TeV}$.

The presented search concentrates on event topologies in which heavy new particles are pair-produced in a proton-proton collision and where at the end of their decay chain a weakly interacting massive particle (WIMP) is produced. The latter remains undetected, thus leading to a missing energy signature. In the case of SUSY, squarks and gluinos could be the heavy particles while the lightest (and stable) neutralino χ_1^0 is the WIMP candidate. Although this search will be carried out in the context of SUSY, it is applicable to other New Physics scenarios as the missing energy signature is common to many models, e.g., Extra Dimensions and Little Higgs models.

We study events with n high-p_T hadronic jets and by using the kinematic variable α_T that is only based on the jet momenta concentrate on providing a robust measurement that is suitable for the early physics data at the LHC, i.e. that is stable with respect to mismeasurements of jets. Our analysis is based on two previous PAS documents [1, 2] and was initially inspired by Ref. [3].

As we will show, the by far dominant background from multi-jet QCD events can be suppressed effectively with the α_T variable. To estimate the remaining backgrounds we make use of data control samples. These are a μ + jets sample for the background from $\text{W} + \text{jets}$ and $t\bar{t}$ events, a photon+jets sample to determine the background from $\text{Z} \to \nu\bar{\nu}$ events and a sample of lower p_T jets than used in the search region to get an estimate of the total background.

This note is organized as follows: In Section 2 we describe the analysis framework followed by a description of the used data and Monte Carlo (MC) samples in Section 3. In Section 4 the event selection is described. Section 5 describes the analysis method and results, followed by some basic cross-checks on the selected events in Section 6. Furthermore we discuss the data-driven methods that were developed for background estimation in Section 7, systematic uncertainties on the signal efficiency in Section 8 and finally interpret our results in the context of different SUSY models in Section 9 before concluding.

2 Analysis Framework

The following describes the workflow and software used to derive at the results presented in this note. All the software used is available in cvs or svn.

From all RECO samples described in Section 3 so called Pat-Tuples have been created on the fly using the following recipe for the Physics Analysis Toolkit (PAT).

Collision data was produced using CMSSW_3_8_4_patch3:

```
cmsrel CMSSW_3_8_4_patch3
cd CMSSW_3_8_4_patch3/src
cmsenv
addpkg PhysicsTools/Configuration V00-08-04
addpkg CommonTools/RecoAlgos CMSSW_3_8_4_patch3
cvs up -r V00-02-15 CommonTools/RecoAlgos/plugins/HBHENoiseFilterResultProducer.cc
cvs up -r V00-02-15 CommonTools/RecoAlgos/python/HBHENoiseFilterResultProducer_cfi.py
cvs up -r V00-02-15 CommonTools/RecoAlgos/BuildFile
cvs co -r V02-3_6_0 -d MyAnalysis/IsolationTools/ UserCode/emanuele/MyAnalysis/IsolationTools/
scram b -j4
```

The recipe follows the SUSYPAT [4] definition from the SUSY group. In the same step flat nTuples have been generated from the on the fly created Pat-Tuples using the producers in UserCode/SusyCAF (V14-00-02). After this step all variables from PAT are accessible in the nTuple.

Unless stated otherwise, we are using ntuples produced in CMSSW_3_6_X for the Monte Carlo samples, again using the SUSYPAT definition of the SUSY group and UserCode/SusyCAF (V00-12-11).

The data and MC ntuples are then analysed by a standalone code that can be found in svn [5].

3 Data and Monte Carlo Samples

The results presented in this note are based on the following data samples,

```
/JetMETTau/Run2010A-Sep17ReReco_v2/RECO
/JetMET/Run2010A-Sep17ReReco_v2/RECO
/Jet/Run2010B-PromptReco-v2/RECO
/MultiJet/Run2010B-PromptReco-v2/RECO
```

corresponding to the official JSON file from November 5th, 2010 and an integrated luminosity of 35 pb^{-1}.

The signal and background MC samples simulated for this analysis have been taken from the Spring10/Summer10 full simulation production for physics at 7 TeV [6]:

```
/QCD_Pt*/Spring10-START3X_V26_S09-v1/GEN-SIM-RECO
/QCD_Pt-*_7TeV-pythia8/Summer10-START36_V10_S09-v1/GEN-SIM-RECO
/QCD_Pt*-madgraph/Spring10-START3X_V26_S09-v2/GEN-SIM-RECO
/PhotonJet_Pt*/Summer10-START36_V9_S09-v1/GEN-SIM-RECO
/PhotonJets_Pt*-madgraph/Spring10-START3X_V26_S09-v1/GEN-SIM-RECO
/TTbarJets-madgraph/Spring10-START3X_V26_S09-v1/GEN-SIM-RECO
/WJets-madgraph/Spring10-START3X_V26_S09-v1/GEN-SIM-RECO
/ZJets-madgraph/Spring10-START3X_V26_S09-v1/GEN-SIM-RECO
/ZinvisibleJets-madgraph/Spring10-START3X_V26_S09-v1/GEN-SIM-RECO
/LM*/Spring10-START3X_V26_S09-v1/GEN-SIM-RECO
/TANB10_CMSW336FASTv0JetID/StoreResults-TANB10_CMSW336FASTv0JetID-46d5c01f684236
```

The cross-sections used for the individual processes are listed in Appendix A. The low mass SUSY signal points LM* are defined in [7].

4 Event and Object Selection

The event and object selection is to good approximation the same as in the two PAS documents [1, 2].

4.1 Trigger

During the data taking period considered in this analysis the trigger menu changed several times. We use a trigger based on the scalar sum of uncorrected jets with $p_{\mathrm{T}j}^{u} > 20\,\mathrm{GeV}$, $\mathrm{H_T} =$

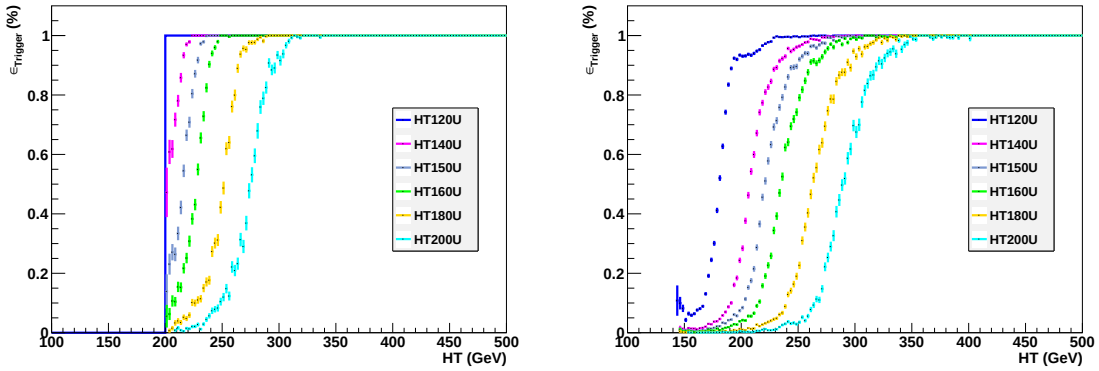

(a) Trigger turn-on for offline jet threshold of 50 GeV. HLT_HT150U, is fully efficient at an offline H_T of 235 GeV.

(b) Trigger turn-on for offline jet threshold of 35 GeV. HLT_HT150U, is 94% efficient at an offline H_T of 250 GeV and fully efficient at H_T = 285 GeV.

Figure 1: H_T trigger turn-on curves with respect to offline jet selection.

$\sum_{i=1}^{n} p_{T_{ji}}^{u}$. The thresholds for this trigger were set to different values during the period of data collection, varying from 100 GeV to 120 GeV and 140 GeV. The corresponding HLT trigger paths are HLT_HT100U, HLT_HT120U, HLT_HT140U and HLT_HT150U. The Level1 seed for each of these triggers is L1_HTT50, i.e. using an L1 H_T threshold of 50 GeV. We use the lowest unprescaled trigger path to select the data events. The turn-on curves for several H_T thresholds with respect to the H_T obtained from the offline jet selection are shown in Figure 1. The trigger with the highest threshold, HLT_HT150U, is 100% efficient at an HT value of 235 GeV when using a corrected jet p_T threshold of 50 GeV in the offline analysis. This is below the H_T region of interest for this analysis. For a jet threshold of 35 GeV, the HLT_HT150U trigger is 94% efficient at H_T = 250 GeV and reaches 100% at H_T = 285 GeV.

4.2 Vertex Requirements

We require at least one good vertex (! fake) with $N_{dof} > 4$ and vertex position along the beam direction of $|z_{vtx}| < 24$ cm and perpendicular to the beam of $\rho < 2$ cm. Furthermore, we remove events with many fake tracks (also known as monster events) by requiring the ratio of HighPurity tracks over the total number of tracks to be greater than 25% in events that have 10 or more tracks.

4.3 Physics Object Definitions

In the following we list the criteria applied to identify jets, muons, electrons and photons.

4.3.1 Jets

In this analysis we use calorimeter based jets (CaloJets) clustered with the anti-kt jet algorithm [8] with radius parameter $R = 0.5$. These jets are required to have a jet-energy corrected (*Spring10* and *v2 residual corrections (for data only)*) transverse momentum $p_T > 50$ GeV and to be within pseudo-rapidity $|\eta| < 3$. In order to reject noise from the calorimeters, jets are furthermore required to pass the *loose* jet identification criteria stated in Ref. [9]. Furthermore we reject events where noise in the HCAL has been identified by the HBHENoiseFilter [10].

4.3.2 Electrons

We base our electron selection criteria on those defined in [11]. Candidate electrons must first pass a transverse momentum requirement of $p_{\mathrm{T}} > 10$ GeV and a pseudo-rapidity requirement of $|\eta| < 2.5$ to be considered relevant to the analysis. We use the identification scheme "WP95" as defined in [11] to select electrons. This scheme places a number of requirements on the isolation and on the properties of the associated track(s), the ratio of deposits in the HCAL and ECAL and the shower shape. The WP95 scheme allows the user to either choose separate relative isolations (i.e. cutting on track, ECAL and HCAL isolations independently) or the combined relative isolation. For consistency and simplicity we use the combined relative isolation:

$$Iso_{\mathrm{comb.}} = \left\{ \sum_{\mathrm{Trk}} p_{\mathrm{T}} + \sum_{\mathrm{ECAL}} E_T + \sum_{\mathrm{HCAL}} E_T \right\}_{\Delta R < 0.3} / p_{\mathrm{T}}^{ele}, \quad (1)$$

The recommended cut value of $Iso_{\mathrm{comb.}} < 0.15$ [11] is used.

4.3.3 Photons

We base our photon selection criteria on those defined in [12]. Candidate photons must first pass a transverse momentum requirement of $p_{\mathrm{T}} > 25$ GeV and a pseudo-rapidity requirement of $|\eta| < 2.5$ to be considered relevant to the analysis. To be considered a photon, the candidate must then pass the criteria associated with the "tight" identification scheme of [12], which uses isolation, HCAL to ECAL deposit ratios and shower shape information.

4.3.4 Muons

Our muon selection is based on the GlobalPromptTight requirement as defined in Refs. [13, 14]. The muons are required to have $p_{\mathrm{T}} > 10$ GeV and $|\eta| < 2.5$ and to be isolated according to $Iso_{\mathrm{comb.}} < 0.15$.

A special case arises if such an identified muon overlaps with a jet (i.e. $\Delta R < 0.5$). If the muon is isolated, both the jet and the muon are kept in the event.

In case that the muon is not isolated it is deemed to be part of the jet. The 4-momentum of the muon is added to the jet and the muon is removed from the event.

4.3.5 Physics object-based event vetoes

Based on the above object definitions, the following events are vetoed:

- Events that contain muons, electrons or photons, identified according to the selection critiera stated above.
- Events that have one or more jets with momentum above threshold, which fail either the $|\eta| < 3$ or the jet-ID requirement. This veto is needed as such jets are not included in the calculation of the energy balance of the event. If these jets are not accounted for the event will look imbalanced and could therefore be misidentified as SUSY signal.
- Events that have at least one global muon which passes the p_{T} and η requirements but is not identified as GlobalPromptTight (Odd Muon)
- Events that have a jet modified by a muon where the muon p_T is more than 50% of the unmodified jet p_{T}. This cut protects against jets containing muons with large p_{T} mismeasurements.

4.4 Event Preselection

Based on the above object definitions and vetoes we select events which have $n \geq 2$ jets and no electron or muon with momentum above $p_T > 10\,\text{GeV}$ or photon with momentum above $p_T > 25\,\text{GeV}$. We furthermore require the leading jet to be within $|\eta| < 2.5$ and the two leading jets to have momentum $p_T > 100\,\text{GeV}$.

In the following we will refer to this selection as "preselection".

We define the following two variables based on the jet momenta:

- the scalar sum of jet E_T's: $H_T = \sum_{i=0}^{n} E_T^{j_i}$
- the missing p_T of the event based on jets from the vectorial sum of the jet momenta: $\not{H}_T = |-\sum_{i=0}^{n} \vec{p}_T^{\,j_i}|$

4.4.1 Data - Monte Carlo comparisons

As we will see, the description of the data by the Monte Carlo simulation is reasonably good, however, there are a few known deficiencies. One of them concerns the jet energy resolution which is modelled as too good in MC, in particular in the HCAL barrel. In our analysis this affects directly the $\not{H}_T$ but also the $\not{E}_T$ distribution.

To obtain an uncertainty on the MC modelling, we increase the MC jet energy resolution by 10% in the barrel ($|| < 1.4$) and 15% in the endcap. This results in about 8% additional gaussian smearing for jets with a p_T of 50 GeV, decreasing to about 4.5% for jets with p_T of 200 GeV in the barrel. In the endcap this corresponds to $\sim 10\%$ additional gaussian smearing for 50 GeV jets, decreasing to $\sim 5\%$ for 200 GeV jets.

Furthermore, we chose to vary the jet energy scale by $\pm 3 - 5\%$ depending on jet p_T and η, according to [15]. This is done right at the beginning of the analysis, i.e. allowing jets to move above or fall below the jet p_T threshold of 50 GeV. It therefore also results in a migration of events above or below the H_T = 350 GeV boundary which is discussed towards the end of this section. We add the deviations obtained from these variations in quadrature to the statistical errors of the MC samples and draw this as a hatched band around the default prediction for Standard Model processes. It should be noted that this is simply done to get an estimate for the MC modelling uncertainty. Our results do not depend on these variations as the background predictions are taken from data control samples.

We furthermore in the bottom part of the figures, we show the ratio of the observed events in data over the events expected from SM processes. The red band indicates an 11% normalization uncertainty due to the uncertainty on the luminosity measurement.

In Figure 2, we show the H_T distribution which is falling steeply for the SM backgrounds other than top, while it is peaking at values of a few hundred GeV for the signal models. For QCD background we use the PYTHIA 6 [16] sample listed in Section 3. In addition to the SM distribution which is the sum of the QCD, W + jets, $Z \to \nu\bar{\nu}$ and $t\bar{t}$ distributions, we have overlaid the expected α_T distributions for two low mass SUSY signal points, LM0 and LM1.

To further reduce background events from Standard Model processes we require $H_T > 350$ GeV. In the following we will refer to this stage of the event selection as "H_T selection".

In Figure 3 we show the jet multiplicity and $\not{H}_T$ distributions after H_T selection. While the jet multiplicity distribution agrees nicely between data and Monte Carlo simulation the $\not{H}_T$ distribution is wider in data compared to the simulation. This can as least in part be attributed to a

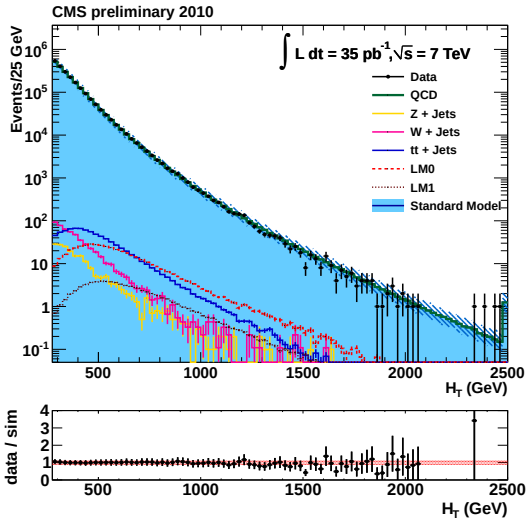

Figure 2: H_T distribution after preselection for data, all Standard-Model backgrounds and two SUSY signal samples with parameter sets LM0 and LM1.

too good jet energy resolution in the simulation. The observed difference is however covered when applying an additional smearing of the jet energies in MC as discussed above.

5 Analysis and Results

In the following we will make use of a kinematic variable (α_T) that allows to one separate QCD events where missing energy is generated through mismeasurements and signal events with real missing energy. It should be noted that our main objective is to understand and to reject QCD events efficiently and not necessarily to optimise the signal efficiency. Hence, we will now mainly discuss properties of QCD events.

5.1 α_T in the di-jet Case

In the di-jet case ($n = 2$) transverse momentum conservation requires the p_T of the two jets in QCD events to be of equal magnitude and back-to-back in the azimuthal angle ϕ. The variable α_T, first introduced in Ref. [2], exploits exactly this requirement. It is defined as

$$\alpha_T = E_T^{j2}/M_T \quad , \tag{2}$$

where E_T^{j2} is the second leading jet in the event and M_T is defined as

$$M_T = \sqrt{\left(\sum_{i=1}^{n} E_T^{j_i}\right)^2 - \left(\sum_{i=1}^{n} p_x^{j_i}\right)^2 - \left(\sum_{i=1}^{n} p_y^{j_i}\right)^2} = \sqrt{H_T{}^2 - \not{H}_T{}^2} \quad , \tag{3}$$

and $n = 2$ in the di-jet case. For a well measured QCD di-jet event, $E_T^{j2} = 0.5 \times H_T$ and $\not{H}_T = 0$, thus α_T is exactly 0.5.

5.2 α_T in the n-jet Case

To define α_T for more than two jets the n-jet system is reduced down to a two-jet system by combining jets into two pseudo-jets. The E_T of the pseudo-jets is calculated as the scalar sum of

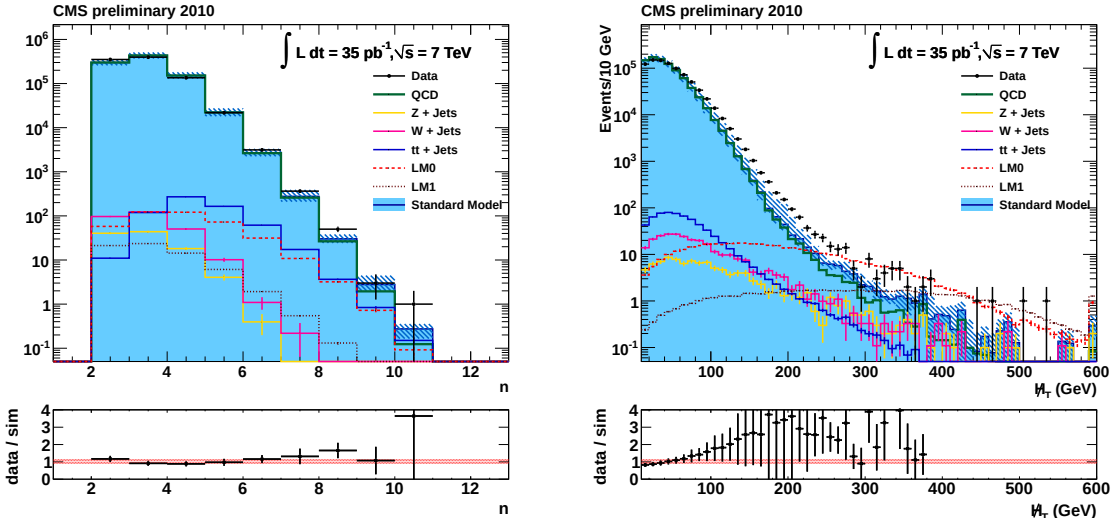

(a) Jet multiplicity after H_T selection.

(b) $\not\!\!H_T$ distribution after H_T selection. The applied systematic uncertainty for jet energy resolution (hased band) leads to a longer tail in $\not\!\!H_T$.

Figure 3: Jet multiplicity and $\not\!\!H_T$ distributions.

the contributing jet E_T. All possibilities of how n jets can be combined into two are tested and the combination is chosen where the resulting pseudo-jet E_T are most similar, i.e., for which the difference $\Delta H_T = E_T^{pj_1} - E_T^{pj_2}$ is minimal. For n jets, α_T is then obtained in the same way as in Eq. 2.

It is however instructive to rewrite Eq. 2 as a function of the variables H_T and $\not\!\!H_T$. As discussed, E_T^{pj2} can be at most $0.5 \cdot H_T$ and with the definition of ΔH_T given above α_T can be written as:

$$\alpha_T = \frac{1}{2}\frac{H_T - \Delta H_T}{M_T} = \frac{1}{2}\frac{H_T - \Delta H_T}{\sqrt{{H_T}^2 - {\not\!\!H_T}^2}} = \frac{1}{2}\frac{1 - \Delta H_T/H_T}{\sqrt{1 - (\not\!\!H_T/H_T)^2}} \tag{4}$$

The quantities H_T and $\not\!\!H_T$ can be unambiguously calculated for any number of jets n. As pointed out above, in a perfectly measured QCD event $\not\!\!H_T$ would be zero while for signal events this quantity is expected to be non-zero. In order to achieve large values of α_T and therefore larger signal efficiencies, ΔH_T should be as small as possible. This reasoning motivates the choice of the pseudo-jet combination that results in the minimal ΔH_T. It can be seen from Eq. 4 that $\not\!\!H_T$ and ΔH_T do not enter into α_T with their absolute values but only relative to H_T and both are generally small for QCD events.

Values of α_T larger than 0.5 are obtained if the jet energy and therefore also the transverse mass is mismeasured, *i.e.*, if there is significant $\not\!\!H_T/H_T$. However, a jet energy mismeasurement also automatically leads to sizeable $\Delta H_T/H_T$ and thus reduces the value of α_T.

For our event selection we require $\alpha_T > 0.55$ which implies $\not\!\!H_T/H_T > 0.4$. The correlation between $\Delta H_T/H_T$ and $\not\!\!H_T/H_T$ is shown in Figure 2 of [17].

Values of α_T significantly greater than 0.5 can be achieved if objects with sizeable p_T were not identified in the event, e.g. jets below threshold. This will be further discussed in Section 5.4.

The α_T distributions for dijet events and events with $n \geq 3$ jets are shown in Figure 4. It can

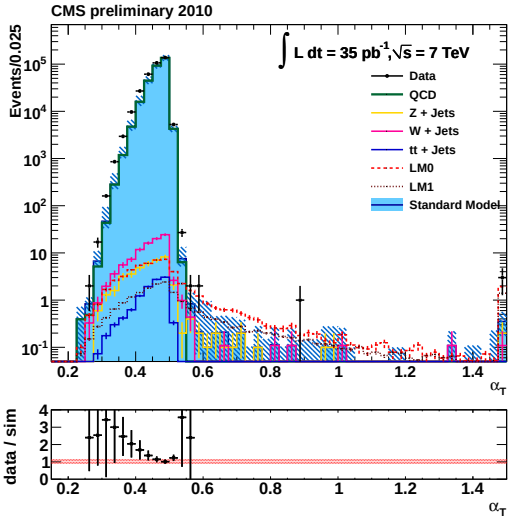

(a) α_T distribution for dijet event.

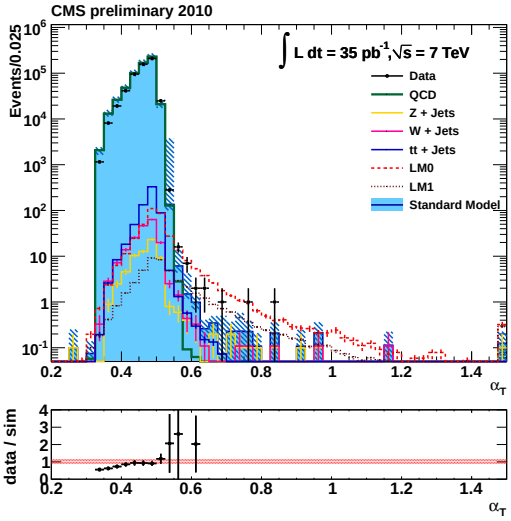

(b) α_T distribution for events with $n \geq 3$ jets.

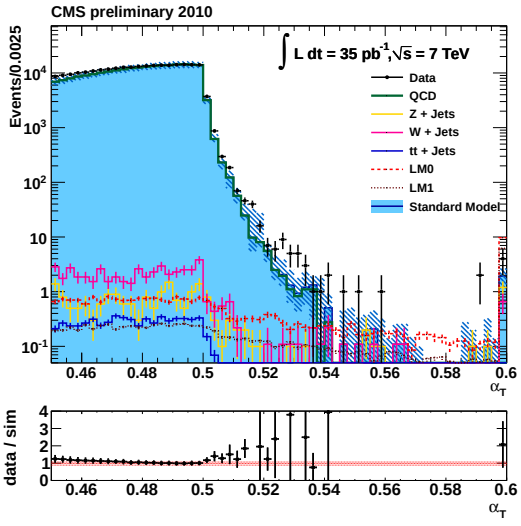

(c) Zoomed α_T distribution for dijet events.

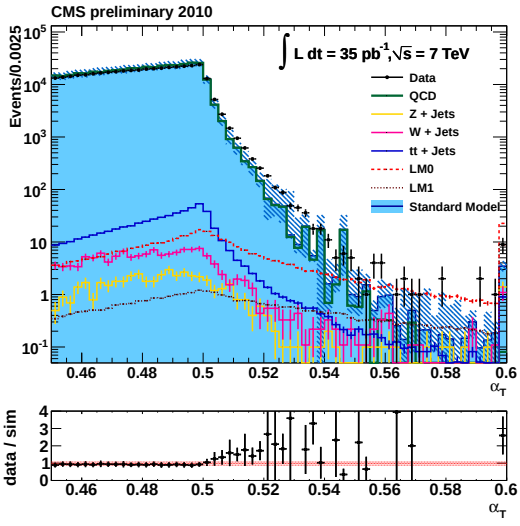

(d) Zoomed α_T distribution for events with $n \geq 3$ jets.

Figure 4: α_T distribution after H_T selection.

be seen that in both figures the QCD background peaks as expected sharply at a value of 0.5.

It should be noted, that the alignment of the missing energy to a jet is not incorporated in α_T and can be used as a cross-check (see Section 5.3).

5.3 Effect of dead ECAL regions

As discussed above, jet mismeasurements can lead to α_T values > 0.5 or even > 0.55 for severe mismeasurements. One known source that can cause such mismeasurements are regions of dead crystals in the ECAL.

A variable to identify mismeasured jets is $\Delta\phi^*$:

$$\Delta\phi^* = \min_k \Big(\Delta\phi((\sum_{i=0}^{n} -\vec{j}_i) + \vec{j}_k; \vec{j}_k) \Big), \tag{5}$$

where n is the number of jets and $\vec{j}_i$ the momentum of jets. This variable tests if there is at least one jet which, if rescaled by a certain factor, would be able to balance the event. For typical QCD events, with one dominating jet mismeasurement, this angle tends to be small. This statement is still true for the QCD events passing the previous selections, as can be seen in Figure 12.

To reject events with severe jet mismeasurement due to a dead ECAL region, we select events with $\Delta\phi^* < 0.5$, i.e. $\not{H}_T$ approximately aligned with a jet in ϕ direction. Here all jets with $p_T > 30\,\text{GeV}$ enter into the $\Delta\phi^*$ calculation. We then check if the jet that resulted in the minimum $\Delta\phi$ is pointing towards a dead ECAL region in (η, ϕ) with 10 or more dead crystals. This list is retrieved for each event directly from the ECAL channel status database [18]. To cause a large energy loss in a jet, it is more likely that the dead region is towards the center of the jet and hence we reject events if $\Delta R_{ECAL} < 0.3$. The ΔR(jet,deadECALregion) = ΔR_{ECAL} is shown on the vertical axis of Figure 6(a).

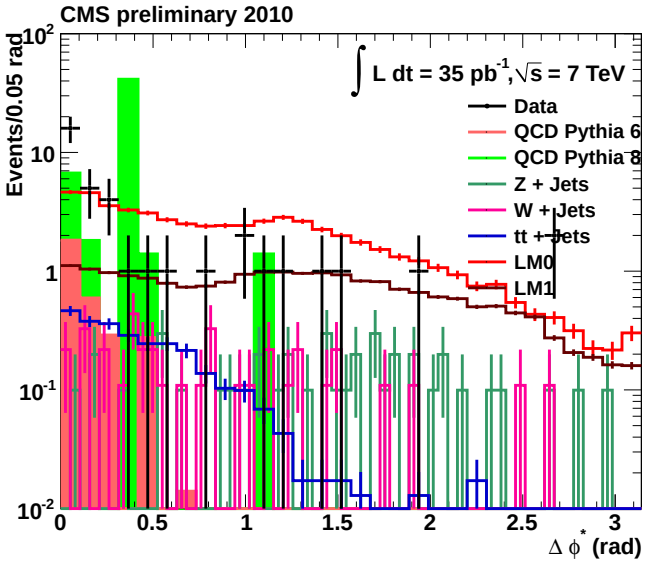

Figure 5: $\Delta\phi^*$ distribution after α_T cut.

For about 2/3 of the dead ECAL regions it is possible to recover the energy seen by the trigger primitives (TP). As a cross-check we plot in Figure 6 the $\sum E_T$ and $\not{E}_T$ seen by the trigger primitives for events surviving the $\alpha_T > 0.55$ requirement. In Figure 6(a) we show ΔR_{ECAL} versus the sum of the energies seen by the recoverable TP cells. It can be seen that our ΔR_{ECAL} requirement rejects two events where the energy in the TP cells was 63.75 GeV, which corresponds to the saturation value.

5.4 Effect of jets below threshold on $\not{H}_T$

We require the total transverse energy from jets to be greater than 350 GeV which is well above the transverse momentum threshold of 50 GeV for a single jet. However several jets below that

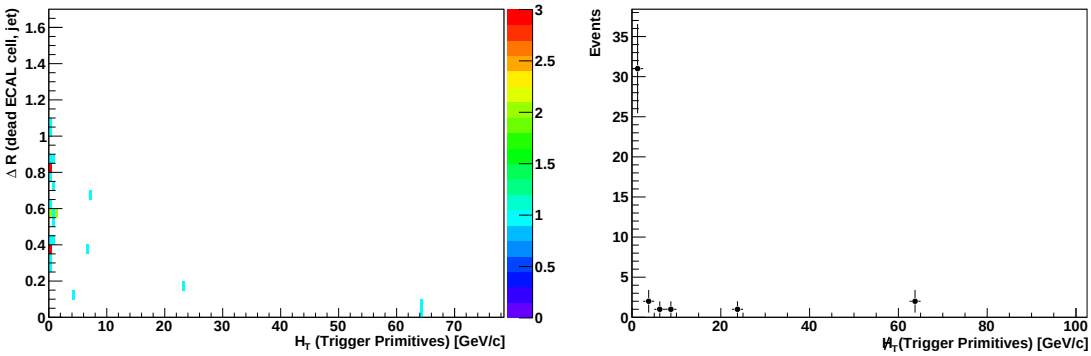

(a) $\sum E_T$ seen by the Trigger Primitives vs ΔR_{ECAL}. (b) $\not{E}_T$ seen by the Trigger Primitives.

Figure 6: $\sum E_T$ and $\not{E}_T$ as measured by the Trigger Primitives for events with $\alpha_T > 0.55$.

threshold could still amount to a considerable amount of ignored momentum. This is illustrated in Figure 7 which shows the missing momentum calculated from jets in the momentum range $10 < p_T < 50\,\text{GeV}$ for well balanced events with $\not{E}_T < 20$ GeV. It can be seen that in rare cases the neglected momentum can amount to $> 100\,\text{GeV}$, mainly for QCD events. We also see that PYTHIA 8 predicts larger $\not{H}_T$ from below threshold jets compared to PYTHIA 6 and that the data is somewhere in between.

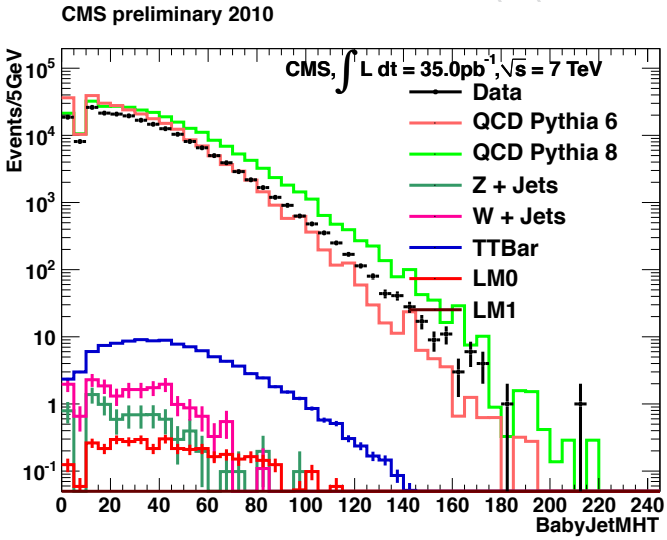

Figure 7: $\not{H}_T$ from jets with $10 < p_T < 50\,\text{GeV}$ in events with $H_T > 350\,\text{GeV}$ and $\not{E}_T < 20$ GeV.

Similar to what was done in [1] – which used the ratio of $\not{H}_T$ calculated from jets with two different thresholds of $p_T > 50\,\text{GeV}$ and $p_T > 30\,\text{GeV}$ to reject events with large $\not{H}_T$ from below threshold jets – we compare $\not{H}_T$ with the missing energy determined from all calorimeter towers, $\not{E}_T$. Specifically, we use $\not{E}_T$ fully calibrated for both clustered and unclustered energy (type-II CaloMET). The ratio $R_{\not{H}_T/\not{E}_T} = \not{H}_T/\not{E}_T$ can be used to single out events where the inclusion of lower momentum jets does significantly improve the balance of the event.

Figure 8(a) shows $R_{\not{H}_T/\not{E}_T}$ for events in a low H_T control region of $250 < H_T < 350\,\text{GeV}$ and $\alpha_T > 0.55$ and $\Delta R_{ECAL} < 0.3$. The majority of QCD events in this distribution has $R_{\not{H}_T/\not{E}_T}$ values well above one which means that there are moderate transverse momentum jets or

other lost objects which when considered do lead to a more balanced event. Figure 8(b) shows $R_{\not H_T/\not E_T}$ in the signal region of $H_T > 350\,\text{GeV}$ after $\alpha_T > 0.55$ and $\Delta R_{ECAL} < 0.3$. Similar to the low H_T region, QCD events are located at values of $R_{\not H_T/\not E_T} > 1$ while signal-like events with true missing energy are closely centered around 1. In analogy to the analysis in [1], we only accept events where $\not H_T$ is no more than 25% larger than $\not E_T$, i.e., where $R_{\not H_T/\not E_T} < 1.25$. This is somewhat stricter than the $R_{\not H_{T50}/\not H_{T30}} < 1.25$ requirement of [1] because the previous cut was derived from a PYTHIA 6 sample that predicts fewer low p_T jets compared to the now available PYTHIA 8 sample.

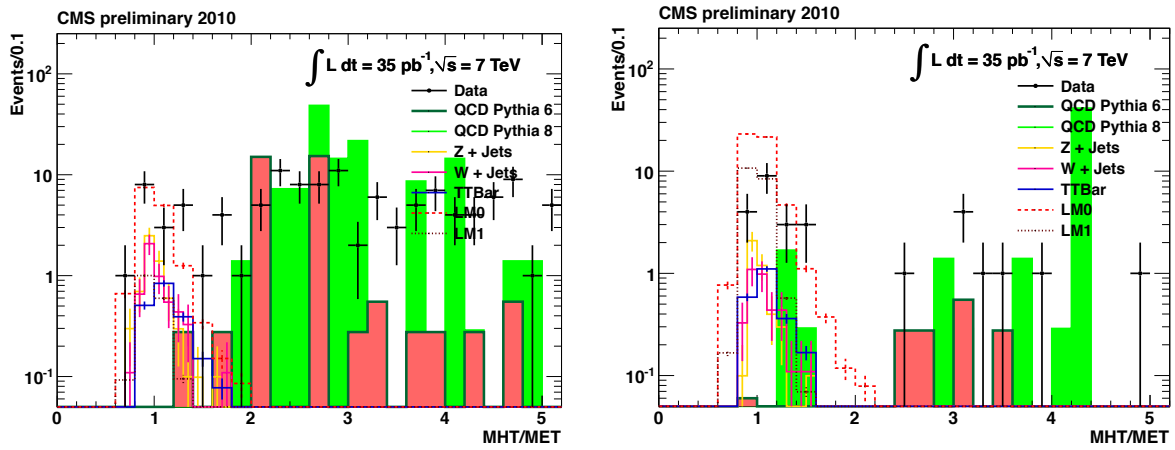

(a) $R_{\not H_T/\not E_T}$ distribution for events in the low H_T control region $250 < H_T < 350\,\text{GeV}$ after α_T and ΔR_{ECAL} cut.

(b) $R_{\not H_T/\not E_T}$ for MC simulated events in the signal region $H_T > 350\,\text{GeV}$ and after α_T and ΔR_{ECAL} cut.

Figure 8: $R_{\not H_T/\not E_T}$ distributions in two different H_T regions.

5.5 Event yields after full selection

To summarise our event selection, we require:

- $H_T > 350\,\text{GeV}$
- $\alpha_T > 0.55$
- $\Delta R_{ECAL} < 0.3$, if $\Delta\phi^* < 0.5$.
- $R_{\not H_T/\not E_T} < 1.25$

The resulting event yields for data and the different Monte Carlo samples at different stages of the event selection are summarised in Tables 1-6. The $H_T > 250\,\text{GeV}$ requirement ensures full efficiency of the HLT_HT150U trigger. A breakdown of the event yields into dijet and ≥ 3 jet events can be found in Tables 25-38.

The α_T distributions with the ΔR_{ECAL} and $R_{\not H_T/\not E_T}$ requirements applied are shown in Figure 9.

The yields from MC background samples are shown for comparison, however it should be noted that the number of background events are determined from data control samples as discussed in Section 7. The expected yields for the SUSY benchmark-points LM0 - LM3 are summarized in Table 6.

We observe 3 events in data with a SM expectation of 4.0 events. Two of the observed events appear in the dijet channel while the third event has three jets. This observation is compatible

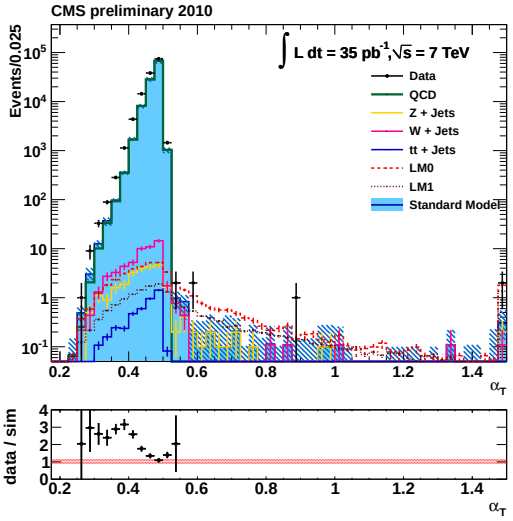

(a) α_T distribution for dijet event.

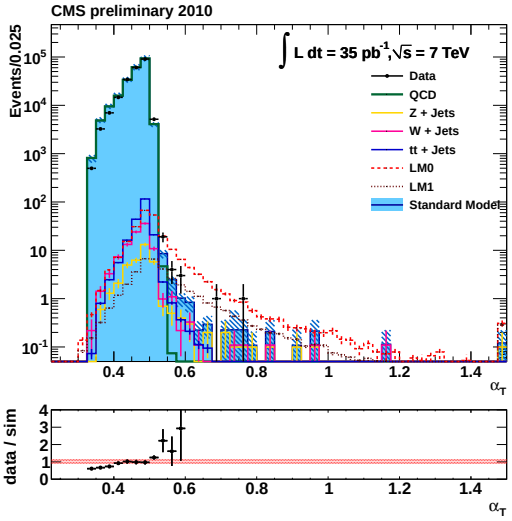

(b) α_T distribution for events with $n \geq 3$ jets.

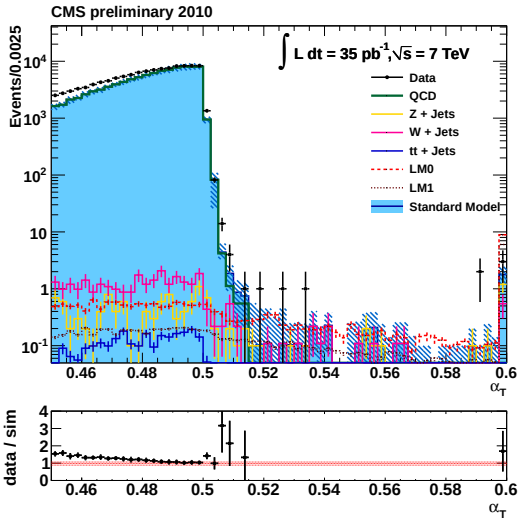

(c) Zoomed α_T distribution for dijet events.

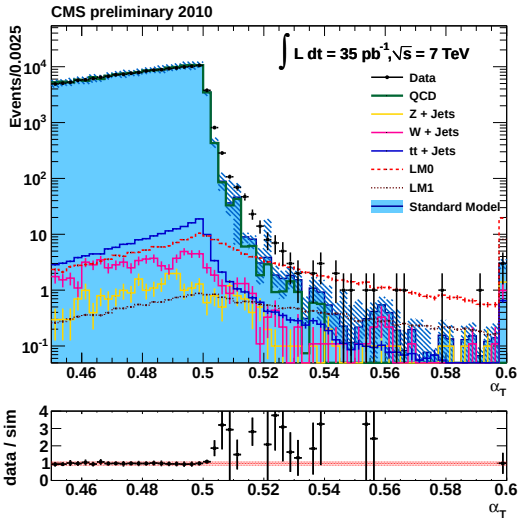

(d) Zoomed α_T distribution for events with $n \geq 3$ jets.

Figure 9: α_T distribution after H_T, ΔR_{ECAL} and $R_{\not{H}_T/\not{E}_T}$ selection.

with the SM expectation.

It can be seen that in the dijet case only $Z \rightarrow \nu\bar{\nu}$ + jets and W + jets events contribute to the expected background. For jet multiplicities ≥ 3, top decays start adding to the background. The contributions from $Z \rightarrow \nu\bar{\nu}$, W + jets and $t\bar{t}$ are all of comparable size. Z decays to charged leptons are negligible.

For the dominant W + jet and $t\bar{t}$ backgrounds it is interesting to take a closer look at their composition as one would expect them to contain leptons which in principle should be easy to identify and reject. As $\alpha_T > 0.55$ requires $\not{H}_T > 140\,\text{GeV}$, we are dealing with boosted W's in both W + jets and $t\bar{t}$ events with similar properties. They can be split into four main categories:

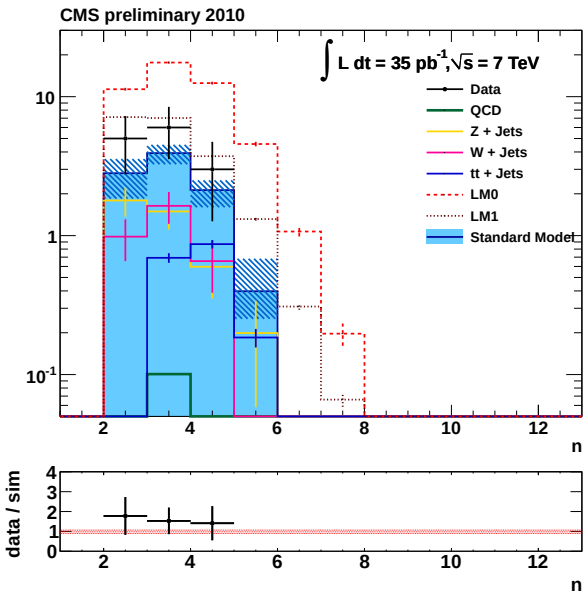

Figure 10: Jet multiplicity distribution after all selection cuts.

- W$\rightarrow \tau\nu(\tau \rightarrow$ hadronic): 37%
- W$\rightarrow (e,\mu)\nu$; e,μ out of p_{T} or η acceptance: 35%
- W$\rightarrow (e,\mu)\nu$; e,μ veto inefficiency: 24%
- both W's from $t\bar{t}$ decaying to leptons: 5%

A detailed discussion of these backgrounds is presented in Section 7.2.

A breakdown of signal and background into the different jet multiplicities is shown in Figure 10. For the PYTHIA 6 QCD sample we obtain 1.3 QCD events after application of the $\alpha_{\mathrm{T}} > 0.55$ cut and integrated over all jet multiplicities. This number is reduced down to 0.05 events after requiring $\Delta\mathrm{R}_{\mathrm{ECAL}} < 0.3$ and $R_{\not\mathrm{H}_{\mathrm{T}}/\not\mathrm{E}_{T}} < 1.25$. The corresponding numbers for the PYTHIA 8 sample are 22.2 events after α_{T} cut and 0.2 events after $\Delta\mathrm{R}_{\mathrm{ECAL}}$ and $R_{\not\mathrm{H}_{\mathrm{T}}/\not\mathrm{E}_{T}}$ cut. The QCD yields and uncertainties should be treated with care, as the equivalent luminosity for the low $\hat{p}_T$ (low H_{T}) samples is smaller than the data luminosity, resulting in weights > 1. However, these yields are only listed for comparison and are not used for the background estimation.

Furthermore, we show the effective mass $M_{\mathrm{eff}} = \mathrm{H}_{\mathrm{T}} + \not\mathrm{H}_{\mathrm{T}}$ distribution after all selection cuts in Figure 11 where we compare the data with the Standard Model background expectation and several SUSY benchmark points.

The shape and yield of the M_{eff} distribution observed in the data is consistent with the expectation from the simulation of the standard model backgrounds. The yields predicted for the LM0 and LM1 benchmark SUSY models are in excess of the data over most of the M_{eff} range.

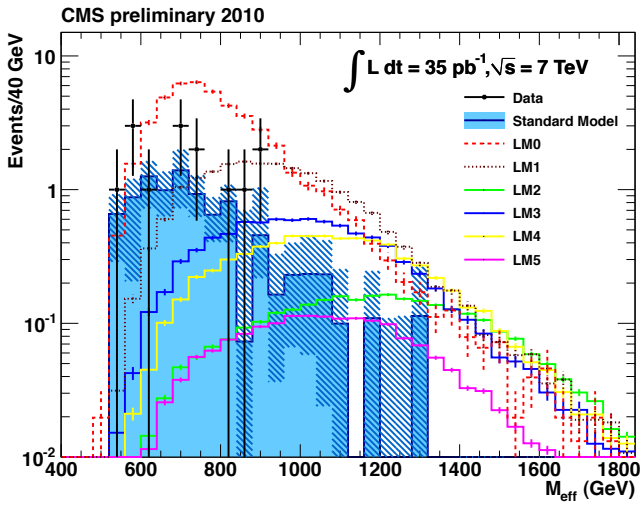

Figure 11: Effective Mass M_{eff} distribution after all selection cuts for SM processes and several low mass SUSY points.

Table 1: Cut flow for $35\,\mathrm{pb}^{-1}$ for $N^j \geq 2$. Column *a)* is the number of events passing the cut, column *b)* is the percentage of events lost of those passing the intial $H_T > 250$ GeV cut (cumulative), and column *c)* is the percentage lost from the previous cut. The QCD PYTHIA sample is from CMSSW_3_6_X.

Cut	SM (Pythia 6 QCD)			SM (Pythia 8 QCD)			SM (MadGraph)			Data		
	a)	b)	c)	a)	b)	c)	a)	b)	c)	a)	b)	c)
Selection	12.03 M	-	-	14.51 M	-	-	8.86 M	-	-	9.91 M	-	-
$H_T > 250\,\mathrm{GeV}$	5.04 M	0.0	58.1	5.47 M	0.0	62.3	3.36 M	0.0	62.1	4.68 M	0.0	52.8
$N^\gamma = 0$	5.02 M	0.2	0.2	5.46 M	0.2	0.2	3.35 M	0.2	0.2	4.67 M	0.2	0.2
$N^e = 0$	5.02 M	0.3	0.1	5.45 M	0.3	0.1	3.35 M	0.2	0.1	4.66 M	0.3	0.1
Odd μ veto	4.91 M	2.5	2.2	5.33 M	2.5	2.2	3.27 M	2.6	2.3	4.52 M	3.3	3.0
$N^\mu = 0$	4.91 M	2.5	0.0	5.33 M	2.5	0.0	3.27 M	2.6	0.0	4.52 M	3.3	0.0
Bad μ in j	4.89 M	3.0	0.5	5.31 M	2.8	0.3	3.25 M	3.0	0.5	4.50 M	3.7	0.4
Odd j veto	4.79 M	4.9	1.9	5.20 M	4.9	2.2	3.22 M	4.1	1.1	4.44 M	4.9	1.3
$j^1 : \lvert\eta\rvert < 2.5$	4.59 M	8.9	4.3	4.98 M	9.0	4.3	3.08 M	8.2	4.4	4.30 M	8.0	3.2
$j^2 : p_T > 100\,\mathrm{GeV}$	2.95 M	41.5	35.7	2.95 M	46.1	40.8	2.15 M	36.1	30.4	2.89 M	38.2	32.8
$H_T > 350\,\mathrm{GeV}$	(849 ± 2) k	83.1	71.2	1.06 M	80.6	64.0	(612 ± 1) k	81.8	71.5	(908 ± 1) k	80.6	68.6
$\alpha_T > 0.55$	14.0 ± 1.2	≥ 99.9	≥ 99.9	63.7 ± 41.5	≥ 99.9	≥ 99.9	41.1 ± 28.4	≥ 99.9	≥ 99.9	38.0 ± 6.2	≥ 99.9	≥ 99.9
Dead ECAL	12.6 ± 1.2	≥ 99.9	9.9	58.7 ± 41.5	≥ 99.9	7.9	11.2 ± 0.9	≥ 99.9	72.6	33.0 ± 5.7	≥ 99.9	13.2
$\not{H}_T / \not{E}_T < 1.25$	9.35 ± 0.88	≥ 99.9	25.7	9.52 ± 0.92	≥ 99.9	83.8	9.45 ± 0.89	≥ 99.9	16.0	14.0 ± 3.7	≥ 99.9	57.6

Table 2: Cut flow for 35 pb^{-1} for $N^j \geq 2$. Column a) is the number of events passing the cut, column b) is the percentage of events lost of those passing the intial $H_T > 250$ GeV cut (cumulative), and column c) is the percentage lost from the previous cut. The QCD PYTHIA sample is from CMSSW_3_8_X.

Cut	SM (Pythia 6 QCD)			SM (Pythia 8 QCD)			Data		
	a)	b)	c)	a)	b)	c)	a)	b)	c)
Selection	14.99 M	-	-	15.00 M	-	-	9.91 M	-	-
$H_T > 250\,\mathrm{GeV}$	5.82 M	0.0	61.2	5.68 M	0.0	62.1	4.68 M	0.0	52.8
$N^\gamma = 0$	5.81 M	0.2	0.2	5.67 M	0.2	0.2	4.67 M	0.2	0.2
$N^e = 0$	5.80 M	0.3	0.1	5.66 M	0.3	0.1	4.66 M	0.3	0.1
Odd μ veto	5.69 M	2.1	1.9	5.57 M	2.0	1.7	4.52 M	3.3	3.0
$N^\mu = 0$	5.69 M	2.1	0.0	5.57 M	2.1	0.0	4.52 M	3.3	0.0
Bad μ in j	5.67 M	2.4	0.3	5.55 M	2.4	0.3	4.50 M	3.7	0.4
Odd j veto	5.57 M	4.3	1.9	5.42 M	4.6	2.3	4.44 M	4.9	1.3
$j^1 : \lvert\eta\rvert < 2.5$	5.34 M	8.1	4.1	5.19 M	8.7	4.3	4.30 M	8.0	3.2
$j^2 : p_T > 100\,\mathrm{GeV}$	3.40 M	41.5	36.3	3.07 M	45.9	40.8	2.89 M	38.2	32.8
$H_T > 350\,\mathrm{GeV}$	1.11 M	80.9	67.4	1.12 M	80.3	63.5	(908 ± 1) k	80.6	68.6
$\alpha_T > 0.55$	30.5 ± 4.7	≥ 99.9	≥ 99.9	35.3 ± 9.3	≥ 99.9	≥ 99.9	38.0 ± 6.2	≥ 99.9	≥ 99.9
Dead ECAL	24.5 ± 4.2	≥ 99.9	19.5	26.5 ± 7.9	≥ 99.9	25.1	33.0 ± 5.7	≥ 99.9	13.2
$\not{H}_T / \not{E}_T < 1.25$	9.26 ± 0.88	≥ 99.9	62.2	9.24 ± 0.88	≥ 99.9	65.1	14.0 ± 3.7	≥ 99.9	57.6

Table 3: Cut flow for $35\,\mathrm{pb}^{-1}$ for $N^j \geq 2$ for the QCD PYTHIA CMSSW_3_6_X samples. Column $a)$ is the number of events passing the cut, column $b)$ is the percentage of events lost of those passing the intial $H_T > 250$ GeV cut (cumulative), and column $c)$ is the percentage lost from the previous cut.

Cut	QCD Pythia 6 (36X)			QCD Pythia 8 (36X)			QCD MadGraph		
	a)	b)	c)	a)	b)	c)	a)	b)	c)
Selection	12.01 M	-	-	14.49 M	-	-	8.83 M	-	-
$H_T > 250\,\mathrm{GeV}$	5.03 M	0.0	58.1	5.46 M	0.0	62.3	3.34 M	0.0	62.1
$N^\gamma = 0$	5.02 M	0.2	0.2	5.45 M	0.2	0.2	3.34 M	0.1	0.1
$N^e = 0$	5.02 M	0.3	0.1	5.45 M	0.3	0.1	3.34 M	0.1	0.1
Odd μ veto	4.90 M	2.5	2.2	5.33 M	2.5	2.2	3.26 M	2.4	2.3
$N^\mu = 0$	4.90 M	2.5	0.0	5.33 M	2.5	0.0	3.26 M	2.5	0.0
Bad μ in j	4.88 M	2.9	0.5	5.31 M	2.8	0.3	3.25 M	2.9	0.5
Odd j veto	4.79 M	4.8	1.9	5.19 M	4.9	2.2	3.21 M	3.9	1.1
$j^1 : \lvert\eta\rvert < 2.5$	4.58 M	8.9	4.3	4.97 M	9.0	4.3	3.07 M	8.1	4.4
$j^2 : p_T > 100\,\mathrm{GeV}$	2.95 M	41.4	35.7	2.94 M	46.1	40.8	2.14 M	36.0	30.3
$H_T > 350\,\mathrm{GeV}$	(848 ± 2) k	83.1	71.2	1.06 M	80.6	64.0	(610 ± 1) k	81.8	71.5
$\alpha_T > 0.55$	3.00 ± 0.83	≥ 99.9	100.0	52.7 ± 41.5	≥ 99.9	100.0	30.1 ± 28.4	≥ 99.9	100.0
Dead ECAL	2.36 ± 0.78	≥ 99.9	21.5	48.4 ± 41.5	≥ 99.9	8.1	1.01 ± 0.28	≥ 99.9	96.6
$\not{H}_T / \not{E}_T < 1.25$	0.12 ± 0.04	≥ 99.9	94.9	0.29 ± 0.29	≥ 99.9	99.4	0.23 ± 0.14	≥ 99.9	76.9

Table 4: Cut flow for 35 pb^{-1} for $N^j \geq 2$ for the QCD PYTHIA CMSSW_3_8_X samples. Column *a*) is the number of events passing the cut, column *b*) is the percentage of events lost of those passing the intial $H_T > 250$ GeV cut (cumulative), and column *c*) is the percentage lost from the previous cut.

Cut	QCD Pythia 6 (38X)			QCD Pythia 8 (38X)		
	a)	b)	c)	a)	b)	c)
Selection	14.98 M	-	-	14.98 M	-	-
$H_T > 250\,\mathrm{GeV}$	5.81 M	0.0	61.2	5.68 M	0.0	62.1
$N^\gamma = 0$	5.80 M	0.2	0.2	5.66 M	0.2	0.2
$N^e = 0$	5.79 M	0.2	0.1	5.66 M	0.3	0.1
Odd μ veto	5.69 M	2.1	1.9	5.56 M	2.0	1.7
$N^\mu = 0$	5.69 M	2.1	0.0	5.56 M	2.0	0.0
Bad μ in j	5.67 M	2.4	0.3	5.54 M	2.3	0.3
Odd j veto	5.56 M	4.2	1.9	5.42 M	4.5	2.3
$j^1 : \lvert\eta\rvert < 2.5$	5.34 M	8.1	4.1	5.19 M	8.6	4.3
$j^2 : p_T > 100\,\mathrm{GeV}$	3.40 M	41.5	36.3	3.07 M	45.9	40.8
$H_T > 350\,\mathrm{GeV}$	1.11 M	80.9	67.4	1.12 M	80.3	63.6
$\alpha_T > 0.55$	19.5 ± 4.6	≥ 99.9	100.0	24.4 ± 9.2	≥ 99.9	100.0
Dead ECAL	14.3 ± 4.1	≥ 99.9	26.7	16.2 ± 7.9	≥ 99.9	33.4
$\not{H}_T / \not{E}_T < 1.25$	0.03 ± 0.02	≥ 99.9	99.8	0.01 ± 0.00	≥ 99.9	100.0

Table 5: Cut flow for $35\,\mathrm{pb}^{-1}$ for $N^j \geq 2$ for the W + jets, $Z \to \nu\bar{\nu}$and $t\bar{t}$ samples. Column a) is the number of events passing the cut, column b) is the percentage of events lost of those passing the intial $H_T > 250$ GeV cut (cumulative), and column c) is the percentage lost from the previous cut.

Cut	$W + nj$			$Z + nj$			$Z \to \nu\nu$			$t\bar{t}$		
	a)	b)	c)	a)	b)	c)	a)	b)	c)	a)	b)	c)
Selection	(4.3 ± 0.0) k	-	-	758.7 ± 8.6	-	-	491.6 ± 7.0	-	-	(3.7 ± 0.0) k	-	-
$H_T > 250\,\mathrm{GeV}$	(2.0 ± 0.0) k	0.0	54.8	279.2 ± 5.2	0.0	63.2	285.3 ± 5.3	0.0	42.0	(2.5 ± 0.0) k	0.0	32.8
$N^\gamma = 0$	(1.7 ± 0.0) k	14.9	14.9	211.9 ± 4.6	24.1	24.1	285.3 ± 5.3	0.0	0.0	(2.3 ± 0.0) k	8.0	8.0
$N^e = 0$	(1.5 ± 0.0) k	20.8	6.9	193.5 ± 4.4	30.7	8.7	285.2 ± 5.3	0.0	0.0	(2.2 ± 0.0) k	11.8	4.1
Odd μ veto	(1.5 ± 0.0) k	23.7	3.8	185.2 ± 4.3	33.7	4.3	275.9 ± 5.2	3.3	3.3	(2.1 ± 0.0) k	14.7	3.3
$N^\mu = 0$	(1.1 ± 0.0) k	44.9	27.7	121.5 ± 3.5	56.5	34.4	275.8 ± 5.2	3.3	0.0	(1.9 ± 0.0) k	25.5	12.6
Bad μ in j	(1.1 ± 0.0) k	46.1	2.2	119.9 ± 3.4	57.1	1.4	274.0 ± 5.2	4.0	0.6	(1.8 ± 0.0) k	26.7	1.6
Odd j veto	(1.0 ± 0.0) k	47.1	1.9	116.4 ± 3.4	58.3	2.9	272.1 ± 5.2	4.6	0.7	(1.8 ± 0.0) k	28.2	2.0
$j^1 : \lvert\eta\rvert < 2.5$	998.0 ± 10.4	48.9	3.4	109.9 ± 3.3	60.6	5.6	266.9 ± 5.2	6.5	1.9	(1.8 ± 0.0) k	29.0	1.1
$j^2 : p_T > 100\,\mathrm{GeV}$	610.3 ± 8.2	68.8	38.8	65.0 ± 2.5	76.7	40.9	160.5 ± 4.0	43.8	39.9	832.4 ± 1.9	66.8	53.2
$H_T > 350\,\mathrm{GeV}$	281.6 ± 5.5	85.6	53.9	27.7 ± 1.7	90.1	57.3	79.1 ± 2.8	72.3	50.7	650.1 ± 1.7	74.1	21.9
$\alpha_T > 0.55$	3.93 ± 0.66	99.8	98.6	0.00 ± 0.00	100.0	100.0	4.18 ± 0.64	98.5	94.7	2.77 ± 0.11	99.9	99.6
Dead ECAL	3.60 ± 0.63	99.8	8.3	0.00 ± 0.00	100.0	-	4.18 ± 0.64	98.5	0.0	2.39 ± 0.10	≥ 99.9	13.5
$\not{H}_T / \not{E}_T < 1.25$	3.28 ± 0.60	99.8	9.1	0.00 ± 0.00	100.0	-	4.08 ± 0.64	98.6	2.4	1.82 ± 0.09	≥ 99.9	23.9

Table 6: Cut flow for 35.0 pb^{-1} for $N^j \geq 2$ for selected LM signal points. Column *a)* is the number of events passing the cut, column *b)* is the percentage of events lost of those passing the intial $H_T > 250$ GeV cut (cumulative), and column *c)* is the percentage lost from the previous cut.

Cut	LM0			LM1			LM2			LM3		
	a)	b)	c)	a)	b)	c)	a)	b)	c)	a)	b)	c)
Selection	(1.0 ± 0.0) k	-	-	132.1 ± 0.3	-	-	15.5 ± 0.0	-	-	93.6 ± 0.2	-	-
$H_T > 250\,\mathrm{GeV}$	954.4 ± 2.5	0.0	9.0	128.2 ± 0.3	0.0	2.9	15.2 ± 0.0	0.0	1.9	90.7 ± 0.2	0.0	3.1
$N^\gamma = 0$	878.6 ± 2.4	7.9	7.9	118.9 ± 0.3	7.2	7.2	14.1 ± 0.0	7.2	7.2	82.6 ± 0.2	8.9	8.9
$N^e = 0$	825.2 ± 2.3	13.5	6.1	110.4 ± 0.3	13.8	7.2	13.3 ± 0.0	12.8	6.1	78.1 ± 0.2	13.9	5.4
Odd μ veto	774.7 ± 2.3	18.8	6.1	100.6 ± 0.3	21.5	8.9	11.7 ± 0.0	23.5	12.2	71.0 ± 0.2	21.7	9.1
$N^\mu = 0$	665.2 ± 2.1	30.3	14.1	86.2 ± 0.3	32.7	14.3	10.4 ± 0.0	31.6	10.6	61.6 ± 0.2	32.1	13.3
Bad μ in j	653.6 ± 2.1	31.5	1.7	85.3 ± 0.3	33.4	1.0	10.3 ± 0.0	32.4	1.2	60.4 ± 0.2	33.3	1.8
Odd j veto	642.8 ± 2.1	32.7	1.6	84.0 ± 0.3	34.5	1.6	10.1 ± 0.0	33.5	1.7	59.5 ± 0.2	34.4	1.5
$j^1 : \lvert\eta\rvert < 2.5$	638.8 ± 2.0	33.1	0.6	83.8 ± 0.3	34.6	0.2	10.1 ± 0.0	33.6	0.1	59.4 ± 0.2	34.5	0.2
$j^2 : p_T > 100\,\mathrm{GeV}$	464.6 ± 1.7	51.3	27.3	71.6 ± 0.2	44.2	14.6	9.14 ± 0.03	40.0	9.7	51.8 ± 0.2	42.8	12.7
$H_T > 350\,\mathrm{GeV}$	420.3 ± 1.7	56.0	9.5	67.9 ± 0.2	47.0	5.1	8.96 ± 0.03	41.2	2.0	50.6 ± 0.2	44.2	2.3
$\alpha_T > 0.55$	55.7 ± 0.6	94.2	86.7	20.8 ± 0.1	83.8	69.3	3.04 ± 0.02	80.0	66.0	9.45 ± 0.07	89.6	81.3
Dead ECAL	51.6 ± 0.6	94.6	7.3	19.9 ± 0.1	84.5	4.6	2.89 ± 0.02	81.0	5.0	8.77 ± 0.07	90.3	7.1
$\not{H}_\mathrm{T}/\not{E}_T < 1.25$	47.1 ± 0.6	95.1	8.8	19.5 ± 0.1	84.8	1.8	2.87 ± 0.02	81.2	0.9	8.45 ± 0.07	90.7	3.7

6 Cross-checks on selected events

As discussed so far, we expect that after the application of all selection cuts, there is a negligible amount of background from QCD processes and all events should be consistent with EWK processes, namely $Z \rightarrow \nu\bar{\nu}$, W+jets and $t\bar{t}$ production. In this section we perform three consistency checks to verify that the events selected have no unforeseen features.

6.1 $\Delta\phi^*$ distribution

As discussed in section 5.3, the $\Delta\phi^*$ variable is useful in identifying mismeasured jets. A discussed, events arising from mismeasurements of the huge background presented by QCD tend to small values of $\Delta\phi^*$, whereas processes with real $\not\!\!E_T$, e.g. from EWK processes) tend to populate $\Delta\phi^*$ evenly. In Fig. 12 we display the $\Delta\phi^*$ distribution for the (14) events in the data passing all selection requirements, i.e. after the $H_T > 350$ GeV requirement and then $\alpha_T > 0.55$, dead-ECAL cleanup and finally $\not\!\!H_T / \not\!\!E_T < 1.25$. As can be seen from the figure, the distribution in the data is consistent with the sum of the EWK processes and there is no indication of an enhanced contribution from QCD processes.

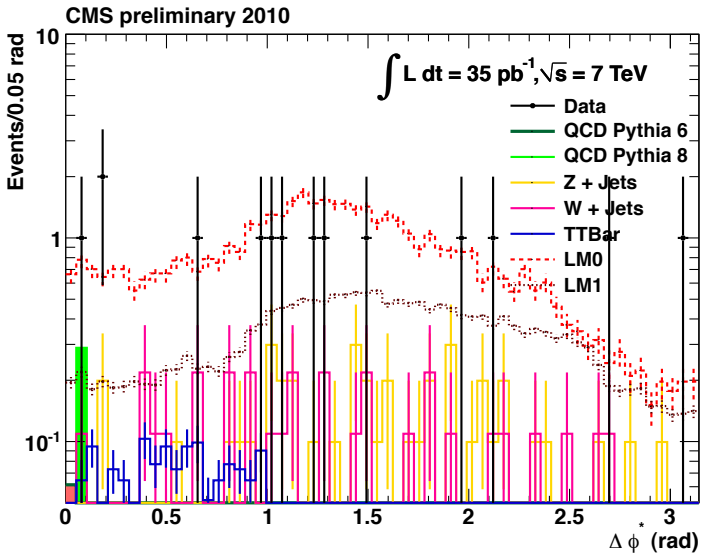

Figure 12: $\Delta\phi^*$ distribution after all selection cuts.

6.2 Possible pile-up effects

The rapidly rising instantaneous luminosity has introduced a time-varying amount of pileup in the data collected in 2010. It is therefore important to check whether there is any dependence of the results on the relative amount of pileup. This check is shown in Fig. 13, where the ratio of the α_T distributions for events with exactly 1 and ≥ 2 primary verteces is shown, once after the H_T selection and once after final selection. Within statistical uncertainties the distributions are flat, i.e., the α_T tail is not enhanced in events with multiple verteces.

6.3 Calorimeter noise cleaning effects

The CMS electromagnetic calorimeter (ECAL) barrel (EB) and endcap (EE), and hadron calorimeter (HCAL) barrel (HB), endcap (HE), and forward (HF) sections are known to record anomalous signals or noise. Anomalous signals are identified based on signal timing and

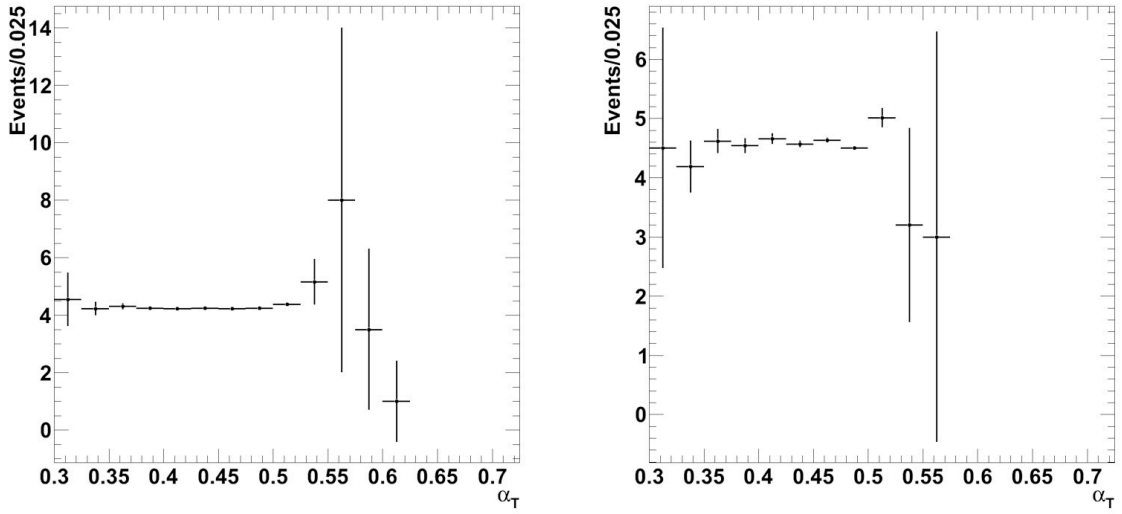

(a) Ratio of the α_T distributions for events with > 1 vertex and events with exactly 1 vertex after $H_T > 350\,GeV$ requirement.

(b) Ratio of the α_T distributions for events with > 1 vertex and events with exactly 1 vertex after $H_T > 350\,GeV$, $\Delta R_{ECAL} < 0.3$ and $R_{\not H_T / \not E_T} < 1.25$ requirement.

Figure 13: Dependence of the α_T distribution on the number of verteces in the event.

topologies. Studies of these effects are documented in detail in Ref. [10] for the HCAL, and in Ref. [19] for the ECAL.

Once a "RecHit" in an HCAL tower or ECAL crystal is determined to be unphysical, it is excluded from the reconstruction of higher level objects such as jets. To verify that our results are not affected by accidental removal of a real signal we plot in Figure 14 the scalar and vectorial sums of the RecHit energies in EB, EE, HB, HE and HF that were removed from the reconstruction for the events surviving our event selection. No significant "cleaned energy" is observed in the remaining events.

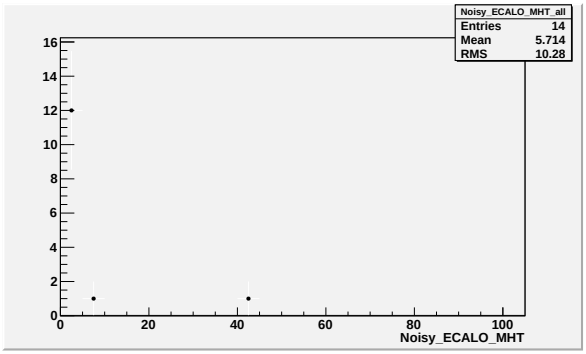

(a) $\not\!\!E_T$ of the cleaned ECAL RecHits.

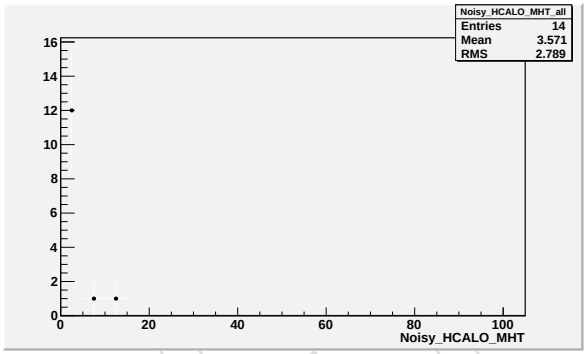

(b) $\not\!\!E_T$ of the cleaned HCAL RecHits.

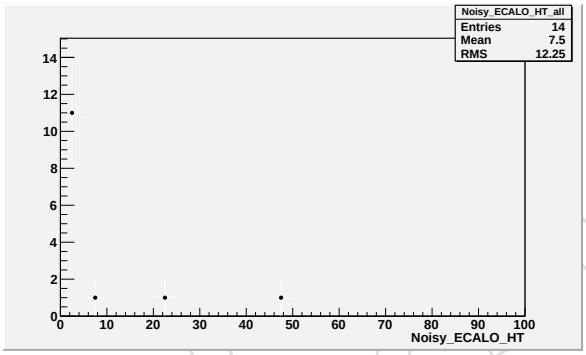

(c) $\sum \mathrm{E_T}$ of the cleaned ECAL RecHits

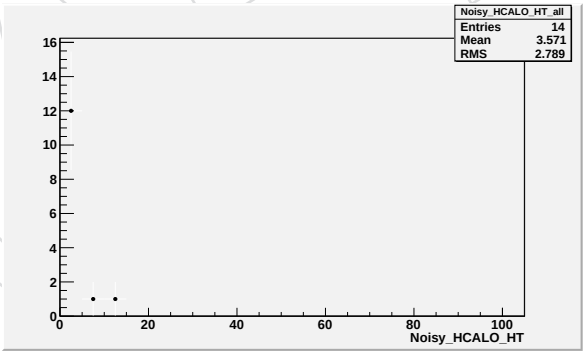

(d) $\sum \mathrm{E_T}$ of the cleaned HCAL RecHits

Figure 14: $\sum \mathrm{E_T}$ and $\not\!\!E_T$ from the cleaned RecHit collections for the remaining events.

7 Data-driven background estimations

In the following we present three different ways of estimating the remaining Standard Model backgrounds from data control samples. As discussed in the previous section, these are mainly $Z \rightarrow \nu\bar{\nu}$, $W + \text{jets}$ and $t\bar{t}$ events. The expected QCD background contribution is small but the associated uncertainties are sizable. We therefore first present a method that is aims to estimate all remaining backgrounds by extrapolating from lower H_T control regions. As a result of this study we conclude that the QCD contribution to the total background is indeed small as suggested by the simulation. We then turn to estimating the remaining electro-weak backgrounds from dedicated control samples to get a more precise background estimation. Specifically, these are photon+jets events for $Z \rightarrow \nu\bar{\nu}$+jets background and events with high-p_T muons for the $W + \text{jets}$ and $t\bar{t}$ backgrounds.

7.1 Total background prediction using lower H_T control regions

The method presented here is based on one documented in [1], known as the "η-H_T" method, that was designed primarily to establish the presence of a signal incompatible with SM expectation, without breaking the SM backgrounds down into their individual components.

The original method relies on the expectation that SUSY signal events are produced more centrally in pseudo-rapidity with respect to QCD, for which the main production mechanism is t-channel exchange, and other SM backgrounds. The pseudo-rapidity of the leading jet, η, is used as a measure of the centrality of an event. An excess is identified through the dependence on $|\eta|$ of the ratio of events passing a cut of $\alpha_T > 0.55$. This dependence is enhanced with increasing H_T in the presence of signal, as shown in Fig. 15(a). No dependence is observed for SM backgrounds only, as indicated in Fig. 15(b).

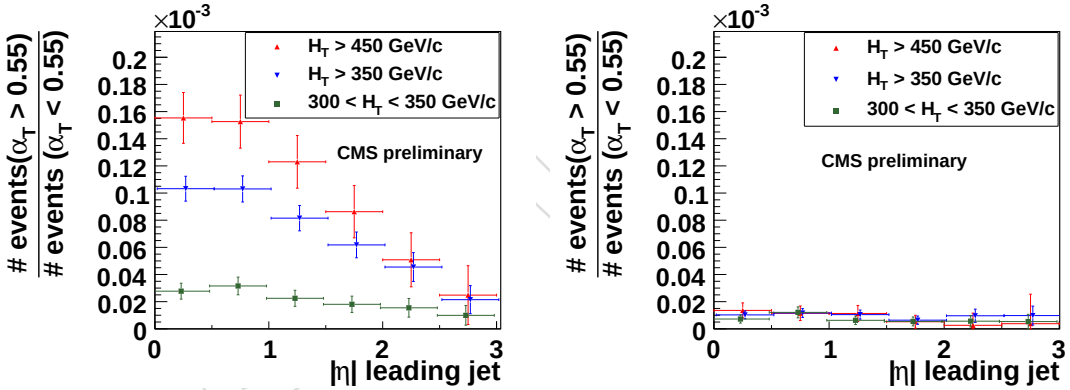

Figure 15: The ratio of events passing a cut of $\alpha_T > 0.55$ plotted as a function of $|\eta|$ of the leading jet for three different H_T bins, in the presence of an LM1 signal (a) and for SM backgrounds only (b), for an integrated luminosity of 100 pb^{-1} at $\sqrt{s} = 10$ TeV. Taken from [1].

Unfortunately, the size of the 2010 dataset is insufficient for a categorisation in bins of $|\eta|$. Therefore, we have investigated modifications to this procedure that are more suitable for a smaller dataset. More specifically, we concentrate on the behaviour of the ratio of events passing a cut on α_T as a function of H_T and do not consider the dependence on η.

7.1.1 Methodology and motivation

An inclusive prediction of the SM background in the signal region of $H_T > 350$ GeV is derived directly from data by making use of two control regions of lower H_T: 250 GeV $< H_T \leq 300$ GeV and 300 GeV $< H_T \leq 350$ GeV, with the main purpose of establishing an excess above SM. In the absence of a significant excess, this method provides an inclusive estimate of the SM backgrounds, including QCD.

One new important development to the method is motivated by the desire to ensure that the same event topologies and kinematic properties are observed in the control regions as for the signal region. This is achieved by scaling all jet kinematic thresholds according to $H_T^{min} + P_T$, where P_T denotes the minimum p_T of jets considered in the analysis, thus defining the jet multiplicity (jets falling below this threshold contribute to the $\not{H}_T$ for the event); and H_T^{min} denotes the lower bound of the H_T region under consideration. Similarly, the p_T thresholds of the leading and secondary jets of an event are also scaled in this way. We define the ratios:

$$x_i = \frac{P_T^i}{H_T^{min} + P_T} \tag{6}$$

where P_T^i is the minimum p_T threshold for the i^{th} jet. Note that in definition of this analysis, $P_T^{i>2} \equiv P_T$. The values of the ratios x_i are determined by the definition of the signal region and kept constant for the two control regions. The values of the scaled p_T jet thresholds for the different H_T regions are listed in Table 7. This scaling affects event selection through all variables that use jets as input (such as the $|\eta|$ of the leading jet, the jet-outside-acceptance veto, α_T, ...). It should be noted that this method is based on simple three-body (jet) kinematics in the transverse plane. In [20], it was pointed out that α_T can be expressed in terms of two relative quantities x_1 and x_2, which can be identified with the ρ normalisation parameters in the Dalitz notation.

Table 7: Scaled p_T jet thresholds for the different H_T regions.

H_T^{min}	(P_{T1}, P_{T2} ,P_T)	$H_T^{min} + P_T$	(x_1, x_2 ,x_3)
250	(71.4, 71.4 ,35.7)	285.7	(0.5,0.5,0.25)
300	(85.7, 85.7 ,42.9)	342.9	(0.5,0.5,0.25)
350	(100.0,100.0,50.0)	400.0	(0.5,0.5,0.25)

The scaling of the jet p_T thresholds ensures that, when ignoring instrumental effects, the allowed kinematic phase space is kept constant for the different H_T regions. Thus, relative kinematic properties like the jet multiplicity should remain unchanged between H_T regions.

Using jet multiplicity as an example, the necessity of scaling can be illustrated by considering the p_T thresholds for the leading and secondary jets in the signal region, for which $H_T > 350$ GeV and both jets are required to have $p_T > 100$ GeV. If these thresholds are also applied in the control regions within the range 250 GeV $< H_T \leq 350$ GeV, the available phase space for high-multiplicity events is restricted with respect to the signal region.

The validity of this approach is illustrated in Fig. 16(a) and Fig. 16(b), which show the jet multiplicity distributions using Monte-Carlo truth information (i.e., "gen-jets") for each of the three H_T regions when the jet p_T thresholds are scaled and not scaled with $H_T^{min} + P_T$, respectively. In the case of the scaled jet p_T thresholds, the mean jet multiplicity remains constant within

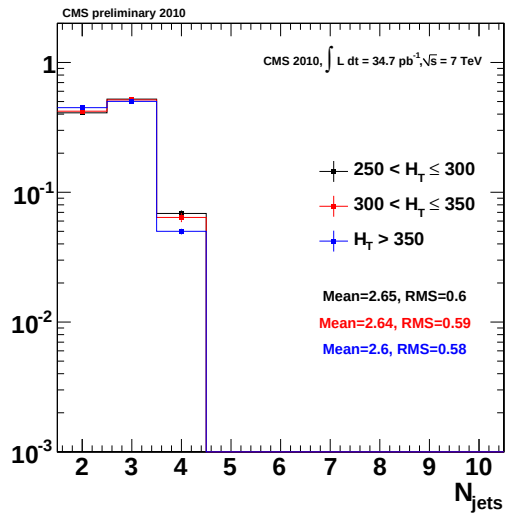

(a) Monte-Carlo truth and scaled jet p_T thresholds.

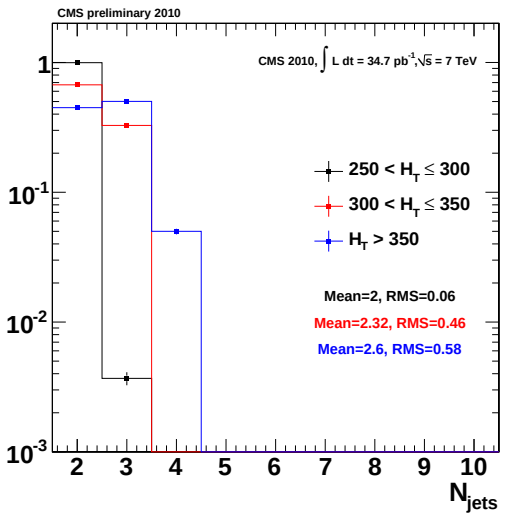

(b) Monte-Carlo truth and fixed jet p_T thresholds.

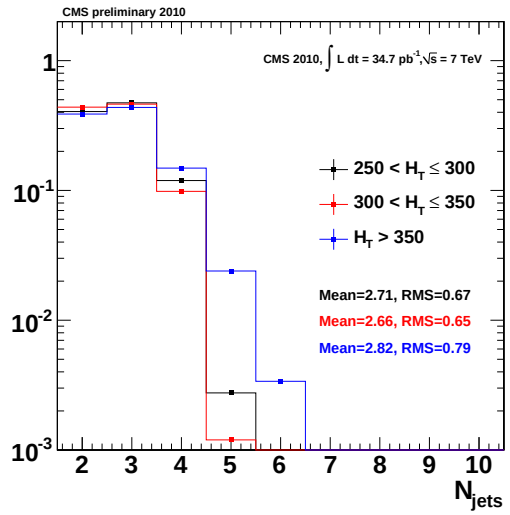

(c) Data and scaled jet p_T thresholds.

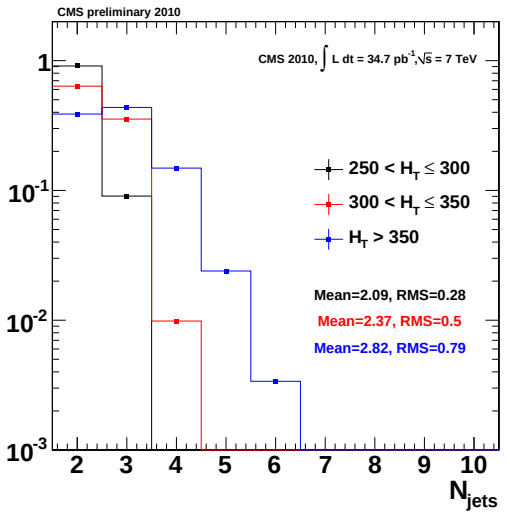

(d) Data and fixed jet p_T thresholds.

Figure 16: Jet multiplicity distributions from Monte-Carlo truth (a and b) and data (c and d), normalised to unit area, for the signal and two control regions using scaled (a and c) and fixed (b and d) jet p_T thresholds. Similar jet multiplicities are observed in each of the three H_T regions only when the jet p_T thresholds are scaled using $H_T^{min} + P_T$. This is especially true in the absence of instrumental effects.

errors; when the jet p_T thresholds are kept fixed for the three H_T regions, the mean jet multiplicity drops from 2.6 for the signal region to 2.0 for the lower control region, highlighting the reduced phase space relative to the signal region. Figs. 16(c) and 16(d) show the jet multiplicity distributions measured from data, again for each of the three H_T regions when the jet p_T thresholds are scaled and not scaled with $H_T^{min} + P_T$, respectively. A similar behaviour to the gen-jet case is again observed: for fixed jet p_T thresholds, the mean jet multiplicity drops from 2.8 for the signal region to 2.1 for the lower control region. The (small) differences with respect to the gen-jet multiplicity distributions are therefore attributed to instrumental effects. Similar arguments apply to other kinematic properties and only with the appropriate scaling of the jet p_T thresholds will it be possible to extract estimators of kinematic properties from lower H_T

regions that can be applied to the signal region in a controllable fashion.

7.1.2 H_T scaling when QCD dominated

Especially important is the application of scaling to the ratio of events passing and failing a given α_T cut, which is defined as:

$$R_{\alpha_T}(\theta) = \frac{N(\alpha_T > \theta)}{N(\alpha_T < \theta)} \tag{7}$$

In this section of the note, plots showing R_{α_T} as a function H_T reflect the values of R_{α_T} and H_T calculated when using scaled or fixed jet p_T thresholds, as indicated on the plots, and are binned according to the value of H_T (scaled or otherwise). Concerning statistical errors: the QCD samples were created in `CMSSW_3_6_X`, which are limited in size for the H_T regime of the two control regions, leading to relatively large uncertainties and a normalisation to 2.2 pb^{-1}; in the case of the SM backgrounds with real $\not\!\!E_T$, the samples were normalised to 415 pb^{-1}, which corresponds to the size of the smallest sample available (W+jets).

As a consequence of maintaining the allowed kinematic phase space constant in each of the three H_T regions, the ratio R_{α_T} is expected to be independent of the scale H_T for QCD events in the absence of instrumental effects.

Figures 17(a) and 17(b) show $R_{\alpha_T}(\alpha_T$ =0.51) as a function of H_T for jets clustered using generator information. These "gen-jets" do not suffer from instrumental effects and therefore approximate the environment of an ideal detector. For the cut value of $\alpha_T > 0.51$, the ratio R_{α_T} is completely dominated by QCD. For scaled quantities, both for di-jets and n-jets, the R_{α_T} calculated from gen-jets is flat within the errors, indicating that the scaling preserves the kinematic phase space for an ideal detector. However, for fixed thresholds, already without any detector effects, R_{α_T} becomes a strong function of H_T, indicating that the kinematic phase space is not preserved.

In the presence of instrumental effects, R_{α_T} calculated from data falls monotonically, as can be seen in Fig. 17(c) and Fig. 17(d). The decrease of R_{α_T} with H_T is more pronounced in n-jet ($n > 2$) events because for these topologies both jet mis-measurements as well as jets falling below threshold can cause events to pass the α_T cut. For di-jets only the effect of jets falling below threshold is typically causing events to pass the cut and therefore the fall of R_{α_T} with H_T is not as strong as in the n-jet case. Comparable behaviour is observed for SM backgrounds using a full detector simulation.

In general, the behaviour of R_{α_T} falling with H_T can be qualitatively understood by assuming that the QCD background has no significant intrinsic $\not\!\!E_T$ and only jet mis-measurements lead to the tail in the $\not\!\!E_T$ distribution. When considering a measurement of R_{α_T} using a real detector, the effect of worsening jet energy resolution with decreasing H_T means that even the scaled p_T thresholds effectively tighten with decreasing H_T, as jets are more likely to fluctuate below rather than above the jet p_T threshold. This leads to a decrease in the measured H_T, an increase in $\not\!\!H_T$, and thus an increase in the number of events passing a given α_T cut value, leading to a larger value of R_{α_T} relative to that for gen-jets (i.e., ideal detector). This effect is reduced with increasing H_T due to the improvement in the jet energy resolutions. Hence, R_{α_T} is expected to be a monotonically falling function of H_T for QCD. This behaviour is observed in data, reported for the first time in [21].

For fixed jet p_T thresholds, the same non-scaling behaviour is also observed in data (and for SM backgrounds using a full detector simulation, not shown here) as for gen-jets, as highlighted in

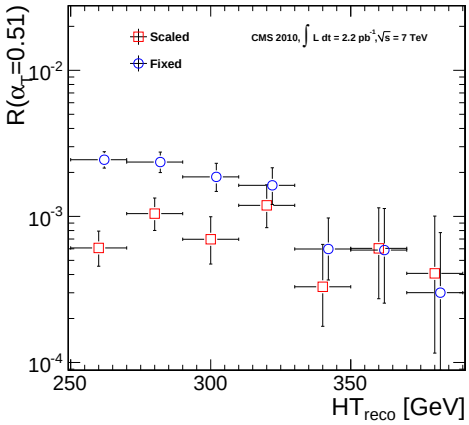

(a) Monte-Carlo truth information, $N_{\text{jet}} = 2$.

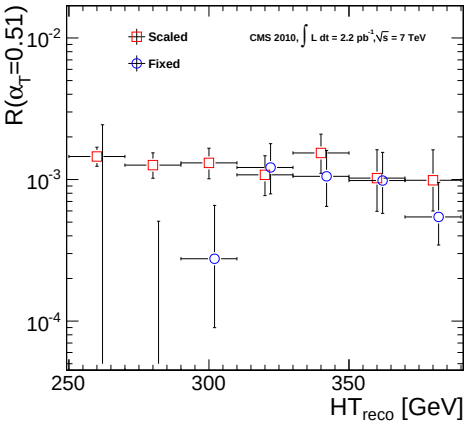

(b) Monte-Carlo truth information, $N_{\text{jet}} \geq 3$.

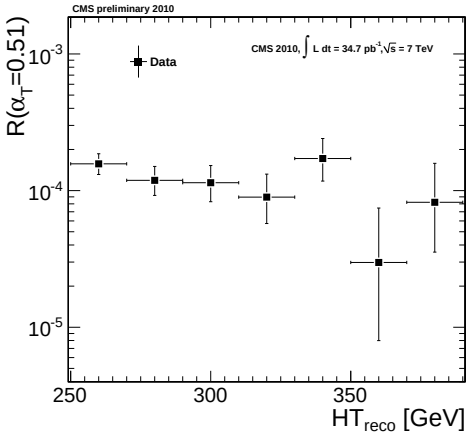

(c) Scaled p_T thresholds, $N_{\text{jet}} = 2$.

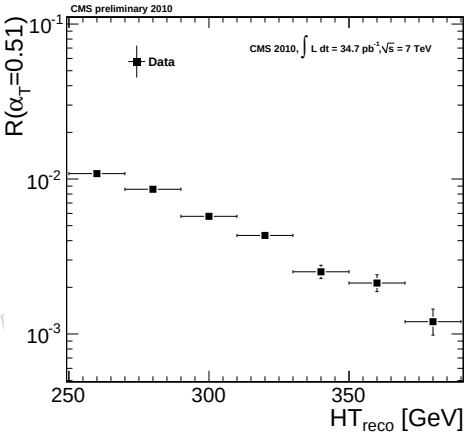

(d) Scaled p_T thresholds, $N_{\text{jet}} \geq 3$.

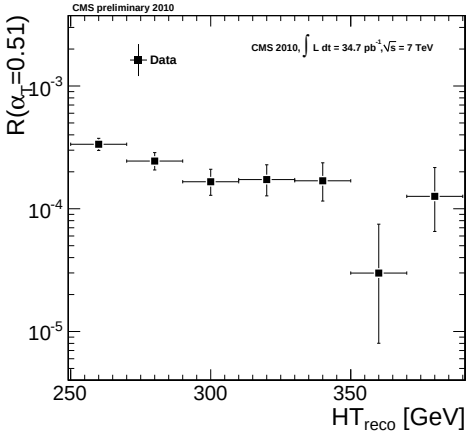

(e) Fixed p_T thresholds, $N_{\text{jet}} = 2$.

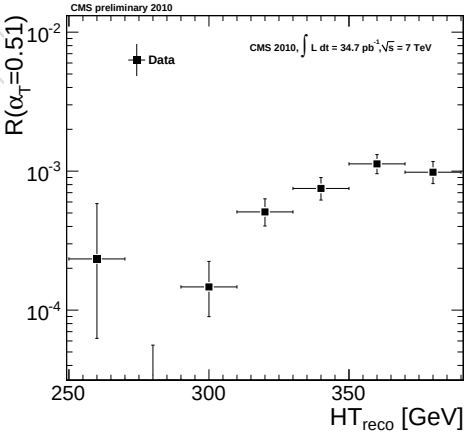

(f) Fixed p_T thresholds, $N_{\text{jet}} \geq 3$.

Figure 17: The evolution of R_{α_T} as a function of H_T for SM backgrounds using Monte-Carlo truth (a and b) and reconstructed quantities with scaled (c and d) and fixed (e and f) jet p_T thresholds and for events with $N_{\text{jet}} = 2$ (a, c and e) and $N_{\text{jet}} \geq 3$ (b, d and f). The α_T cut value used is 0.51. (Markers are artificially offset for clarity.)

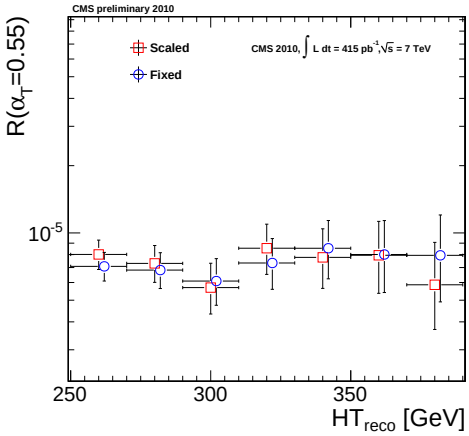

(a) Monte-Carlo truth information, $N_{\text{jet}} = 2$.

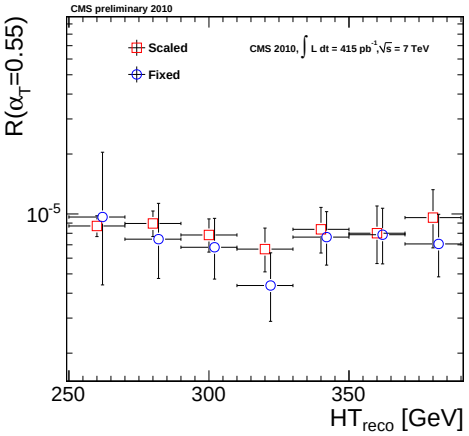

(b) Monte-Carlo truth information, $N_{\text{jet}} \geq 3$.

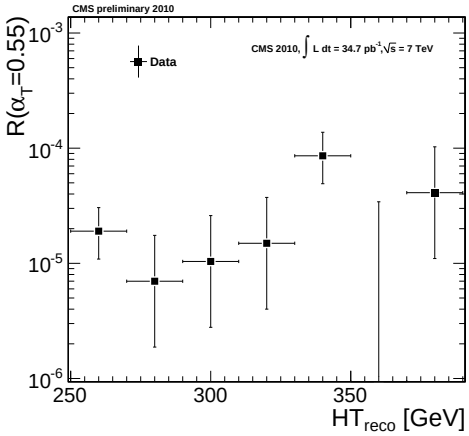

(c) Scaled p_{T} thresholds, $N_{\text{jet}} = 2$.

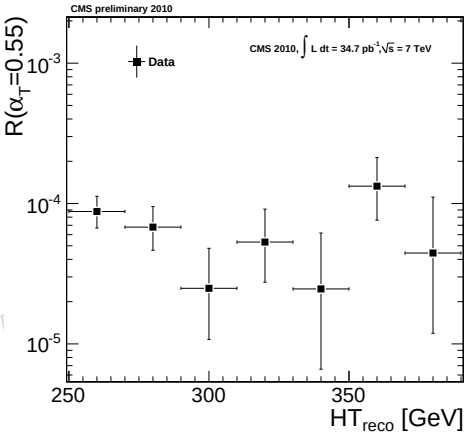

(d) Scaled p_{T} thresholds, $N_{\text{jet}} \geq 3$.

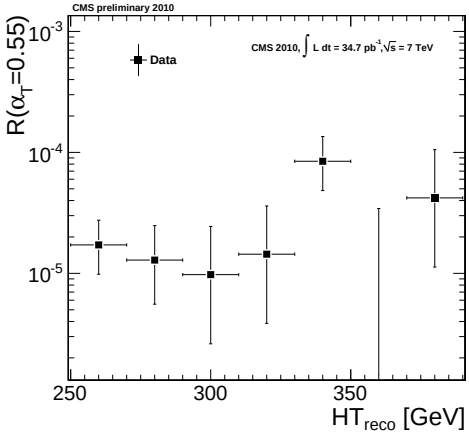

(e) Fixed p_{T} thresholds, $N_{\text{jet}} = 2$.

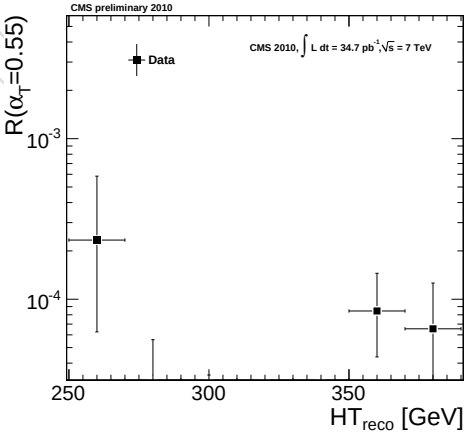

(f) Fixed p_{T} thresholds, $N_{\text{jet}} \geq 3$.

Figure 18: The evolution of $R_{\alpha_{\text{T}}}$ as a function of H_{T} for SM backgrounds using Monte-Carlo truth (a and b) and reconstructed quantities with scaled (c and d) and fixed (e and f) jet p_{T} thresholds and for events with $N_{\text{jet}} = 2$ (a, c and e) and $N_{\text{jet}} \geq 3$ (b, d and f). The α_{T} cut value used is 0.55. (Markers are artificially offset for clarity.)

Fig 17(e) and Fig. 17(f) for di-jets and $N_{jet} \geq 3$, respectively. Therefore, the measured R_{α_T} (H_T) with fixed thresholds will be a convolution of instrumental effects and kinematic phase space changes, which are almost impossible to separate. On the other hand, for scaled thresholds the gen-jet ratio stays stable within errors over the entire range of H_T, thus leaving detector effects as the only source for R_{α_T} (H_T) to change with H_T.

7.1.3 H_T scaling when dominated by SM processes with real $\not{E}_T$

As shown in Sec. 5.5, after a cut of $\alpha_T > 0.55$ and all other cleaning cuts, only SM backgrounds with real $\not{E}_T$ (primarily $W^{\pm}$+jets, $Z^0 \rightarrow \nu\nu$+jets and $t\bar{t}$) are expected to survive. Therefore, the numerator of R_{α_T} is completely dominated by events with real $\not{E}_T$, while the denominator is effectively QCD events. Figure 18(a) and Fig. 18(b) show a comparison of "fixed" and "scaled" $R_{\alpha_T}(\alpha_T > 0.55)$ after all cuts for di-jets and $N_{jet} \geq 3$, respectively. In contrast to the same comparison where QCD was dominating, described in the previous section, the "fixed" and "scaled" ratio for the sum of all EWK process are constant within errors. However, when this is split in the individual process, it becomes apparent that the observed "flatness" in the case of "fixed" thresholds for $N_{jet} \geq 3$ is caused by an accidental compensation of the three individual background components $W^{\pm}$+jets, $Z^0 \rightarrow \nu\nu$+jets and $t\bar{t}$. In particular, the $t\bar{t}$ behaviour displayed in Fig. 19(d) for $N_{jet} \geq 3$ reveals a strong dependence in R_{α_T}, which is explained by the restriction of phase space caused by the fixed jet p_T thresholds. For lower H_T bins the available space space is strongly reduced for $t\bar{t}$ leading to a bias in the R_{α_T} distribution towards lower values. The vector boson backgrounds, $W^{\pm}$+jets and $Z^0 \rightarrow \nu\nu$+jets, exhibit a smaller bias in R_{α_T} but also suffer from lower statistics due to the fixed thresholds at lower H_T values, as reflected by the error bars.

For scaled thresholds, however, the phase space is preserved over the entire range in H_T and therefore no R_{α_T} bias in the three individual background components is observed. Furthermore, the scaling of the thresholds also preserves the statistical power of the control sample at low H_T. This is a clear indication that also in an EWK-dominated environment, as in the case of $\alpha_T > 0.55$, scaling of cut thresholds is desirable in order to obtain estimators of kinematic properties in lower H_T bins that can be applied to the signal region (i.e. higher H_T).

7.1.4 An empirical H_T scaling law

As shown in the previous two sections, after an appropriate scaling of the jet p_T thresholds, R_{α_T} is either a monotonically falling function of H_T when QCD dominates (fake $\not{E}_T$) or constant with H_T when real $\not{E}_T$ processes are overwhelming. Since R_{α_T} is expected to be flat for an ideal detector (i.e. Gen-Jets) after scaling, the differences between these two scenarios can be qualitatively understood as the different response of detector effects for fake and real $\not{E}_T$ signatures. While for fake $\not{E}_T$ topologies (i.e. QCD events) the resolution and mis-measurements effects typically improve with energy (i.e. H_T), the impact of mis-measurements on real $\not{E}_T$ signatures for events passing the α_T cut is small. Therefore, events with significant (real) $\not{E}_T$ are expected to preserve the behaviour observed for an ideal detector (i.e. R_{α_T} being flat as a function of H_T), whereas for fake $\not{E}_T$ events R_{α_T} is expected to decrease with increasing H_T. This qualitative behaviour has been observed in the Monte Carlo and is also confirmed by the data.

Furthermore, Monte Carlo studies have shown that for both of these extreme scenarios (fake $\not{E}_T$ dominating and real $\not{E}_T$ dominating) the H_T behaviour can be well approximated by assuming the double ratio R_R:

$$R_R = \frac{R_{\alpha_T}(H_T)}{R_{\alpha_T}(H_T - X)} = \frac{R_{\alpha_T}(H_T + X)}{R_{\alpha_T}(H_T)} \tag{8}$$

is constant for three adjacent H_T bins: $H_T - X, H_T, H_T + X$.

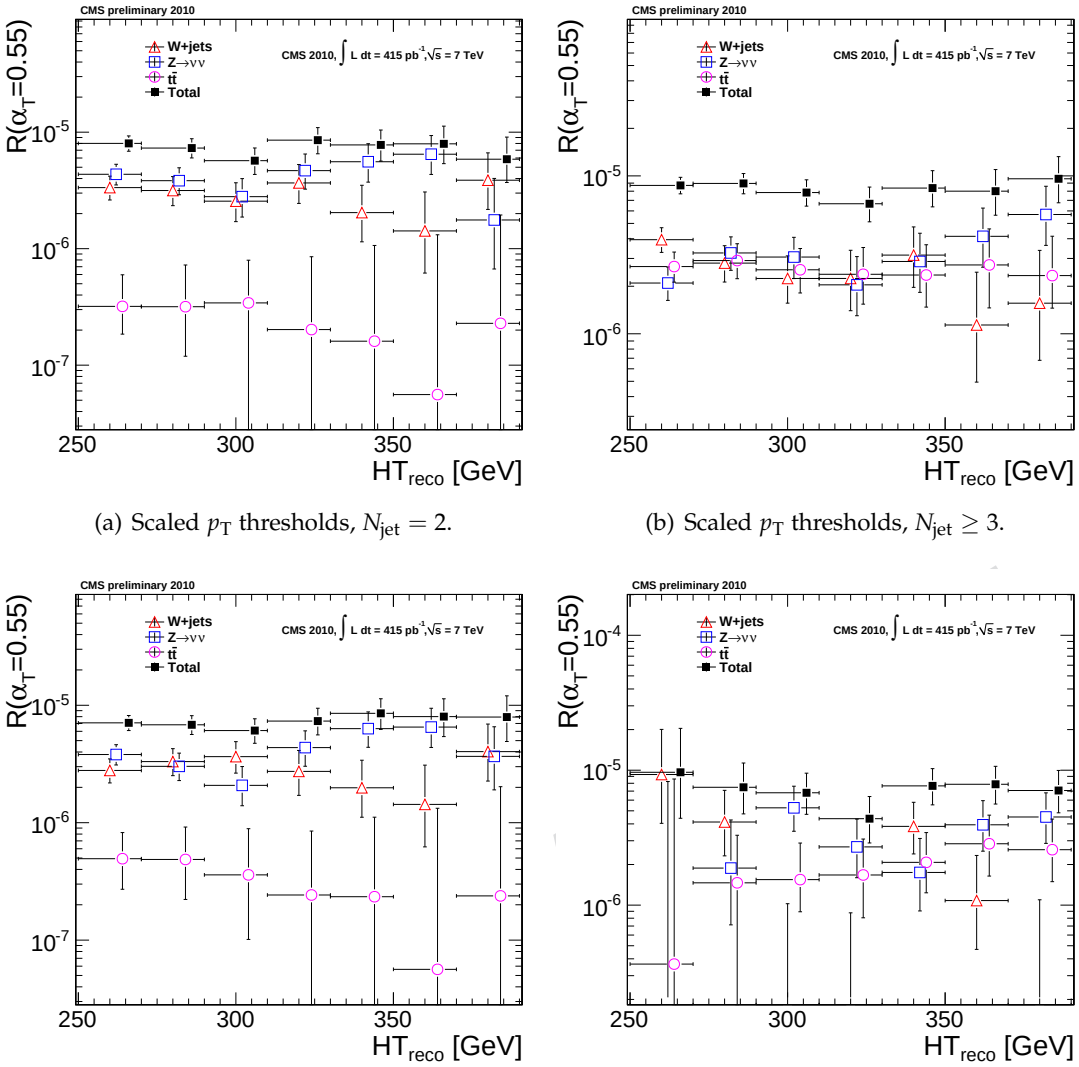

(a) Scaled p_T thresholds, $N_{jet} = 2$.

(b) Scaled p_T thresholds, $N_{jet} \geq 3$.

(c) Fixed p_T thresholds, $N_{jet} = 2$.

(d) Fixed p_T thresholds, $N_{jet} \geq 3$.

Figure 19: The evolution of R_{α_T} as a function of H_T for SM backgrounds using Monte-Carlo truth, with scaled (a and b) and fixed (c and d) jet p_T thresholds and for events with $N_{jet} = 2$ (a and c) and $N_{jet} \geq 3$ (b and d). The α_T cut value used is 0.55. (Markers are artificially offset for clarity.)

We observe that this ratio is a constant, independent of H_T. In the case of a QCD-dominated sample, the value of this ratio can be $R_R \ll 1$, whereas for real $\not{E}_T$ processes, $R_R \approx 1$. While this functional behaviour can be likely motivated on more general grounds by quantifying the detector response of real and fake $\not{E}_T$ processes, this goes beyond the scope of this study. For the present analysis we take this "double scaling" as an empirical fact motivated by the Monte Carlo. In the following we will demonstrate that this method closes in the Monte Carlo and that its general behaviour and assumptions are reproduced in data. It should be noted that for the analysis only the real $\not{E}_T$ scenario ($\alpha_T > 0.55$) is of numerical importance. Therefore, instead of using the double ratio scaling, the assumption of constant R_{α_T} could have also been a working hypothesis. However, since the double ratio scaling applies to both scenarios (i.e., QCD-dominated and EWK-dominated), even though it suffers from larger statistical uncertain-

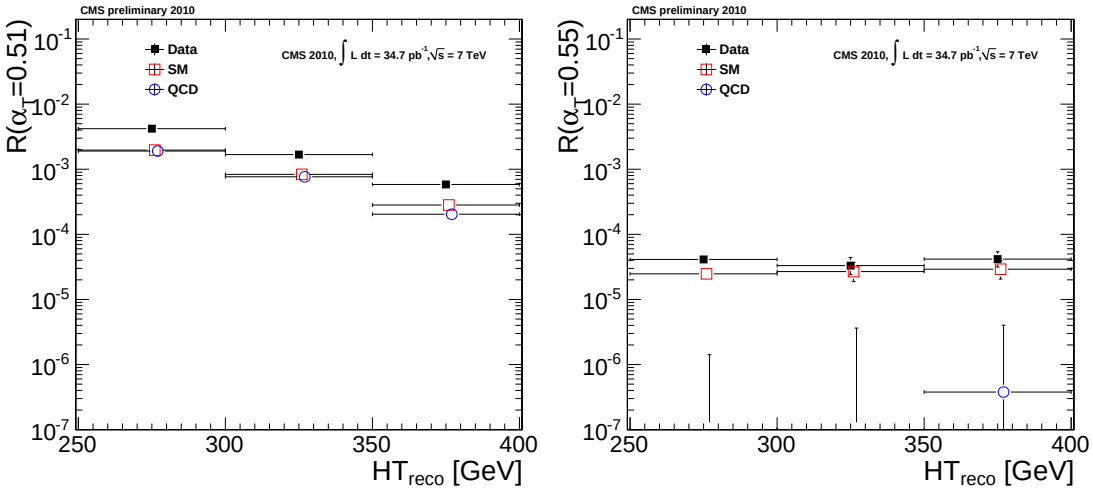

(a) $R_{\alpha_T}(0.51)$ as a function of H_T. (b) $R_{\alpha_T}(0.55)$ as a function of H_T.

Figure 20: The evolution of the ratio R_{α_T} as a function of H_T for events with $N_{\text{jet}} \geq 2$ and two different α_T cut values: (a) 0.51 and (b) 0.55. (Markers are artificially offset for clarity.)

ties because R_{α_T} (H_T) enters quadratically rather than a constant as in the case of a the "flat" assumption, the authors decided to adopt this more conservative extrapolation approach as the baseline. In the following the method is defined in detail.

Applying this independence of the double ratio on H_T, we obtain:

$$\frac{R^{350}_{\alpha_T}}{R^{300}_{\alpha_T}} = \frac{R^{300}_{\alpha_T}}{R^{250}_{\alpha_T}} \tag{9}$$

This equation can thus be solved to yield an expectation for $R^{350}_{\alpha_T}$ given $R^{250}_{\alpha_T}$ and $R^{300}_{\alpha_T}$:

$$R^{350,\text{pred}}_{\alpha_T} = \frac{R^{300,\text{meas}}_{\alpha_T}}{R^{250,\text{meas}}_{\alpha_T}} \cdot R^{300,\text{meas}}_{\alpha_T} \tag{10}$$

where $R^{350,\text{pred}}_{\alpha_T}$ is the prediction for the signal region. This ratio is then multiplied with the number of events observed to fail the α_T cut, $N^{350,\text{meas}}_{\theta<\alpha_T}$ in the signal region, again measured from data, to obtain an estimate of the number of events that satisfy $H_T > 350$ GeV and $\alpha_T > \theta$:

$$N^{350,\text{pred}}_{\theta>\alpha_T} = N^{350,\text{meas}}_{\theta<\alpha_T} \cdot \frac{R^{300,\text{meas}}_{\alpha_T}}{R^{250,\text{meas}}_{\alpha_T}} \cdot R^{300,\text{meas}}_{\alpha_T} \tag{11}$$

Figure 20(a) shows the dependence of R_{α_T} on H_T for data, all SM processes combined and QCD separately, for events with $N_{\text{jet}} \geq 2$ and passing an α_T cut value of 0.51. For the larger, nominal cut value of 0.55, essentially only severe mis-measurements result in QCD events passing the α_T cut, even for the lower H_T bins, leading to very small ratios and a weak (i.e., essentially flat) dependence on H_T, as expected from EWK processes and as shown in Fig. 20(b). Essentially no QCD events pass the α_T cut and only electroweak processes remain.

7.1.5 Results

The extrapolation into the signal region yields a predicted number of events, $N_{\text{predicted}}$, passing the α_T cut, which can be compared with the number of observed events, N_{observed}, in the signal

region. Figure 21 shows the difference in the number of events predicted and observed as a function of the α_T cut value, for data and Monte Carlo simulations of SM processes, with and without the addition of a SUSY LM1 signal. The cleaning cuts described in Sec. 5.3 and 5.4 (ΔR_{ECAL} and $R_{H_T/\not{E}_T}$) are also applied after the α_T cut.

For both data and SM processes, the behaviour is flat and consistent with zero as a function of the α_T cut value. Thus, the predicted and observed number of events are consistent with one another for all α_T cut values above 0.55, implying that the prediction provides an estimate of the total remaining background in the signal region. Importantly, the difference is always consistent with zero for the simulation of SM processes, which implies that the method does not under-predict the number of events in the signal region. The contribution from QCD is negligible and the background composition is dominated by processes with real $\not{E}_T$. Data and SM are in agreement for all cut values of α_T. Also shown is the behaviour when the SUSY LM1 signal is added to the SM backgrounds: negative values would be observed, reflecting an excess above SM expectation.

Table 8 summarises the predicted and observed number of events in the signal region of $H_T > 350$ GeV and after an α_T cut of 0.55 for data, QCD, all SM processes combined and SM+LM1. There is good agreement between data and SM Monte-Carlo and the QCD contribution is observed to be negligible. Table 9 summarises the values of the variables used in Equ. 11 to give a prediction for data and SM backgrounds with $\alpha_T > 0.55$

Table 8: Predicted and measured yields for data and simulated SM, QCD and LM1 processes for $H_T \geq 350$ and a cut value $\alpha_T = 0.55$. Only statistical uncertainties are listed.

N_{jet}	$N^{data}_{predicted}$	$N^{data}_{observed}$	$N^{SM}_{predicted}$	$N^{SM}_{observed}$	$N^{QCD}_{predicted}$	$N^{QCD}_{observed}$	$N^{SM+LM1}_{predicted}$	$N^{SM+LM1}_{observed}$
2	$4.9 \pm ^{4.7}_{3.4}$	5 ± 2.2	$3.1 \pm ^{3.5}_{2.4}$	2.8 ± 0.5	$0.0 \pm ^{0.0}_{0.0}$	0.0 ± 0.0	$4.7 \pm ^{4.2}_{2.9}$	9.8 ± 0.5
≥ 3	$5.2 \pm ^{3.4}_{2.6}$	9 ± 3	$6.1 \pm ^{4.5}_{3.4}$	6.4 ± 0.7	$0.0 \pm ^{0.0}_{0.0}$	0.1 ± 0.0	$7.2 \pm ^{5.3}_{4.1}$	18.6 ± 0.7
≥ 2	$9.0 \pm ^{4.5}_{3.8}$	14 ± 3.7	$9.1 \pm ^{5.4}_{4.3}$	9.2 ± 0.9	$0.0 \pm ^{0.0}_{0.0}$	0.1 ± 0	$11.8 \pm ^{6.4}_{5.2}$	28.5 ± 0.9

Table 9: Values of the variables used in Equ. 11 to give a prediction for data and SM backgrounds with $\alpha_T > 0.55$. Only statistical uncertainties are listed.

N_{jet}	$R^{250,data}_{\alpha_T}$ $[10^{-6}]$	$R^{300,data}_{\alpha_T}$ $[10^{-6}]$	$N^{350,data}_{\alpha_T<\theta}$	$R^{250,SM}_{\alpha_T}$ $[10^{-6}]$	$R^{300,SM}_{\alpha_T}$ $[10^{-6}]$	$N^{350,SM}_{\alpha_T<\theta}$
≥ 2	$41.1 \pm ^{7.4}_{6.6}$	$33.1 \pm ^{11.1}_{9.1}$	336063 ± 580	$24.7 \pm ^{6.0}_{5.1}$	$26.8 \pm ^{10.1}_{8.0}$	315312 ± 562

7.1.6 Systematic studies

As shown already, when scaling the jet p_T thresholds, the kinematic properties of the signal region are to a good approximation preserved in the lower H_T control regions. This largely negates any contribution to systematic uncertainty due to differing kinematics in each of the control regions. Also, any systematic effects, such as jet mis-measurement or identification, that may occur in the signal region will also affect the control regions. Thus, to a good approximation, these systematic effects are already accounted for in the method. Therefore, in the absences of significant QCD contributions to the ratio, the H_T scaling method is expected to

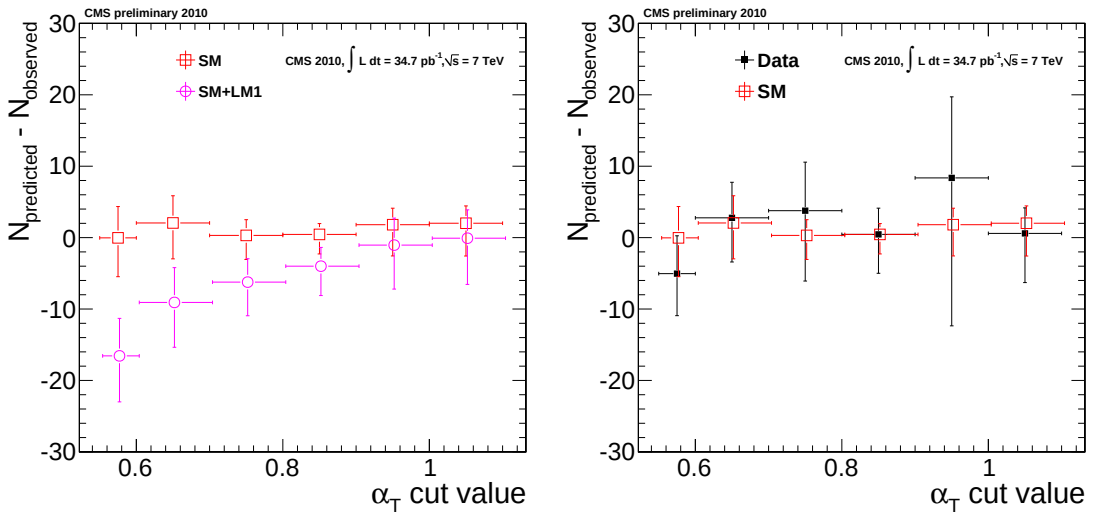

(a) Monte-Carlo closure test. (b) Comparison of data and simulation.

Figure 21: The difference in the number of events predicted by the method and observed as a function of the α_T cut value. (a) A Monte-Carlo closure test, showing expected behaviour for SM processes, with and without the addition of a SUSY LM1 signal. (b) Comparison of data with SM expectation, as also shown in Fig (a). (Markers are artificially offset for clarity.)

provide an estimate of the remaining SM backgrounds with real $\not\!\!E_T$. In the following sections we discuss additional cross checks and systematic studies in support of this expectation.

7.1.7 Closure in the Monte Carlo and comparison with data

Using a full Monte-Carlo detector simulation, a consistent closure test was carried out in order to establish that the method provides an unbiased estimator of the number of total SM background events surviving all in cuts in the signal region. The result of this test is displayed in Fig. 21(a), which shows the difference between the number of predicted and observed events as a function of the α_T cut value. The Monte Carlo closure test is within errors distributed around $N_{\text{predicted}} - N_{\text{observed}} = 0$, demonstrating that at least for the Monte Carlo the method provides a good estimator of the measured number of background events after all cuts. When adding signal (LM1) to Monte Carlo sample, a clear under prediction is observed showing that in the presence of significant signal contamination this method would be a good indicator to establish a deviation from the SM hypothesis without first measuring the individual background components. As can be seen from Fig. 21(b), $N_{\text{predicted}} - N_{\text{observed}}$ measured in data is compatible with zero and therefore indicates that no significant deviation from the SM hypothesis is observed.

7.1.8 Variation of EWK background in the Monte Carlo

Although the method closes in the Monte Carlo it is important to check the assumption of the double ratio scaling behaviour of R_{α_T} as a function of H_T, i.e. the independence of R_{α_T} on H_T, which is used when extrapolating into the signal region. After all cuts, the numerator of R_{α_T} is dominated by EWK processes with real $\not\!\!E_T$. Figure 22(a) shows the behaviour of R_{α_T} as a function of H_T for each of the individual background processes ($W^{\pm}$+jets, $Z^0 \rightarrow \nu\nu$+jets, $t\bar{t}$) and their total, in the absence of QCD events passing the α_T cut. All the plots have been normalised to the same effective cross-section in the signal region, so that the shapes can be compared

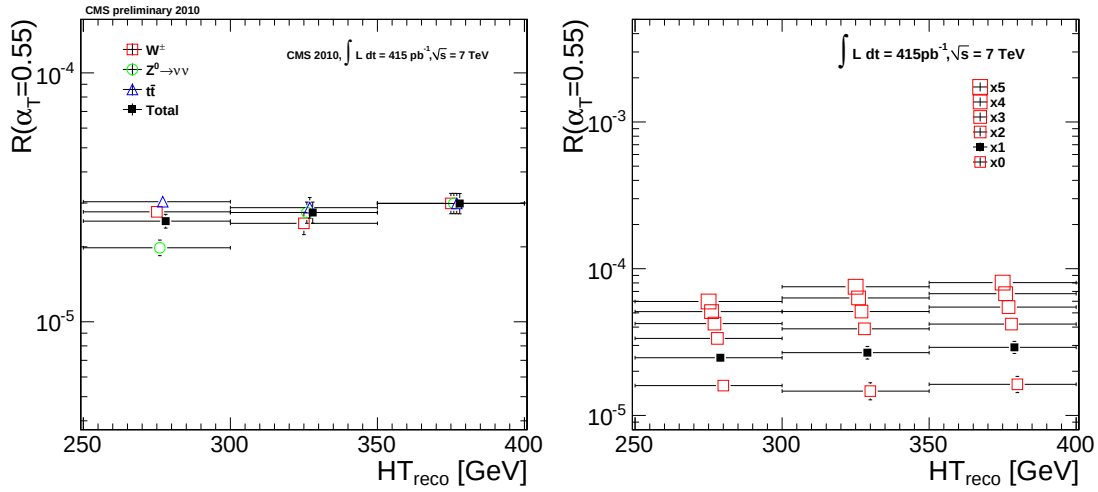

(a) R_{α_T} versus H_T for SM processes with real $\not{E}_T$. (b) R_{α_T} versus H_T when varying $t\bar{t}$ contribution.

Figure 22: (a) The behaviour of R_{α_T} as a function of H_T for each of the individual background processes $W^{\pm}$+jets, $Z^0 \to \nu\nu$+jets, $t\bar{t}$ and their total, in the absence of QCD events passing the α_T cut. (b) Dependence of R_{α_T} on H_T for the sum of the three processes above and the effect of varying the $t\bar{t}$ component only, after an α_T cut value of 0.55. (Markers are artificially offset for clarity.)

easily. The shapes are essentially flat and the ratio, R_{α_T}, in the 250 GeV $< H_T \leq$ 300 GeV bin differs at most by 20% relative to the total.

Given the very weak dependence of R_{α_T} on H_T, a stress test was devised to see the effect of drastically varying the composition of the SM background. This was done by effectively scaling the cross-sections of each of the $W^{\pm}$+jets, $Z^0 \to \nu\nu$+jets and $t\bar{t}$ processes in turn.[1] The cross-sections of each of the backgrounds under consideration were varied very conservatively by $\pm$100%, +200%, +300%, +400% and +500%. The extrapolation into the signal region was then repeated for each of the various mixtures. Figure 22(b) shows the dependence of R_{α_T} on H_T for the sum of the three processes above and the effect of varying the $t\bar{t}$ component only, after an α_T cut value of 0.55. While the absolute values of R_{α_T} change by as much as $\sim$ 250% relative to the nominal value, the shape of the R_{α_T} distribution versus H_T is largely unaffected. The same behaviour is observed when varying the $W^{\pm}$+jets and $Z^0 \to \nu\nu$+jets processes. This is highlighted by Fig. 23, which shows the difference in the number of events predicted for each different background composition and the corresponding number of events observed in the signal region, $N_{\text{predicted}} - N_{\text{observed}}$. The spread of the distribution is 11% and the bias of 1% is consistent with zero when considering the statical uncertainties associated with the predicted and observed numbers.

Therefore, even after varying drastically the composition of the individual EWK components, no significant bias in the number of predicted events is observed in the Monte Carlo, suggesting that the method is very robust against the composition of the total EWK background.

[1] QCD was not considered here, as the number of events passing $\alpha_T > 0.55$ is negligible.

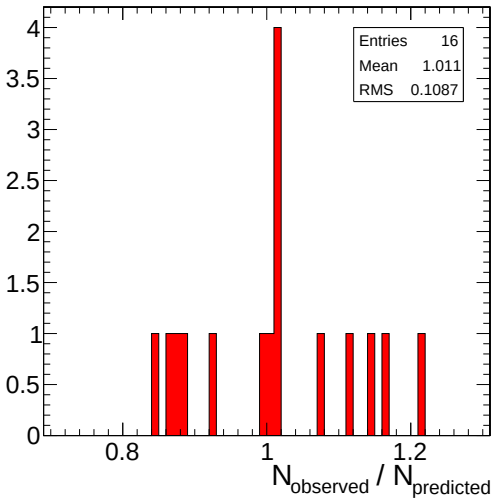

Figure 23: The difference in the number of predicted and observed events, $N_{\text{predicted}} - N_{\text{observed}}$, for different mixtures of SM backgrounds.

7.1.9 Validation of the constant R_R expectation, when dominated by SM processes with real $\not{E}_T$, with data

The observed constant behaviour of R_{α_T} with H_T can also be validated in data using the EWK estimate defined in section Sec. 7.2. This method uses a muon control sample measured in data to predict the remaining background of $W^{\pm}$+jets, $Z^0 \rightarrow \nu\nu$+jets and $t\bar{t}$ (Table 15). Based on these estimates, for these processes with real $\not{E}_T$, the ratio R_{α_T} can be calculated by dividing the EWK estimates for the different H_T bins by the corresponding number of events failing all cuts. Table 10 lists the number of EWK events predicted by the muon control sample to survive all cuts, the number of events measured in data failing all cuts, as well as the corresponding ratio, $R^{\text{data}}_{\text{all cuts}}$, for the three H_T bins. Also listed are the predictions of the ratio, $R^{\text{SM}}_{\text{all cuts}}$, from Monte-Carlo for the remaining EWK background.

While overall the ratios measured in data are approximately 30% higher than in the Monte Carlo, the ratio is constant with H_T within errors and therefore confirms the expectation from Monte Carlo that R_{α_T} is flat as a function of H_T after all cuts. Therefore, the assumed H_T scaling behaviour is expected to predict an unbiased estimator of the R_{α_T} in the signal regions when SM processes with real $\not{E}_T$ dominate the numerator of the ratio.

Table 10: Validation of the scaling law with measurements from data of R_{α_T} in the control regions using a muon control sample.

H_T	$N^{\text{data}}_{\text{all cuts}}$	$N^{\text{data}}_{\text{all cuts}}$	$R^{\text{data}}_{\text{all cuts}}$ $[10^{-5}]$	$N^{\text{MC}}_{\text{all cuts}}$	$N^{\text{MC}}_{\text{all cuts}}$	$R^{\text{MC}}_{\text{all cuts}}$ $[10^{-5}]$
250	$29.1 \pm {}^{6.7}_{8.7}$	851177 ± 923	$3.9 \pm {}^{0.9}_{1.2}$	16.9 ± 1.2	810613 ± 900	$2.4 \pm {}^{0.6}_{0.5}$
300	$9.3 \pm {}^{5.2}_{3.3}$	332284 ± 576	$3.2 \pm {}^{1.8}_{1.1}$	7.0 ± 0.8	316844 ± 563	$2.6 \pm {}^{1.0}_{0.8}$
350	$11.0 \pm {}^{6.0}_{4.8}$	336063 ± 580	$3.3 \pm {}^{1.8}_{1.4}$	7.5 ± 0.8	315312 ± 562	$2.4 \pm {}^{1.1}_{0.9}$

7.1.10 Cross-checks using alternative methods

We present here two alternative methods for predicting the SM backgrounds in the signal region as an independent cross-check to the double ratio scaling.

In the first case, the background prediction is based on the measurement of $R^{300}_{\alpha_T}$ from data in the control region 300 GeV $< H_T \leq$ 350 GeV. A small correction from Monte Carlo is then used to extrapolate into the signal region:

$$R^{350,\text{pred}}_{\alpha_T} = \frac{R^{350,\text{MC}}_{\alpha_T}}{R^{300,\text{MC}}_{\alpha_T}} \cdot R^{300,\text{meas}}_{\alpha_T} \tag{12}$$

where $R^{350,\text{pred}}_{\alpha_T}$ is the prediction for the signal region. No assumption on the functional form of R_{α_T} is made in this case and the method relies purely on Monte Carlo to extrapolate to the signal region. Again, the ratio then multiplied with the number of events observed to fail the α_T cut in the signal region, $N^{350,\text{meas}}_{\theta<\alpha_T}$, to obtain an estimate of the number of events from SM backgrounds that satisfy $\alpha_T > \theta$:

$$N^{350,\text{pred}}_{\theta>\alpha_T} = N^{350,\text{meas}}_{\theta<\alpha_T} \cdot \frac{R^{350,\text{MC}}_{\alpha_T}}{R^{300,\text{MC}}_{\alpha_T}} \cdot R^{300,\text{meas}}_{\alpha_T} \tag{13}$$

Figure 24(a) shows the difference between the number of events predicted and observed in the signal region as a function of the α_T cut value, for data and also for the sum of SM processes and a SUSY LM1 signal.[2] The prediction for data is again consistent with the observation for all cut values of α_T and the expected behaviour is observed when the SUSY LM1 signal is added to the SM backgrounds: negative values reflecting an excess above SM expectation.

For both data and SM+LM1, the MC-based correction used to extrapolate into the signal region encompasses all the SM processes. However, as shown in the previous sections, the contribution from QCD is negligible and the behaviour of R_{α_T} versus H_T for the remaining processes (with real $\not{E}_T$) is essentially flat for an α_T cut of 0.55. Thus, the correction factor, $R^{\text{SM}}_{350/300}$, is close to 1, as shown in Table 11. For comparison purposes only, the same ratios measured from data and for SM+LM1 are also shown. Again, there is good agreement between predicted and observed numbers of events in the signal region for data.

Table 11: Predicted and measured yields for data and simulated SM, QCD and LM1 processes for $H_T \geq 350$ and a cut value $\alpha_T = 0.55$. Only statistical uncertainties are listed.

N_{jet}	$R^{\text{SM}}_{350/300}$	$R^{\text{data}}_{350/300}$	$R^{\text{SM+LM1}}_{350/300}$	$N^{\text{data}}_{predicted}$	$N^{\text{data}}_{observed}$	$N^{\text{SM+LM1}}_{predicted}$	$N^{\text{SM+LM1}}_{observed}$
2	$1.1 \pm ^{0.3}_{0.3}$	$1.5 \pm ^{1.2}_{0.9}$	$3.2 \pm ^{2.1}_{1.5}$	$3.8 \pm ^{2.5}_{1.9}$	5 ± 2.2	$3.5 \pm ^{2.2}_{1.5}$	9.8 ± 0.5
$\geq$3	$1.0 \pm ^{0.2}_{0.2}$	$1.1 \pm ^{0.6}_{0.5}$	$2.7 \pm ^{1.5}_{1.1}$	$8.5 \pm ^{4.0}_{3.2}$	9 ± 3	$7.1 \pm ^{3.6}_{2.8}$	18.6 ± 0.7
$\geq$2	$1.1 \pm ^{0.2}_{0.1}$	$1.3 \pm ^{0.6}_{0.5}$	$2.9 \pm ^{1.1}_{0.9}$	$12.0 \pm ^{4.4}_{3.7}$	14 ± 3.7	$10.6 \pm ^{4.0}_{3.2}$	28.5 ± 0.9

The correction taken from Monte-Carlo has a systematic uncertainty associated with it, which can be estimated by repeating the same method reported earlier of varying the effective cross-section of the individual background components by $\pm$100%, +200%, +300%, +400% and

[2] Again, the cleaning cuts ΔR_{ECAL} and $R_{\not{H}_T/\not{E}_T}$ are applied after the α_T cut.

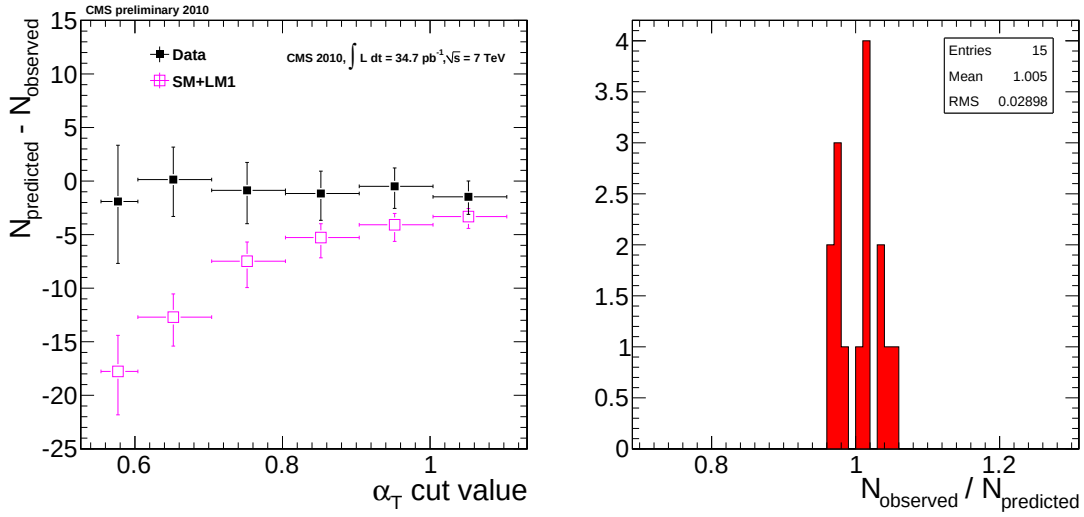

(a) (b)

Figure 24: (a) The difference in the number of events predicted and observed for data and SM+LM1, as a function of the α_T cut value. (b) The difference in the number of predicted and observed events for different background compositions.

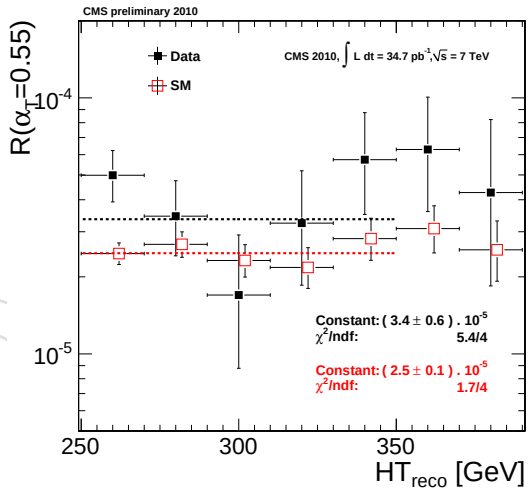

Figure 25: The behaviour of R_{α_T} as a function of HT with scaled jet p_T thresholds and an α_T cut value of 0.55 for events with $N_{jet} \geq 2$. The five bins within 250 GeV $\geq HT <$ 350 GeV are used by a fitting procedure that assumes flat behaviour. (Markers are artificially offset for clarity.)

+500%. Figure 24(b) shows the difference in the number of events predicted for each different background composition and the corresponding number of events observed in the signal region, $N_{predicted} - N_{observed}$. The spread of the distribution is 3% and the bias is negligible.

A further cross-check can be made by assuming a flat behaviour for R_{α_T} as a function of H_T and fitting in the control regions to predict the number of events in the signal region. Figure 25 shows the behaviour of R_{α_T} as a function of H_T with scaled jet p_T thresholds and an α_T cut value of 0.55 for events with $N_{jet} \geq 2$ (i.e., the fully inclusive sample, which corresponds to the sum of Fig. 18(c) and Fig. 18(d)). The five bins within 250 GeV $\leq H_T <$ 350 GeV are used

Table 12: Values of the variables used in Equ. 11 to give a prediction for data and SM backgrounds with $\alpha_T > 0.55$. Only statistical uncertainties are listed.

Sample	$R_{\alpha_T}^{\text{fit,meas}}$ $[10^{-5}]$	$N_{\alpha_T<\theta}^{350,\text{meas}}$	$N_{\text{predicted}}^{350}$	$N_{\text{observed}}^{350}$
Data	3.4 ± 0.6	336063 ± 580	11.4 ± 2.0	14 ± 3.7
SM	2.5 ± 0.1	315312 ± 562	7.9 ± 0.4	9.2 ± 0.9

by a fitting procedure that assumes flat behaviour. The fit results are summarized in Table 12, along with a prediction for the signal region, given by multiplying the value from the fit by the number of events failing the α_T cut in the signal region, $N_{\alpha_T<\theta}^{350,\text{meas}}$, measured from data. Again, the prediction agrees well with observed.

7.1.11 Summary

Using this data-driven method, we predict the total number of background events in the signal region defined by $H_T > 350$ GeV and $\alpha_T > 0.55$ to be $9.0 \pm^{4.5}_{3.8}$ (*stat*). Various cross-checks and systematic studies have been performed without revealing any significant bias in the measurement, primarily due to its data-driven nature. For that reason, we do not assign a systematic uncertainty to this measurement.

A second independent method, that uses a small correction from Monte Carlo, provides a cross-check that gives $12.0 \pm^{4.4}_{3.7}$ (*stat*) ± 0.4 (*sys*). A third method, based on the assumption of R_{α_T} being independent of H_T (i.e., flat) when being EWK-dominated gives 11.4 ± 2.0 (*stat*).

All methods are based on scaling the jet p_T thresholds in the lower H_T control regions and their results agree within the errors. Furthermore, all methods have been shown in the MC to provide an unbiased estimator of the number of total background events after all cuts.

For the final result, we choose the first method, which relies entirely on properties measured in the data (i.e., the ratios), and describes both the QCD-dominated and EWK-dominated H_T scaling behaviours. Alternatively, we could have also adopted a more aggressive approach that explicitly relies on the assumption of flat behaviour of R_{α_T} for the EWK-dominated environment when extrapolating into the signal region.

7.2 Estimating EWK backgrounds using high-p_T W+jets events

In order to estimate the background from high-p_T W bosons we explicitly select W bosons decaying to a muon and neutrino in the phase-space region of the signal, i.e. $H_T > 350$ GeV. These leptonically-decaying W bosons constitute a control sample with which we estimate the number of expected events in the hadronic signal region.

7.2.1 W Selection and validation

All cuts on jet-based quantities are equivalent to those used in the cut flow in the search region. For the muon ID and kinematic cuts we use the recommendations of the $t\bar{t}$ group. The requirements applied are:

- number of valid tracker hits > 11
- identified as global and tracker muon
- transverse impact parameter with respect to beam spot < 2 mm

Table 13: The expected and observed numbers of events for 35pb^{-1} in the muon control sample selection for three different H_T thresholds. A muon-enriched Pythia MC sample was used for the lower H_T bins.

Selection cut	data	SM	W+jets	$t\bar{t}$	Z+jets	QCD
HT250 selection	134	135.5 $\pm$ 3.2	78.0$\pm$2.9	54.7$\pm$1.1	2.6$\pm$0.5	0.0$\pm$0.0
HT250+ $\alpha_T > 0.55$	32	29.2$\pm$ 1.4	14.7$\pm$ 1.3	14.4 $\pm$ 0.6	0.1 $\pm$0.1	0.0$\pm$0.0
HT250+ $\alpha_T^{leptonic} > 0.55$	8	6.6$\pm$ 0.7	2.6$\pm$0.6	3.1$\pm$0.3	0.0 $\pm$0.1	0.0$\pm$0.0
HT300 selection	52	56.7$\pm$2.2	33.0$\pm$1.9	22.3$\pm$ 1.1	1.4 $\pm$ 0.4	0.0 $\pm$ 0.0
HT300+ $\alpha_T > 0.55$	12	11.1	6.4$\pm$0.8	4.7$\pm$0.5	0.0$\pm$0.1	0.0$\pm$0.0
HT300+ $\alpha_T^{leptonic} > 0.55$	3	2.2 $\pm$0.4	1.2 $\pm$ 0.4	1.0 $\pm$0.2	0 $\pm$ 0.1	0.0 $\pm$ 0.0
HT350 selection	25	29.4$\pm$1.5	17.5$\pm$1.4	11.0$\pm$0.3	0.9 $\pm$0.3	0.0 $\pm$0.0
HT350 + $\alpha_T > 0.55$	7	5.9$\pm$0.6	3.4$\pm$0.6	2.5$\pm$0.2	0.0 $\pm$0.1	0.0 $\pm$0.0
HT350 + $\alpha_T^{leptonic} > 0.55$	3	1$\pm$0.3	0.7$\pm$0.3	0.4$\pm$0.1	0.0 $\pm$0.1	0.0 $\pm$0.0

- χ^2/ndof of global muon fit < 10
- number of valid hits in the muon chambers used in the global fit > 0
- $|\eta| < 2.1$
- $P_T^{\mu} > 20$ GeV
- $M_T > 30$ GeV, with M_T the transverse mass of the W candidate, using the transverse missing energy computed with particle flow
- ΔR(jet,muon) > 0.5
- $\not{H}_T > 140$ GeV. This is a cut on $P_T(W)$, since for a W+jet event the W boson P_T is given by the quantity $\not{H}_T$
- no second global muon $P_T^{\mu} > 10$ GeV, $|\eta| < 2.5$, and combined isolation < 0.2 (reduces Z$\rightarrow \mu\mu$)

The $\not{H}_T > 140$ GeV requirement is introduced in order to confine the analysis to W bosons which can pass the α_T cut. This results in a significant loss of statistics, and for this reason we also consider lower thresholds on H_T and the jet P_T. For this purpose we utilize the HT300 and HT250 selections, for which the jet thresholds and the cut on the transverse momentum of the second jet are scaled, as described in Table 7.1. The $\not{H}_T$ cut has been accordingly adapted to $\not{H}_T > 120$ GeV for HT300 and to $\not{H}_T > 100$ GeV for the HT250 selection. The trigger efficiency for the HT250 sample can be seen in Table **??**, only a single event out of 104 events failed the HT150U trigger. The estimated trigger efficiency for the scaled jet thresholds is $> 95\%$ at $H_T \approx 250$ GeV. Moreover, only $\approx 1/4$ of the data was taken at a time were we relied on using the HTU150. Therefore, the overall trigger efficiency inefficiency is small, and we thus neglect it in the following.

The event yields in the data and in the MC, for the three different H_T regions, are listed in Table 13. We observe very good agreement between data and MC both before and after the α_T cut. This agreement is maintained also after an $\alpha_T^{leptonic}$ cut, in which the muon is treated as a jet in the α_T calculation.

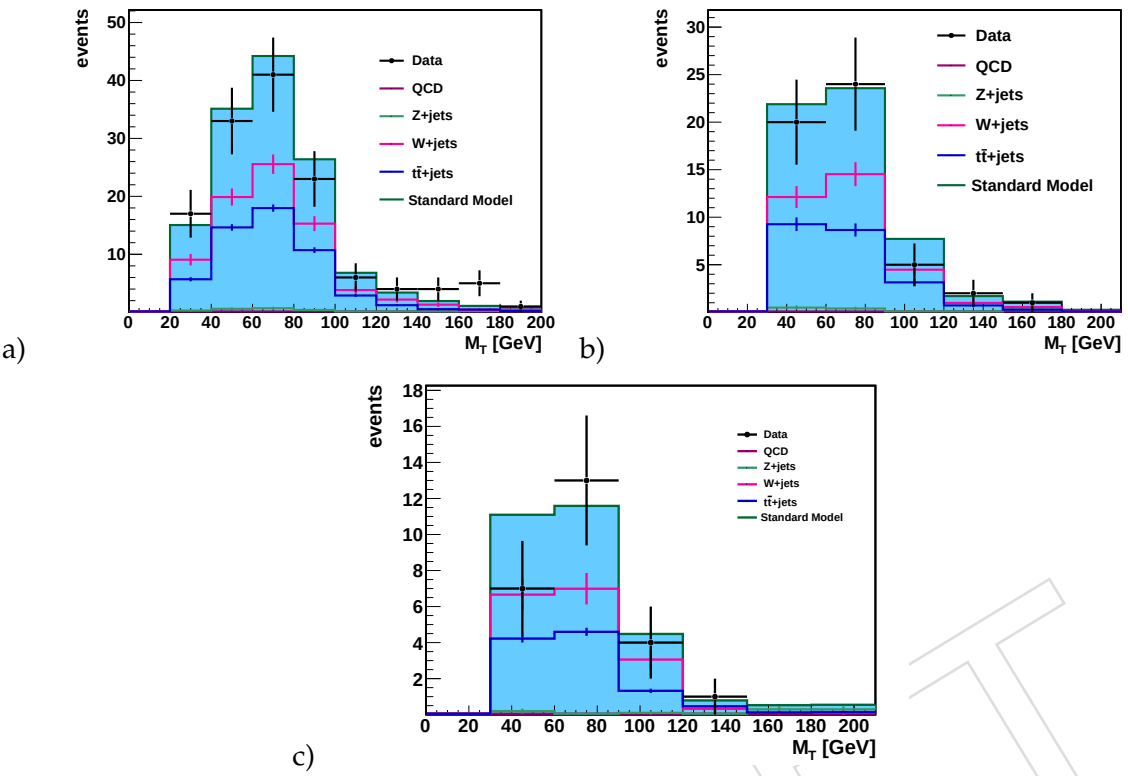

Figure 26: Transverse mass for HT selection a) HT250, b) HT300, and c) HT350

The transverse mass distribution of the samples, shown in Fig. 26, indicates that indeed the sample is dominated by W bosons. The jet-multiplicities, shown in Fig. 27, are also reproduced well by the MC. Altogether these control plots confirm that the combined W signal from W+jet and $t\bar{t}$ production is quite clean and that it is modeled well, as observed also in other studies [22]. The α_T distribution also shows good agreement between data and MC as can be seen in Fig. 28.

7.2.2 Background estimation procedure

In order to estimate the background from W+jet events in the hadronic channel, W^{had}_{data}, from the number of events in the muon sample (W^{μ}_{data}), we need the expected relative ratio of these two types of events. We take the value of this ratio from the Monte Carlo, and thus the estimated number of W events passing the hadronic selection in the data is given by

$$W^{had}_{data} = W^{\mu}_{data} \frac{W^{had}_{MC}}{W^{\mu}_{MC}}$$

The actual values of $\frac{W^{had}_{MC}}{W^{\mu}_{MC}}$ is 0.86. A detailed list of Monte Carlo issues which affect this estimation can be found in Appendix C.

A variant of this method is to require $\alpha_T > 0.55$ before calculating the ratio $W^{had}_{MC}/W^{\mu}_{MC}$. In this case, the α_T parameter is computed ignoring the muon in the event. The advantage of including the α_T cut is that it reduces the dependence of the estimated background on the modeling of α_T in the Monte Carlo, albeit at the price of a reduced control sample: as can be seen from Table 13, the $\alpha_T > 0.55$ requirement has an efficiency of $\approx 20\%$ on the EWK processes. To counter this, we consider this ratio in lower H_T regions as well.

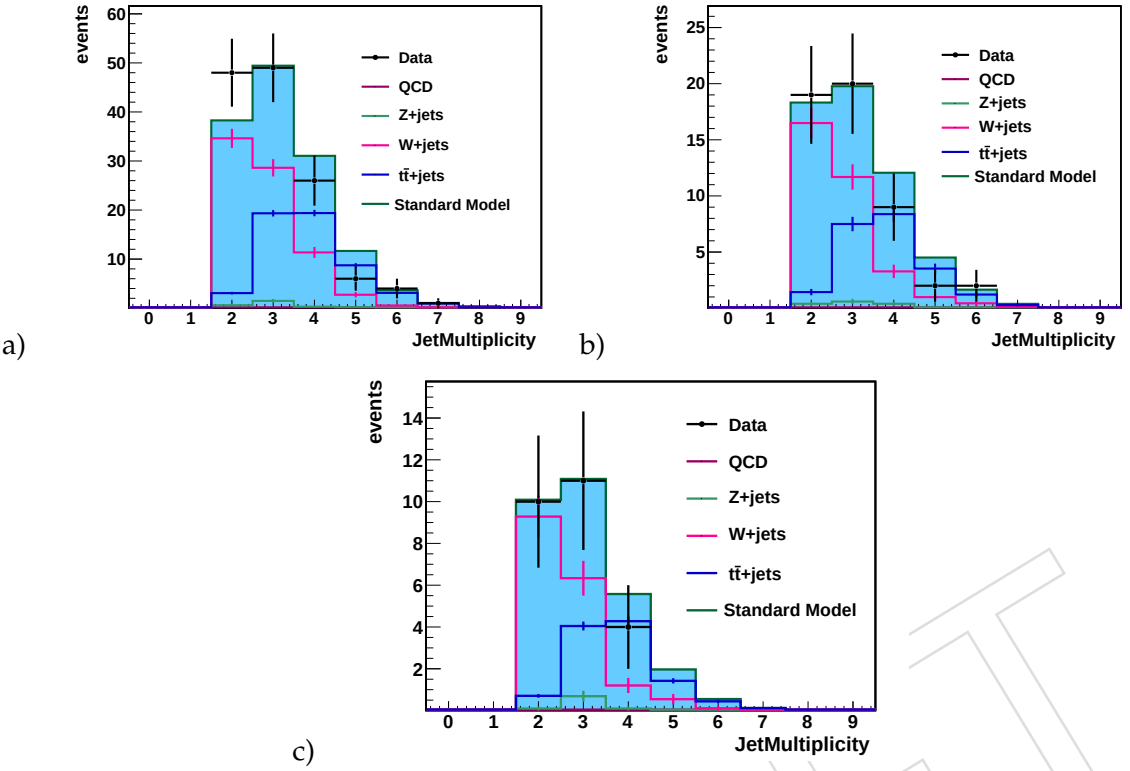

Figure 27: Jet multiplicity for HT selection a) HT250, b) HT300, and c) HT350

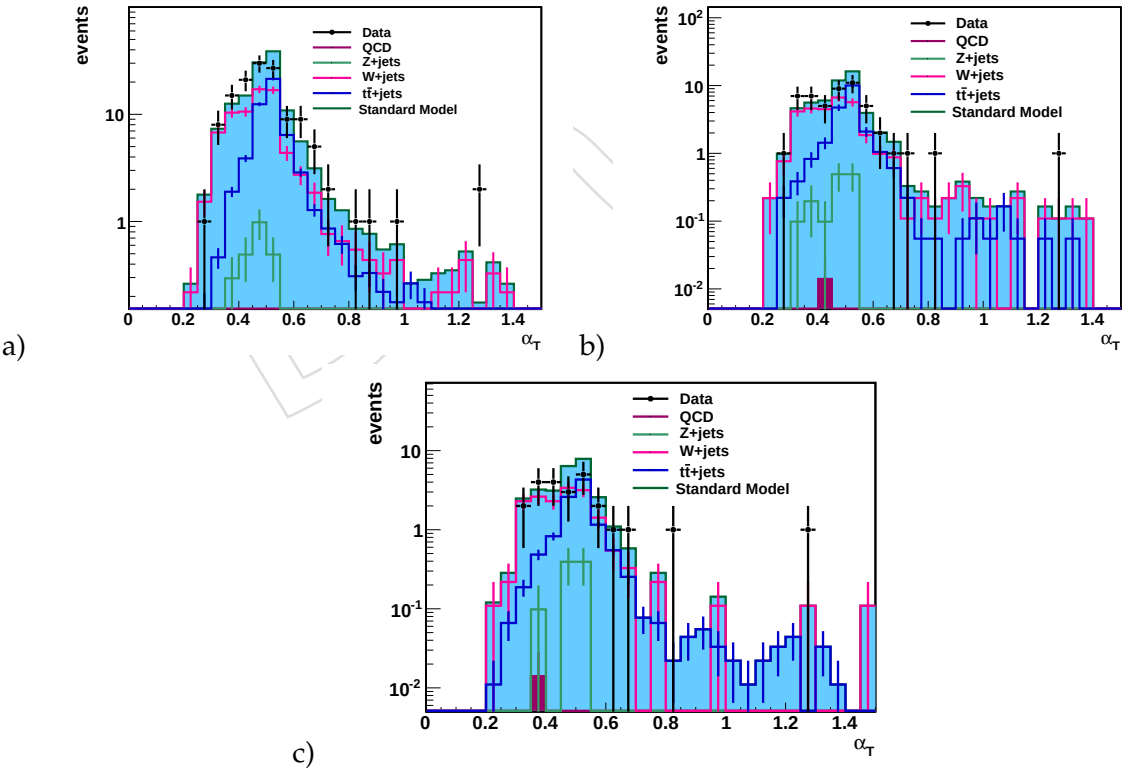

Figure 28: α_T for selection a) HT250, b) HT300, and c) HT350

In what follows we present both variants of the background estimation method, i.e. both with and without the α_T cut.

7.2.3 Systematic Uncertainties

Since the ratio W^{had}/W^{μ} is taken from the Monte Carlo we conservatively assign large uncertainties on all the parameters which affect this ratio.

- $\frac{1}{a\times\epsilon}$: 6.1%. In the W and Z cross section measurements, which are dominated by lower H_T values, the difference between MC and data is less than 1.5 % [23]. The corresponding figure from the $t\bar{t}$ cross section measurement is 6.1% [24]. We assign the latter figure (despite being an overestimate given the W fraction).
- The probability of the lepton veto missing a W decay, p, is discussed in more detail in the Appendix C. Varying all the input parameters which affect p (6.1% on the lepton acceptance and efficiency, 7% on tau-jet modeling, 100% on the lepton reconstruction inefficiency and 50% on the relative fraction of $t\bar{t} \to \tau\tau$ to the total number of boosted Ws) we estimate an uncertainty of 33%.
- The fraction of EWK events (i.e. due to W and $t\bar{t}$ production) in the control sample, $f_W + f_{tt}$: we estimate an uncertainty of 3%. The combination of the tight muon selection, along with the kinematic requirements ($M_T > 30$, $\Delta R(\mu, \text{jet}) > 0.5$ and $\not{H}_T > 140$ GeV cut reduces the QCD background to negligible levels. Even if the expected QCD background is assigned an uncertainty of 200%, the resulting effect on $f_W + f_{tt}$ is $< 3\%$.
- $\epsilon(\alpha_T)$, lower-H_T regions show good modeling of $\epsilon(\alpha_T)$ within the statistics of the comparison which has an uncertainty of 25%. We thus assign a 25% uncertainty on this parameter. In the region $250 < H_T < 350$ GeV, 25 out of 109 data events have $\alpha_T > 0.55$; this agrees, within the statistical uncertainty of 17%, with the ratio from the MC. No significant dependence on α_T is expected; nevertheless, to err on the conservative side we assign twice the precision of the measurement in the lower H_T region to the higher H_T region, yielding 34%.

If the α_T cut is applied, the majority of the systematic uncertainty on the efficiency of the $\alpha_T > 0.55$ requirement is removed. This yields an uncertainty of 30% for the combined W+jet and $t\bar{t}$ backgrounds.

The muon control sample can also be used to obtain an estimate of the background from Z+jets events with $Z \to \nu\bar{\nu}$. For this purpose, the ratio between $t\bar{t}$ and W+jet as well as the ratio between W+jet and Z+jet is taken from the generators, for which only a Leading-Order version is available. These processes are generally adequately modeled and therefore a 25% uncertainty on this generator ratio factor is a conservative estimate. The uncertainties on the $Z \to \nu\bar{\nu}$add up to 30%.

For the case where the α_T cut is not applied, the addition, in quadrature, of the uncertainties described yields an estimate of the total systematic uncertainty of 50% for W+jet and $t\bar{t}$ and 40% for Z invisible.

7.2.4 Background estimate for 35 pb^{-1}

The final estimates and uncertainties for the two variants of the background estimation method for 35 pb^{-1} are listed in table 14. The two variants are seen to agree, within the uncertainties, with each other.

Table 14: Estimate of EWK background for 35 pb^{-1} from the W $\rightarrow \mu\nu$sample.

predicted sample	prediction
W and $t\bar{t}$ (with α_T cut)	6.1 $^{+2.8}_{-1.9}$ (stat) $\pm$ 1.8 (syst)
Z invisible (with α_T cut)	4.9 $^{+2.6}_{-1.8}$ (stat) $\pm$ 1.5 (syst)
W and $t\bar{t}$	4.4 $^{x}_{-x}$ (stat) $\pm$ 2.2 (syst)
Z invisible	3.5 $^{x}_{-x}$ (stat) $\pm$1.4 (syst)

Table 15: The numbers of events estimated for the total EWK background (from Z $\rightarrow \nu\bar{\nu}$, $t\bar{t}$ and W+jets) vs the those observed in 35 pb^{-1} for three different H_T selections as in 7.1.

HT region	data	prediction
HT250-300 (with α_t)	35	29.1 $\pm$ 6.7 (stat)$\pm$ 8.7 (syst)
HT300-350 (with α_t)	11	9.3 $^{+5.2}_{-3.3}$ (stat) $\pm$ 3.1 (syst)
HT350 (with α_t)	14	11.0 $^{+5.0}_{-3.5}$ (stat) $\pm$ 3.3 (syst)

7.2.5 Cross-checks of QCD content lower HT regions

Even in the lower H_T regions, the events passing the fully hadronic selection are dominated by the EWK backgrounds. This provides an opportunity to perform the background estimate with higher statistics in a region which is still depleted in signal. Using the variant with the α_T cut, the estimates of the non-QCD background in the different H_T regions are compared to the data in Table 15. The W,Z and $t\bar{t}$ backgrounds are derived using the procedure described above. We used the H_T bins as described in section 7.1 and predicted the non-QCD background for each bin in H_T. In all cases the background estimate agrees, within the uncertainties, with number of events observed.

This demonstrates that even in the lower H_T region there are no backgrounds in addition to those from W, Z and $t\bar{t}$.

7.3 Estimating Z $\rightarrow \nu\bar{\nu}$+ jets background using photon + jets events

Events in which a Z^0 is produced along with jets and decays to a pair of neutrinos is a large source of background. To estimate the number of such events, we select events with a high p_T photon, ignore the photon when computing the kinematic variables, and use Monte Carlo to connect the expected yield of photon + jet events to that of Z $\rightarrow \nu\bar{\nu}$+ jet events:

$$Z^{predicted}_{data;invisible} = \gamma^{measured}_{data} \times MC^{ratio}_{Z\rightarrow\nu\bar{\nu}/\gamma}$$

where $\gamma^{measured}_{data}$ is the number of events in data in the photon control sample. We expect the kinematics of the Z $\rightarrow \nu\bar{\nu}$ events and γ + jet events to be similar, especially when the transverse momentum of the photon exceeds the Z^0 mass. This idea was already developed and described in detail in [25]. The samples for QCD and photon+jet in this section have been generated with madgraph [26].

7.3.1 Selection of photon + jet events

We select events with one photon satisfying the recommendations for isolated photons as described in [27]. The photon ID criteria are:

- $|\eta^{\gamma}| < 1.45$
- application of the criteria listed in table 16
- ΔR(jet, photon) > 1.0
- $P_T^{\gamma} > 100$ GeV
- $\not{H}_{\mathrm{T}} > 140$ GeV

The requirement on P_T^{γ} is applied to reduce the contamination of the control sample from QCD jet production with large mismeasurements and a fake photon, e.g. a π^0. The requirement on $\not{H}_{\mathrm{T}}$ is applied as in the W+jet selection in order to include events which can pass the α_{T} cut. The similarities of events with a photon and with a Z are enhanced at large values of the p_T of the vector boson. In the data, this p_T is measured by $\not{H}_{\mathrm{T}}$, so the requirement on $\not{H}_{\mathrm{T}}$ also increases the similarity between the photon and Z $\rightarrow \nu\bar{\nu}$ samples. We consider two different cut-flows which satisfy these criteria. The event selection for the first cut-flow resembles the hadronic-search criteria for quantities based on jets:

- $P_T^{jet2} > 100$ GeV
- $H_{\mathrm{T}} > 350$ GeV

In the following this cutflow is denoted as "hadronic-signal-like" selection.

For the second cut-flow, the requirements are:

- $P_T^{jet2} > 50$ GeV
- $250 < \mathrm{H_T} < 350$ GeV,

where $\mathrm{H_T}$ and $\not{H}_{\mathrm{T}}$ are calculated from jets alone. The photon is ignored, as are any reconstructed "jets" within $\Delta R < 0.5$ of the photon. In the second cut-flow a larger number of events is selected, the corresponding statistical uncertainty is therefore smaller than for the first cut-flow. This cutflow will be denoted as "lower $\mathrm{H_T}$" selection.

Table 16: Variables and upper thresholds used for photon identification. They correspond to the "tight" requirements in [27].

Variable	Barrel	Endcap
pixel seed	require none	
$\mathrm{Iso_{TRK}}$	0.9 GeV	
$\mathrm{Iso_{ECAL}}$	2.4 GeV	
$\mathrm{Iso_{HCAL}}$	1.0 GeV	
H/E	0.03	
$\sigma_{i\eta i\eta}$	0.01	0.028

The distributions of α_T and N_{jets} are shown in Figures 29 and 30. The green histograms contain MadGraph photon + jet events; the blue histograms contain Madgraph QCD events. A "k-factor" of 1.27 has been applied to the MC samples. The factor was determined by comparing the cross section for Z + jets production calculated at NNLO and at LO [28], thus the same "k-factor" is applied to Z $\rightarrow \nu\bar{\nu}$ and photon plus jets, so that the ratio between them is the same as in LO (which is used for the prediction). The contribution from $t\bar{t}$/W/Z events was found to be negligible. The yields are shown in table 17.

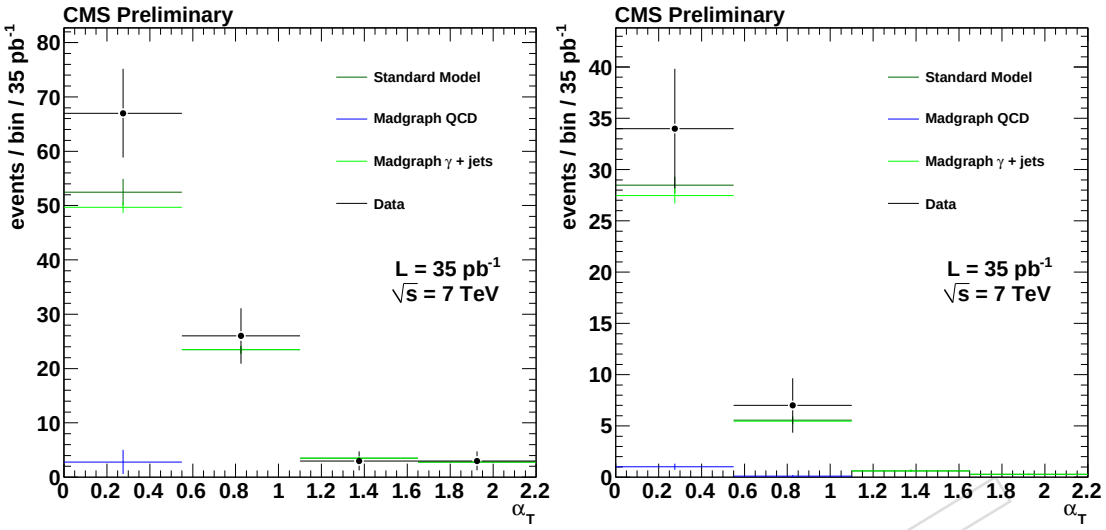

Figure 29: Distribution of α_T for two different selections: lower H_T (left); hadronic-signal-like (right).

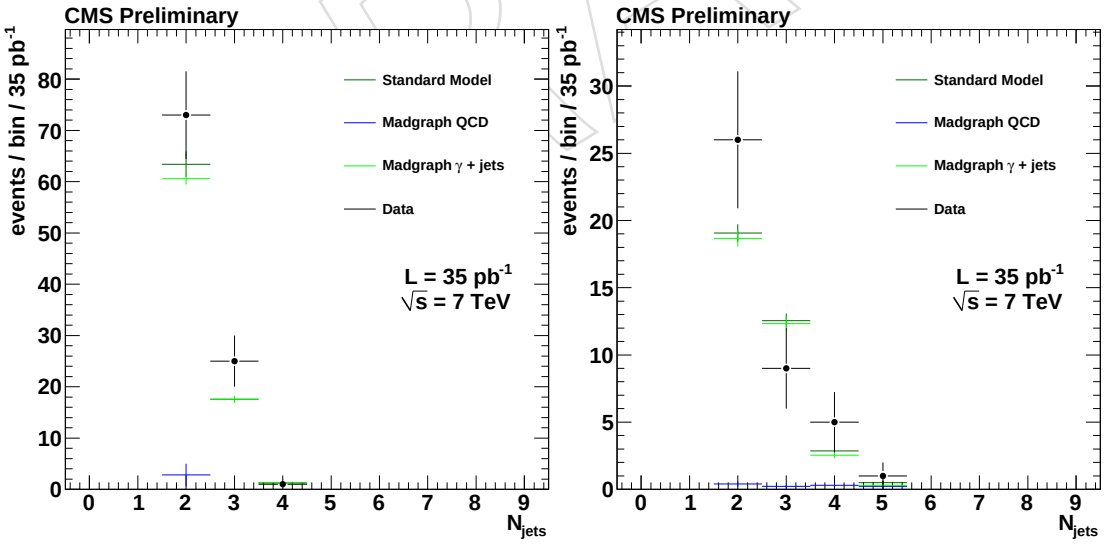

Figure 30: Distribution of N_{jets} for two different selections: lower H_T (left); hadronic-signal-like (right).

Table 17: Expected number of events and observed events for 35 pb^{-1} the photon control sample selection for different HT selections

Selection cut	data	SM	ratio	Selection cut	data	SM	ratio
$250 < H_T < 350$	99	82 ± 3	1.21	$350 < H_T$	41	35.0 ± 0.9	1.17
$N_{jets} = 2$	73	63 ± 2	1.16	$N_{jets} = 2$	26	19.1 ± 0.7	1.36
$N_{jets} >= 3$	26	18.8 ± 0.6	1.38	$N_{jets} >= 3$	15	15.9 ± 0.6	0.94
$+ \alpha_T > 0.55$	32	29.8 ± 0.8	1.07	$+ \alpha_T > 0.55$	7	6.5 ± 0.4	1.08
$N_{jets} = 2$	19	18.8 ± 0.6	1.01	$N_{jets} = 2$	3	2.6 ± 0.2	1.15
$N_{jets} >= 3$	13	10.9 ± 0.5	1.19	$N_{jets} >= 3$	4	3.9 ± 0.3	1.03

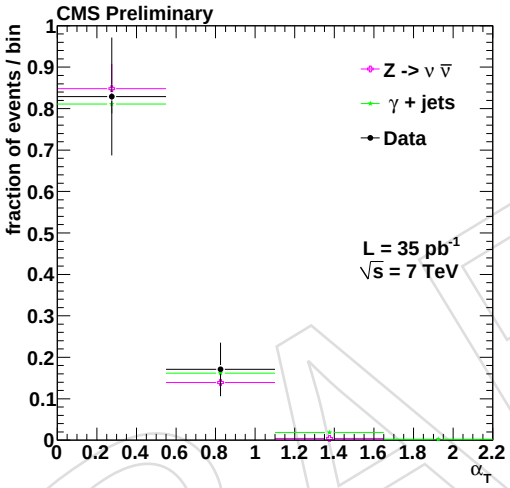

Figure 31: Distribution of α_T for the hadronic-signal-like selection. Each sample is scaled to unit area.

7.3.2 Background estimation procedure

For both sets of selection criteria, the hadronic quantities will resemble closely those of a $Z \rightarrow \nu\bar{\nu}$+ jets event. The distributions of α_T for $Z \rightarrow \nu\bar{\nu}$ and photon + jet events are shown together for the data and Monte Carlo simulation in Fig. 31, for the first cut-flow. The events have been selected as described above, except for the photon requirement, which has been left out for simulated $Z \rightarrow \nu\bar{\nu}$ events. As expected, the α_T efficiencies are similar for $Z \rightarrow \nu\bar{\nu}$ and for photon+jet events.

We express the predicted number of $Z \rightarrow \nu\bar{\nu}$ events in the hadronic signal region, $Z^{had}_{data;inv}$, as

$$Z^{had}_{data;inv} = \frac{Z^{true}_{MC}}{\gamma^{true}_{MC}} \times \frac{P}{a_\gamma \times \epsilon_\gamma} \times \gamma_{data}$$

where:

- Z^{true}_{MC} is the generator truth number of expected $Z \rightarrow \nu\bar{\nu}$ events in the hadronic signal sample.
- γ^{true}_{MC} is the generator truth number of expected γ + jet events in the photon control sample.

Table 18: Left: observed yields in muon low-H_T control sample and expectations from MC for 35 pb^{-1}. Right: predictions for the muon sample using the photon sample.

Selection cut	data	W	$t\bar{t}$	$N_\mu^{pred.by\gamma}$
$250 < H_T < 350$ and $N_{jets} = 2$	30	23.2	3.6	29.9 ± 3.0 stat ± 10.5 syst
+ $\alpha_T > 0.55$	10	6.6	2.0	8.5 ± 1.5 stat ± 2.6 syst

- P is the purity in MC of the sample ($\frac{\gamma+jet}{allevents}$)
- $a \times \epsilon$ is the acceptance times efficiency for photons in such events.
- γ_{data} is number of events in the photon control sample.

7.3.3 Systematic uncertainties

Since the ratio Z^{true}/γ^{true} is taken from the Monte Carlo we conservatively assign large uncertainties on all the parameters which affect this ratio.

- We assign a 30% theoretical uncertainty to the $Z_{MC}^{true}/\gamma_{MC}^{true}$, which we take from MadGraph [29].
- We assign a 5% uncertainty on a, given that photon plus jet are understood processes.
- The recommended IDs and ID variables are validated by tag and probe in [27]. However, given that these tests have been performed at low H_T we assign 20% uncertainty in ϵ; and a 20% uncertainty in P.

The theoretical and systematic uncertainties are added in quadrature, yielding a total systematic uncertainty of 40%.

7.3.4 Background estimate for 35 pb^{-1}

The final prediction is $4.4 \pm^{2.3}_{1.6}$ (stat) $\pm$ 1.8(syst). This agrees within uncertainties with the prediction from the W boson control sample.

7.3.5 Cross-check by predicting W+jets sample, where W $\to \mu\nu$

To check the background estimation procedure, we use the γ+jets sample to predict the jets+$W \to \mu\nu$ sample, with 250 GeV $< H_T <$ 350 GeV and $N_{jets} = 2$.

We estimate $N_\mu^{pred.by\gamma} = W_\mu^{NNLO} \times \frac{\sigma_W^{LO}}{\sigma_W^{NNLO}} \times \frac{N_\gamma^{obs}}{\gamma^{fakeNLO}} \times \frac{\sigma_\gamma^{fakeNLO}}{\sigma_\gamma^{LO}} + t\bar{t}^{NLO}$.

where:

- W_μ^{NNLO} is taken from Table 18 ("W" column).
- $t\bar{t}^{NLO}$ is taken from Table 18 ("$t\bar{t}$" column).
- $\frac{\sigma_W^{LO}}{\sigma_W^{NNLO}}$ = 0.77 [28].
- $\frac{\sigma_\gamma^{fakeNLO}}{\sigma_\gamma^{LO}}$ = 1.27, as mentioned above.
- $\frac{N_\gamma^{obs}}{\gamma^{fakeNLO}}$ is taken from Table 17 ("ratio" column).
- $N_\mu^{pred.by\gamma}$ is shown in Table 18.

We apply the same systematic uncertainty (40%) to the prediction of N_μ that we applied above to the estimate of $Z^{had}_{data;inv}$. The agreement between the numbers of observed muon events and the prediction gives confidence that the systematic errors quoted are not under-estimated.

8 Systematic studies on signal efficiency

8.1 Luminosity uncertainty

The uncertainty on the luminosity measurement propagates directly into an uncertainty on the signal efficiency for any new physics model. At the moment is still 11% [30].

8.2 Jet energy scale uncertainties

Uncertainties in the jet energy scale results in jets falling below or migrating above the jet p_{T} threshold of 50 GeV or the $\mathrm{H_T} > 350\,\mathrm{GeV}$ requirement. To address this, we vary the jet energy scale between $\pm 3 - 5\%$ depending on jet p_{T} and η, according to the results of [15]. The signal yields for LM0-LM5 vary on average by +1.9% and -2.4% when appying the above corrections. As only an overestimate of the signal yield would result in a better limit, we use 2% as a systematic uncertainy on the signal efficiency due to jet energy scale uncertainties. We verified that the effect is of similar size for other signal points.

8.3 Jet energy resolution

As described in Section 4.4.1 the jet energy resolution in the Monte Carlo is found to be better than in the data at the 10-15% level. We therefore increase the jet energy resolution of the MC by 10% in the barrel ($|\eta| < 1.4$) and by 15% in the endcap. This results in about 8% additional gaussian smearing for jets with a p_{T} of 50 GeV, decreasing to about 4.5% for jets with p_{T} of 200 GeV in the barrel. In the endcap this corresponds to $\sim$ 10% additional gaussian smearing for 50 GeV jets, decreasing to $\sim$ 5% for 200 GeV jets.

The variation we apply results in a change in signal yield of $\sim$ 1% for the LM0-LM5 points, and we use this as a systematic uncertainty.

8.4 Uncertainty on lepton and photon veto efficiencies

To define our desired event topology, we reject events with prompt leptons and photons as described in Section 4.3.5. The effect of the individual selections and vetoes are listed in Tables 1 and 2. In general, we observe good agreement between data and the three types of QCD MC (PYTHIA 6, PYTHIA 8 and MadGraph) for each of the vetoes. The largest effect of a single veto is 3% with the maximum difference between any of the four samples being 1.3%. The combined vetoes amount to rejecting at maximum 4.9% of the events where again the maximum difference between any of the four samples is 0.8%. We assign half of the total veto inefficiency, i.e. 2.5% as a systematic uncertainty on the vetoes.

8.5 Influence of the $\not\!\!\mathrm{H_T}/\not\!\!E_T$ modelling

A different modelling of low p_{T} jets between data and MC simulation could result in a different efficiency of the $R_{\not\!\!\mathrm{H_T}/\not\!\!E_T}$ requirement for signal like events in data compared to MC. In practise, this effect is only of relevance for QCD events with typically small $\not\!\!E_T$ and to a much lesser extend for events with real missing energy. As shown in Figure 32 for LM1, the $R_{\not\!\!\mathrm{H_T}/\not\!\!E_T}$ cut has a very high efficiency for events with large $\not\!\!E_T$ and hence additional $\not\!\!E_T$ introduced by, e.g., pile-up would shift the distribution only by a small amount where the $R_{\not\!\!\mathrm{H_T}/\not\!\!E_T}$ cut is practically

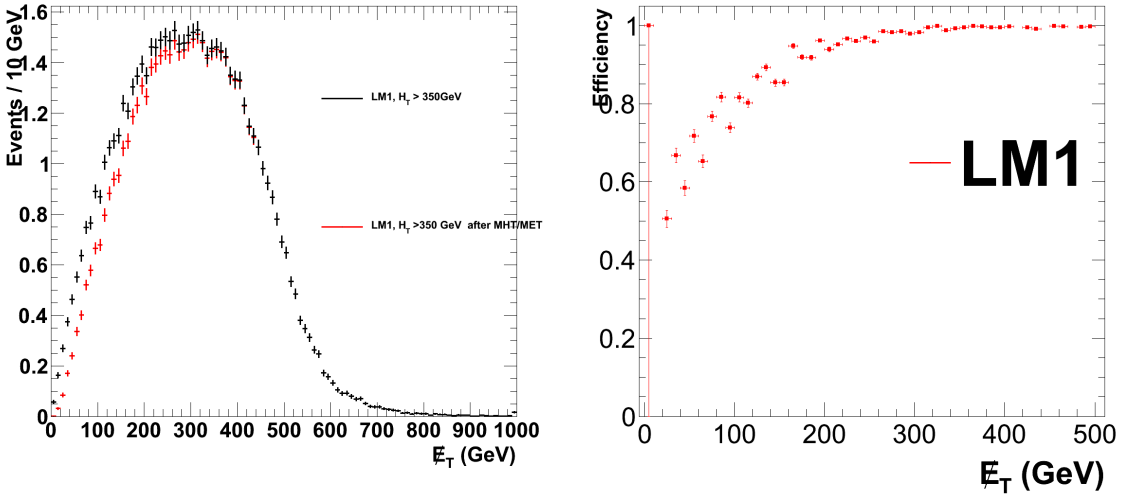

(a) $\not{E}_T$distribution for LM1 before and after the $\not{H}_T/\not{E}_T$¡ 1.25 requirement.

(b) Efficiency of the $R_{\not{H}_T/\not{E}_T}$ cut as a function of $\not{E}_T$.

Figure 32: Effect of the $R_{\not{H}_T/\not{E}_T}$ requirement on signal (before $\alpha_T > 0.55$ requirement).

fully efficient. We observe, that the $R_{\not{H}_T/\not{E}_T} < 1.25$ requirement rejects only a small fraction of the LM1 signal, namely 2.1%. We use the half of the average efficiency loss due to the $R_{\not{H}_T/\not{E}_T}$ requirement on signal points LM0-LM5 of 3% as a systematic uncertainty.

8.6 Veto against jets pointing to dead ECAL crystal regions

The signal efficiency of this cut varies from 94% for the LM1 signal point up to 92% for the LM5 signal point. The mean signal efficiency for the cMSSM points LM1, LM2, LM4 and LM5 is about 92%. The uncertainty on this mean signal efficiency, due to the variations between different points in the CMSSM space, is estimated by the standard deviation for the four studied points. It is about 2%. Another uncertainty on the signal efficiency of this cut is due to the ΔR resolution of the jets which enter into the calculation. For jets with a $p_T > 100$ GeV/c the resolution is about 0.05 [31]. A variation by this 0.05 leads to an additional uncertainty of 2.2% on the mean signal efficiency. To decrease the statistical uncertainty of these numbers the α_T cut has been relaxed to 0.53 for these studies. A comparison with an $\alpha_T > 0.55$ cut shows no significant change of signal efficiency for the two different α_T cuts.

Table 19 gives a summary of the considered systematic uncertainties for the signal efficiency. The total uncertainty is obtained by adding the individual contributions in quadrature.

9 Statistical Interpretation

To quantify which points in a CMSSM parameter-space can be excluded with 95% confidence level the different data-driven background estimations have been combined and interpreted in a statistical manner.

The number of counted events in each of the control samples, i.e. at $\alpha_T < 0.55$, the two low HT regions, both for $\alpha_T > 0.55$ and $\alpha_T < 0.55$, the muon control sample and the photon control sample, are combined in a profile likelihood calculation to extract a confidence interval on the

Table 19: Summary of systematic uncertainties on signal efficiency

Source	Uncertainty
Luminosity	11%
Jet energy corrections	2%
Jet energy resolution	1%
Lepton/photon vetoes	2.5%
$\not{H}_T / \not{E}_T$ modelling	1.5%
dead ECAL veto modelling	3%
Total	12%

number of possible SUSY events in the signal region. The profile likelihoood method is also known as MINOS method in the physics community, and is implemented as MINOS algorithm in the Minuit program [32].

For this profile likelihood calculation a likelihood function has been set up, which describes the complete set of measurements including systematic uncertainties.

The numbers of events in the signal region and for each auxiliary measurement are treated as Poisson distributed:

$$Pois(n|\mu) = \frac{\mu^n}{n!} e^{-\mu}, \tag{14}$$

where μ is the expected number of events and n the observed number of events. The combined likelihood function is the product of these Poisson distributions and of terms which describe the systematic uncertainties.

It can be written as:

$$L_{total} = L_{signal} \cdot L_{muon} \cdot L_{photon} \cdot L_{lowH_T} \tag{15}$$

where:

- L_{signal} is the likelihood of the measurement in the signal-like region

$$L_{signal} = Pois(x|s + b_{tt+W} + b_{Zinv} + b_{QCD}), \tag{16}$$

  x is the number of events measured in the signal-like region, b_{tt+W} is the expected background from $t\bar{t}$ and W events, b_{Zinv} is the expected background from $Z \rightarrow \nu\bar{\nu}$ events and b_{QCD} is the expected background from QCD events.
- L_{muon} is the likelihood of the auxiliary measurement in the muon control sample. It is used to constrain b_{tt+W}.
- L_{photon} is the likelihood of the auxiliary measurement in the photon control sample. It is used to constrain b_{Zinv}.
- L_{lowH_T} is the likelihood of the auxiliary measurements in the low H_T and inverted α_T control regions. These measurements are used to constrain the total background $b = b_{tt+W} + b_{Zinv} + b_{QCD}$.

Table 20 summarizes the number of events measured in each control region.

9.1 Muon and Photon control samples

Both the estimation of the $W + t\bar{t}$ background b_{tt+W} from the muon control sample and the estimation of the $Z \rightarrow \nu\bar{\nu}$ background b_{Zinv} use a measurement of y events in a control sideband

Table 20: Observed number of events for an integrated luminosity of $\mathcal{L} = 35\,\mathrm{pb}^{-1}$ in the signal-like region and the different control regions.

Control Sample	# events measured
Signal-like region	14
Muon control sample (α_T cut applied)	7
Photon control sample (α_T cut applied)	7
$250 < HT < 300$ and $\alpha_T > 0.55$	35
$250 < HT < 300$ and $\alpha_T < 0.55$	851177
$300 < HT < 350$ and $\alpha_T > 0.55$	11
$300 < HT < 350$ and $\alpha_T < 0.55$	332284
$HT > 350$ and $\alpha_T < 0.55$	336063

to estimate a part of the expected background in the signal-like region. The number of expected events in the sideband and the expected background in the signal-like region are connected by a factor of τ. The likelihood functions L_{muon} for the muon and L_{photon} for the photon auxiliary measurement can be written as:

$$\begin{aligned} L_{muon}(y_{muon}|b_{tt+W}) &= Pois(y_{muon}|\tau_{muon} \cdot b_{tt+W}), \\ L_{photon}(y_{photon}|b_{Zinv}) &= Pois(y_{photon}|\tau_{photon} \cdot b_{Zinv}), \end{aligned} \tag{17}$$

if systematic uncertainties on τ_{muon} and τ_{photon} are neglected.

The systematic uncertainties on the estimated values of the $t\bar{t}$ + W and the $Z \to \nu\nu$ background have been discussed in section 7.2 and 7.3. To include these uncertainties the likelihood function for the true value of τ is assumed to follow a gaussian, with a σ that reflects the uncertainty on τ. The likelihood function L_{muon} and L_{photon} can then be written as:

$$\begin{aligned} L_{muon}(y_{muon}, \tau_{nom,muon}|b_{tt+W}, \tau_{muon}) &= Pois(y_{muon}|b_{tt+W} \cdot \tau_{muon}) \cdot Gauss(\tau_{nom,muon}|\tau_{muon}, \sigma_{muon}), \\ L_{photon}(y_{photon}, \tau_{nom,photon}|b_{Zinv}, \tau_{photon}) &= Pois(y_{photon}|b_{Zinv} \cdot \tau_{photon}) \cdot Gauss(\tau_{nom,photon}|\tau_{photon}, \sigma_{photon}), \end{aligned} \tag{18}$$

where τ_{nom} are the values of τ derived from Monte Carlo, as stated in the previous sections.

The factors $\tau_{nom,muon}$ and $\tau_{nom,photon}$ and the systematic uncertainties on τ_{muon} and τ_{photon} are stated in table 21.

Table 21: The factors τ relate the expected numbers of events in the control region to the expected number of background events in the signal-like region. The factor τ_{nom} is an estimate of τ obtained from Monte Carlo studies.

Control Sample	τ_{nom}	systematic uncertainty on τ
Muon control sample (α_T cut applied)	1.2	30%
Photon control sample (α_T cut applied)	1.6	40%

9.2 Low H_T control samples

The method described in section 7.1 is used to estimate the total background b. The low H_T control and the high H_T signal region are related by factors of τ and τ', both are constrained by further measurements at $\alpha_T < 0.55$. The measurements in low and high H_T regions are related

by factors of $\rho\tau$ and $\rho'\tau'$ for the inverted α_T cut. A total of five auxiliary measurements are used in this method.

The corresponding likelihood function, ignoring for the moment systematic uncertainties is:

$$\begin{aligned} L_{lowH_T}(y_1, y_2, y_3, y_4, y_5 | b, \bar{b}, \tau, \tau', \rho, \rho') = & \quad Pois(y_1|\bar{b}) \\ & \cdot Pois(y_2|b\tau\rho)\cdot \quad Pois(y_3|\bar{b}\tau) \\ & \cdot Pois(y_4|b\tau'\rho')\cdot \quad Pois(y_5|\bar{b}\tau'), \end{aligned} \tag{19}$$

where:

- y_1 is the number of events measured at $\alpha_T < 0.55$ and $H_T > 350\,\mathrm{GeV}/c$,
- y_2 is the number of events measured at $\alpha_T > 0.55$ and $300 < H_T < 350\,\mathrm{GeV}/c$,
- y_3 is the number of events measured at $\alpha_T < 0.55$ and $300 < H_T < 350\,\mathrm{GeV}/c$,
- y_4 is the number of events measured at $\alpha_T > 0.55$ and $250 < H_T < 300\,\mathrm{GeV}/c$,
- y_5 is the number of events measured at $\alpha_T < 0.55$ and $250 < H_T < 300\,\mathrm{GeV}/c$,
- $\bar{b}$ is the expected background at $\alpha_T < 0.55$ and $H_T > 350\,\mathrm{GeV}/c$

The assumption of section 7.1 is that, in the absence of signal contamination, the expected number of events in each of these α_T, H_T regions are related by the following equation:

$$f \cdot \frac{\hat{R}_{\alpha_T}(H_T > 350\,\mathrm{GeV}/c)}{\hat{R}_{\alpha_T}(300 < H_T < 350\,\mathrm{GeV}/c)} = \frac{\hat{R}_{\alpha_T}(300 < H_T < 350\,\mathrm{GeV}/c)}{\hat{R}_{\alpha_T}(250 < H_T < 300\,\mathrm{GeV}/c)}, \tag{20}$$

where $\hat{R}_{\alpha_T}$ are the expected values of R_{α_T}. In terms of ρ and ρ', this equation states that $\rho' = f\rho\rho$. The assumption made in method 2 (Sect. 7) is that $f = 1$.

Possible uncertainties on $f = 1$ are estimated by applying systematic variations as described in Sect. 7. The estimated systematic uncertainty is 11%. The likelihood function associated with f is modeled by a gaussian curve with a σ_f that corresponds to the spread observed in Monte Carlo studies after the application of the systematic variations.

$$Gauss(1|f, \sigma_f) \tag{21}$$

The likelihood function corresponding to the background estimation from low H_T regions is the likelihood function of equation (19) multiplied by this gaussian.

9.3 Uncertainty on the signal efficiency and acceptance

The components which contribute most to the uncertainty on the signal efficiency and uncertainty have been discussed in detail in section 8. The total systematic uncertainty on the signal has been estimated to be about 13%.

In order to include this systematic uncertainty into the calculation of the limits, the likelihood function corresponding to the signal acceptance times efficiency is modeled as a gaussian with a σ that corresponds to the before mentioned systematic uncertainty (similar to that in equation 21.

Possible variations of this systematic uncertainty as functions of the CMSSM parameters have not been taken into account. It can however be noted that these systematic uncertainty is expected to decrease with the effective mass range of the CMSSM signal as the signal efficiency of the selection increases with this mass range.

9.4 Signal contamination in auxiliary measurements

The signal contamination of the different control samples varies from point to point in the CMSSM parameter-space. For this reason it has been calculated from Monte Carlo studies for each separate point and fed as a parameter into the full likelihood function. The likelihood function for the auxiliary measurement in the muon control sample changes in this case from equation 18 to:

$$L_{muon}(y_{muon}, \tau_{nom,muon}|b_{tt+W}, \tau_{muon}) = Pois(y_{muon}|b_{tt+W} \cdot \tau_{muon} + s \cdot \tau_S) \cdot Gauss(\tau_{nom,muon}|\tau_{muon}, \sigma_{muon}), \quad (22)$$

where τ_S is the ratio of the expected number of SUSY events in the auxiliary measurement to the number of SUSY events expected in the signal-like region. A further discussion of the results of this contamination can be found in Appendix D .

A profile likelihood fit has been issued for every parameter-set and the resulting 95% CL on the number of signal events has been compared with the corresponding event yields for the specific parameter-set in the signal-like region. The whole program has been set up in the RooStats environment [33]

9.5 Results

Ignoring the signal contamination in each point of the CMSSM parameter-space, the 95% CL exclusion limit can be expressed as a single number, which represents the number of signal events compatible with the measured data.

The background from tt+W+jet events is estimated using the muon control sample. The α_T efficiency is taken from data, i.e. the muon control sample contains only the events after the α_T cut. The background from Z events in which the Z decays into neutrinos is estimated using the photon control sample. The total background (tt+W+$Z \rightarrow \nu\nu$+QCD events) is estimated using the low H_T control region.

The measured upper limit on the number of signal events is 14.8. The p-value of this observation given the null hypothesis of 0 SUSY signal events is 0.3. The measured limit can be compared to the expected limit. For the expected limit the number of events in the signal region is set to the number of background events expected given by the muon and photon control sample estimate ($\approx$ 11 events). The expected limit is 10.8 signal events.

In order to estimate the effect of the inclusion of systematic uncertainties on signal and background, the limit has been calculated once without including these uncertainties and once with. If no systematic uncertainties are taken into account the upper limit improves to 13.4 events.

The analysis has been set up in such a way as to distinguish between dijet events and events with more than two jets. A natural way to include this in the limit setting would be analyze the two channels separately and later to multiply the corresponding probability density functions. Of course to do this properly all correlations which might enter into the background estimations need to be taken into account. Also the systematic uncertainty on the signal multiplicity needs to be included.

In order to estimate if the gain in reach would justify the usage of this somewhat more complex procedure, the upper limit on the number of signal events for the separate treatment of the two channels has been calculated in a simplified way. Instead of using the low H_T control regions

the QCD background contamination has been assumed to be negligible. Only the muon and photon auxiliary measurements are taken into account. The jet multiplicity splitting of the signal events has been assumed to follow the ones predicted for the LM1 CMSSM point, i.e. 37% of all events are dijet events 63% have more than two jets. In this case the upper limit on the number of signal events observed with the measurements would improve from 14.8 to 13.4 events.

9.5.1 Limits on CMSSM

In case that the signal contamination in the control regions is taken into account the exclusion limit can be better expressed as a curve in a m_0 vs. $m_{1/2}$ CMSSM parameter-plane for fixed values of A_0, sign(μ) and tan β. Where μ is the common mass of the scalars at the supersymmetric GUT scale, $m_{1/2}$ is the common gaugino mass, A_0 is the common soft trilinear SUSY breaking paramter, tan β is the ratio of the two Higgs vacuum expectation values, and sign(μ) is the sign of the Higgsino mass parameter. For the CMS sensitivity the chosen values are A_0, tan $\beta = 3$ or 10, and sign(μ) to be positive.

In Fig. 33 the 95% CL for tan $\beta = 10$ is presented as obtained from 35 pb^{-1}, the α_T efficiency for the muon control sample is taken from data.

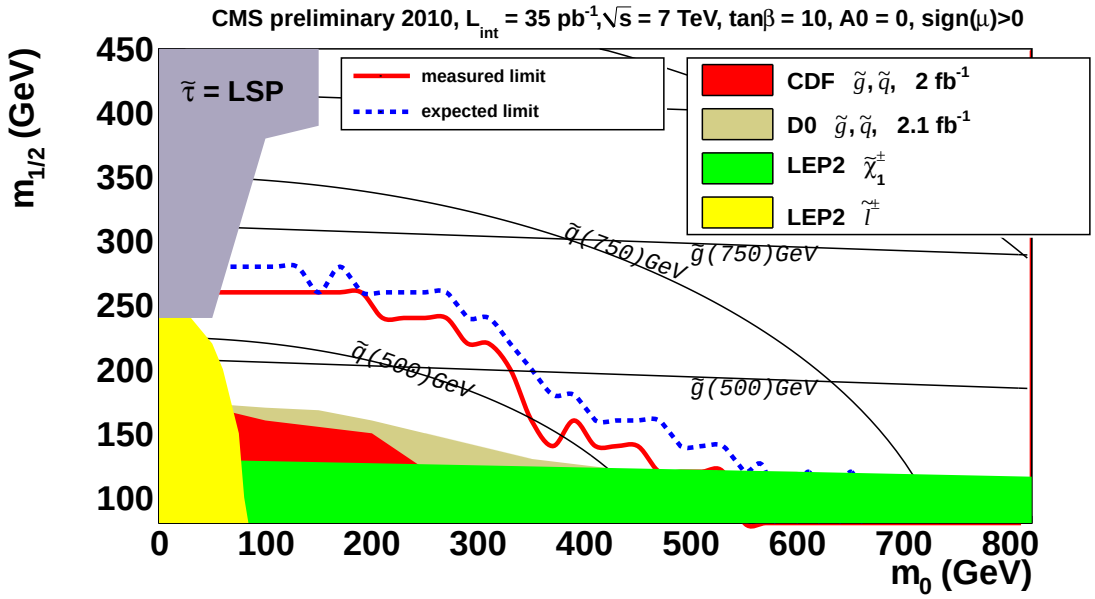

Figure 33: Measured and expected 95% CL exclusion contours in the cMSSM $m_0 - m_{1/2}$ plane (tan $\beta = 10$, $A_0 = 0$, sign$(\mu) > 0$).

The expected limit covers a larger part of the m_0-$m_{1/2}$ plane than the actual measured limit, as the observed number of events is somewhat larger than the number of background events predicted.

The exclusion regions for the CDF [34] measurement shown in figure 33 are defined for tan $\beta = 5$, while those from D0[35] are defined for tan $\beta = 3$. These Tevatron searches are both based on jets + missing tranverse momentum signatures using approximately 2 fb^{-1}. The LEP exclusion regions are based on searches for sleptons and charginos [36]. Preliminary CMS studies of the hadronic channel indicate that its sensitivity is only weakly dependent on the value of tan β.

In Appendix D a discussion of further studies on exclusion limits can be found.

10 Conclusions

We have presented a first study of events with hadronic jets and significant missing energy using the α_T technique. We find the data reflect the behavior expected from Monte Carlo simulations, i.e. that the huge QCD background can be reduced by several orders of magnitude down to a negligible level using a requirement of $\alpha_T > 0.55$. The only remaining backgrounds stem from electro-weak processes, namely W+jet, Z+jet and $t\bar{t}$ production where the weak decays of the vector bosons involve high-momentum neutrinos. We estimate the sum of the backgrounds using a data-driven technique which utilizes events at lower values of H_T. This estimate confirms that the magnitude of the QCD contribution is reduced to negligible levels. Prompted by this observation, we estimate the remaining EWK backgrounds using data and Monte Carlo simulation events with leptonic W+jets decays as well as γ+jets events. We assign large systematic uncertainties to the background predictions, however these uncertainties do not result in a significant deterioration of the physics reach of the analysis due to the smallness of the backgrounds. We observe no excess of events in the data, over the expectations from the Standard Model, and we interpret this lack of events in terms of the CMSSM. With 35 pb^{-1} we already extend significantly the current limits from the Tevatron experiments.

References

[1] CMS Physics Analysis Summary, CMS PAS SUS-09-001.

[2] CMS Physics Analysis Summary, CMS PAS SUS-08-005.

[3] L. Randall and D. Tucker-Smith, "Dijet Searches for Supersymmetry at the LHC", *Phys.Rev.Lett.* **101 221803** (2008).

[4] https://twiki.cern.ch/twiki/bin/view/CMS/SusyPatLayer1DefV9.

[5] See: https://svn.cern.ch/reps/icfsusy/trunk/AnalysisV2/.

[6] See: https://twiki.cern.ch/twiki/bin/viewauth/CMS/ProductionReProcessingSummer10.

[7] CMS Collaboration, "CMS Physics Technical Design Report, Volume II: Physics Performance", *J. Phys. G: Nucl. Part. Phys.* **34** (2007) 995–1579.

[8] M. Cacciari, G. P. Salam, and G. Soyez, "The anti-kt jet clustering algorithm", *JHEP* **0804:063** (2008).

[9] Calorimeter Jet Quality Criteria for the First CMS Collision Data, and preparations for calibrating their efficiencies, CMS AN-2009/087.

[10] CMS Collaboration, "HCAL performance from first collisions data", *CMS Detector Performance Summary* **DPS-2010/025** (2010).

[11] CMS Collaboration, "Measurements of inclusive W and Z cross Sections in pp collisions at 7 TeV", *CMS Note* **2010/116** (2010).

[12] See: https://twiki.cern.ch/twiki/bin/view/CMS/PhotonID.

[13] CMS Collaboration, "Muon reconstruction in the CMS detector", *CMS Note* **2008/097** (2008).

[14] CMS Collaboration, "Muon identification in CMS", *CMS Note* **2008/098** (2008).

[15] CMS Physics Analysis Summary, CMS PAS JME-10-010.

[16] T. Sjöstrand, S. Mrenna, and P. Skands, "PYTHIA 6.4 Physics and Manual; v6.420, tune D6T", *JHEP* **05** (2006) 026, arXiv:hep-ph/0603175.

[17] CMS Analysis Note, CMS-AN 2009/056.

[18] See: https://twiki.cern.ch/twiki/bin/view/CMS/EcalChannelStatus.

[19] CMS Collaboration, "Electromagnetic calorimeter commissioning and first results with 7 TeV data", *CMS Note* **2010/012** (2010).

[20] See: http://cousins.web.cern.ch/cousins/drafts/rhorho_cousins.pdf.

[21] CMS Physics Analysis Summary, CMS PAS SUS-10-001.

[22] CMS Analysis Note, CMS-AN 2010/309.

[23] CMS Analysis Note, CMS AN-2010/264.

[24] CMS Physics Analysis Summary, CMS PAS TOP-10-001.

[25] CMS Physics Analysis Summary, CMS PAS SUS-08-002.

[26] J. Alwall et al., "MadGraph/MadEvent v4: The New Web Generation", *JHEP* **09** (2007) 028, arXiv:0706.2334.

[27] CMS Physics Analysis Summary, CMS PAS EGM-10-006.

[28] K. Melnikov and F. Petriello, "Electroweak gauge boson production at hadron colliders through O(alpha(s)**2)", *Phys. Rev.* **D74** (2006) 114017, arXiv:hep-ph/0609070. doi:10.1103/PhysRevD.74.114017.

[29] L. Dixon, private communication.

[30] CMS Physics Analysis Summary, CMS PAS EWK-10-004.

[31] CMS Physics Analysis Summary, CMS PAS JME-10-003.

[32] F. James, "MINUIT Reference Manual", *CERN Program Library Writeup* **D506**.

[33] C. Moneta, Belasco et al., "The RooStats Project", *Proceedings of Science* (2010).

[34] CDF Collaboration, "the CDF exclusion region in the $m_{1/2}$ vs. m_0 plane", *Phys. Rev. Lett* **102** (2009) 121801, arXiv:011.2512.

[35] D0 Collaboration *Phys. Lett. B* **660** (2008) 449, arXiv:0712.3805.

[36] ALEPH, DELPHI, L3 and OPAL Collaboration *LEPSUSYWG/02-06-2*. http://lepsusy.web.cern.ch/lepsusy.

A Cross sections used for MC samples

Table 22: Cross-section and sample size information for the QCD Monte Carlo samples used in the analysis.

Process	Notes	σ / pb	# events
QCD (Pythia 6)	$\hat{p}_T > 15$ GeV	8.762×10^{8}	6,095,857
	$\hat{p}_T > 30$ GeV	6.041×10^{7}	5,069,664
	$\hat{p}_T > 80$ GeV	9.238×10^{5}	2,065,792
	$\hat{p}_T > 170$ GeV	2.547×10^{4}	3,171,950
	$\hat{p}_T > 300$ GeV	1.256×10^{3}	2,976,108
	$\hat{p}_T > 470$ GeV	8.798×10^{1}	2,159,497
	$\hat{p}_T > 800$ GeV	2.186×10^{0}	2,181,700
	$\hat{p}_T > 1400$ GeV	1.122×10^{-2}	1,185,024
QCD (Pythia 8)	$0 < \hat{p}_T < 15$ GeV	2.117×10^{12}	770,000
	$15 < \hat{p}_T < 20$ GeV	5.638×10^{8}	520,650
	$20 < \hat{p}_T < 30$ GeV	2.264×10^{8}	613,650
	$30 < \hat{p}_T < 50$ GeV	5.018×10^{7}	651,444
	$50 < \hat{p}_T < 80$ GeV	6.035×10^{6}	517,758
	$80 < \hat{p}_T < 120$ GeV	7.519×10^{5}	635,905
	$120 < \hat{p}_T < 170$ GeV	1.120×10^{5}	540,280
	$170 < \hat{p}_T < 230$ GeV	1.994×10^{4}	499,306
	$230 < \hat{p}_T < 300$ GeV	4.123×10^{3}	499,912
	$300 < \hat{p}_T < 380$ GeV	9.593×10^{2}	263,570
	$380 < \hat{p}_T < 470$ GeV	2.434×10^{2}	217,924
	$470 < \hat{p}_T < 600$ GeV	7.410×10^{1}	252,885
	$600 < \hat{p}_T < 800$ GeV	1.657×10^{1}	206,888
	$800 < \hat{p}_T < 1000$ GeV	1.997×10^{0}	163,350
	$1000 < \hat{p}_T < 1400$ GeV	3.621×10^{-1}	165,000
	$1400 < \hat{p}_T < 1800$ GeV	1.179×10^{-2}	164,710
	$1800 < \hat{p}_T < 2200$ GeV	3.743×10^{-4}	164,500
	$2200 < \hat{p}_T < 2600$ GeV	7.590×10^{-6}	109,800
	$2600 < \hat{p}_T < 3000$ GeV	5.458×10^{-8}	109,800
	$3000 < \hat{p}_T < 3500$ GeV	3.283×10^{-11}	107,500
QCD (MadGraph)	$50 < H_T < 100$ GeV	3.00×10^{7}	220,715
	$100 < H_T < 250$ GeV	7.00×10^{6}	8,617,266
	$250 < H_T < 500$ GeV	1.71×10^{5}	3,413,036
	$500 < H_T < 1000$ GeV	5.20×10^{3}	2,334,762
	$1000 < H_T < \infty$ GeV	8.30×10^{1}	432,404

Table 23: Cross-section and sample size information for the electroweak and top quark Monte Carlo samples used in the analysis.

Process	Notes	σ / pb	# events
$\gamma +$ jets (Pythia 6)	$\hat{p}_T > 15$ GeV	1.922×10^5	1,223,390
	$\hat{p}_T > 30$ GeV	2.007×10^4	1,026,794
	$\hat{p}_T > 80$ GeV	5.565×10^2	1,187,711
	$\hat{p}_T > 170$ GeV	2.437×10^1	939,400
	$\hat{p}_T > 300$ GeV	1.636×10^0	1,024,266
	$\hat{p}_T > 470$ GeV	1.360×10^{-1}	1,091,179
	$\hat{p}_T > 800$ GeV	3.477×10^{-3}	1,065,640
	$\hat{p}_T > 1400$ GeV	1.286×10^{-5}	1,291,025
$\gamma +$ jets (MadGraph)	$40 < H_T < 100$ GeV	2.362×10^4	700,000
	$100 < H_T < 200$ GeV	3.476×10^3	800,000
	$H_T > 200$ GeV	4.850×10^2	925,198
$Z \to \nu\bar{\nu}$	NNLO	5.715×10^3	2,010,493
$Z +$ jets	NNLO	3.048×10^3	1,084,921
$W +$ jets	NNLO	3.131×10^4	10,034,822
$t\bar{t} +$ jets	NLO	1.575×10^2	1,282,199

Table 24: Cross-section and sample size information for the signal Monte Carlo samples used in the analysis.

Process	Notes	σ / pb	# events
LM0	–	38.93	207,522
LM1	–	4.888	207,273
LM2	–	0.6027	190,240
LM3	–	3.438	229,750
LM4	–	1.879	255,954
LM5	–	0.4734	250,000

B Detailed cutflows for data and MC samples

B.1 Cutflow for n = 2 jets

Table 25: Cut flow for 35 pb^{-1} for $N^j = 2$. Column *a*) is the number of events passing the cut, column *b*) is the percentage of events lost of those passing the intial $H_T > 250$ GeV cut (cumulative), and column *c*) is the percentage lost from the previous cut. Pythia samples produced with CMSSW_3_6_X.

Cut	SM (Pythia 6 QCD)			SM (Pythia 8 QCD)			SM (MadGraph)			Data		
	a)	b)	c)	a)	b)	c)	a)	b)	c)	a)	b)	c)
Selection	7.97 M	-	-	8.87 M	-	-	6.33 M	-	-	6.41 M	-	-
$H_T > 250\,\mathrm{GeV}$	2.12 M	0.0	73.5	1.95 M	0.0	78.0	1.73 M	0.0	72.7	2.23 M	0.0	65.2
$N^\gamma = 0$	2.11 M	0.3	0.3	1.94 M	0.2	0.2	1.73 M	0.2	0.2	2.23 M	0.2	0.2
$N^e = 0$	2.11 M	0.3	0.1	1.94 M	0.4	0.1	1.72 M	0.3	0.1	2.23 M	0.3	0.1
Odd μ veto	2.05 M	2.9	2.6	1.89 M	2.8	2.5	1.68 M	2.8	2.6	2.15 M	3.6	3.4
$N^\mu = 0$	2.05 M	2.9	0.0	1.89 M	2.9	0.0	1.68 M	2.8	0.0	2.15 M	3.7	0.0
Bad μ in j	2.04 M	3.4	0.5	1.89 M	3.2	0.3	1.67 M	3.3	0.5	2.15 M	4.0	0.3
Odd j veto	2.00 M	5.6	2.2	1.84 M	5.3	2.2	1.66 M	4.2	1.0	2.12 M	5.2	1.3
$j^1 : \lvert\eta\rvert < 2.5$	1.89 M	10.5	5.2	1.77 M	9.0	3.9	1.59 M	8.1	4.0	2.06 M	7.6	2.6
$j^2 : p_T 100\,\mathrm{GeV}$	1.81 M	14.6	4.6	1.67 M	14.2	5.7	1.54 M	11.2	3.3	1.96 M	12.3	5.1
$H_T > 350\,\mathrm{GeV}$	(309 ± 1) k	85.4	82.9	(286 ± 1) k	85.3	82.9	(255 ± 1) k	85.2	83.4	(351 ± 1) k	84.3	82.1
$\alpha_T > 0.55$	3.01 ± 0.55	≥ 99.9	≥ 99.9	4.38 ± 1.50	≥ 99.9	≥ 99.9	3.12 ± 0.56	≥ 99.9	≥ 99.9	8.00 ± 2.83	≥ 99.9	≥ 99.9
Dead ECAL	2.85 ± 0.53	≥ 99.9	5.2	4.25 ± 1.50	≥ 99.9	2.9	2.90 ± 0.54	≥ 99.9	6.9	8.00 ± 2.83	≥ 99.9	0.0
$\not{H}_T / \not{E}_T < 1.25$	2.84 ± 0.53	≥ 99.9	0.5	2.84 ± 0.53	≥ 99.9	33.2	2.81 ± 0.53	≥ 99.9	3.1	5.00 ± 2.24	≥ 99.9	37.5

Table 26: Cut flow for $35\,\mathrm{pb}^{-1}$ for $N^j = 2$. Column a) is the number of events passing the cut, column b) is the percentage of events lost of those passing the intial $H_T > 250$ GeV cut (cumulative), and column c) is the percentage lost from the previous cut. Pythia samples produced with CMSSW_3_8_X.

Cut	SM (Pythia 6 QCD)			SM (Pythia 8 QCD)			Data		
	a)	b)	c)	a)	b)	c)	a)	b)	c)
Selection	9.88 M	-	-	9.16 M	-	-	6.41 M	-	-
$H_T > 250\,\mathrm{GeV}$	2.47 M	0.0	75.1	2.01 M	0.0	78.0	2.23 M	0.0	65.2
$N^\gamma = 0$	2.46 M	0.2	0.2	2.01 M	0.2	0.2	2.23 M	0.2	0.2
$N^e = 0$	2.46 M	0.3	0.1	2.01 M	0.3	0.1	2.23 M	0.3	0.1
Odd μ veto	2.40 M	2.5	2.2	1.97 M	2.3	2.0	2.15 M	3.6	3.4
$N^\mu = 0$	2.40 M	2.5	0.0	1.96 M	2.4	0.0	2.15 M	3.7	0.0
Bad μ in j	2.40 M	2.8	0.3	1.96 M	2.6	0.3	2.15 M	4.0	0.3
Odd j veto	2.35 M	4.6	1.9	1.92 M	4.8	2.2	2.12 M	5.2	1.3
$j^1 : \lvert\eta\rvert < 2.5$	2.26 M	8.3	3.8	1.84 M	8.5	3.9	2.06 M	7.6	2.6
$j^2 : p_T 100\,\mathrm{GeV}$	2.17 M	12.2	4.3	1.74 M	13.7	5.7	1.96 M	12.3	5.1
$H_T > 350\,\mathrm{GeV}$	(390.7 ± 0.5) k	84.2	82.0	(299 ± 1) k	85.1	82.8	(351 ± 1) k	84.3	82.1
$\alpha_T > 0.55$	3.43 ± 0.71	≥ 99.9	≥ 99.9	2.98 ± 0.55	≥ 99.9	≥ 99.9	8.00 ± 2.83	≥ 99.9	≥ 99.9
Dead ECAL	3.30 ± 0.70	≥ 99.9	3.7	2.85 ± 0.53	≥ 99.9	4.3	8.00 ± 2.83	≥ 99.9	0.0
$\not{H}_T / \not{E}_T < 1.25$	2.84 ± 0.53	≥ 99.9	14.0	2.84 ± 0.53	≥ 99.9	0.5	5.00 ± 2.24	≥ 99.9	37.5

Table 27: Cut flow for $35\,\mathrm{pb}^{-1}$ for $N^j = 2$. Column a) is the number of events passing the cut, column b) is the percentage of events lost of those passing the intial $H_T > 250$ GeV cut (cumulative), and column c) is the percentage lost from the previous cut.

Cut	QCD Pythia 6 (361p4)			QCD Pythia 8 (361p4)			QCD MadGraph		
	a)	b)	c)	a)	b)	c)	a)	b)	c)
Selection	7.96 M	-	-	8.85 M	-	-	6.31 M	-	-
$H_T > 250\,\mathrm{GeV}$	2.11 M	0.0	73.5	1.94 M	0.0	78.0	1.72 M	0.0	72.7
$N^\gamma = 0$	2.11 M	0.2	0.2	1.94 M	0.2	0.2	1.72 M	0.1	0.1
$N^e = 0$	2.11 M	0.3	0.1	1.94 M	0.3	0.1	1.72 M	0.1	0.0
Odd μ veto	2.05 M	2.9	2.6	1.89 M	2.8	2.5	1.68 M	2.7	2.6
$N^\mu = 0$	2.05 M	2.9	0.0	1.89 M	2.8	0.0	1.68 M	2.7	0.0
Bad μ in j	2.04 M	3.4	0.5	1.88 M	3.1	0.3	1.67 M	3.1	0.5
Odd j veto	2.00 M	5.5	2.2	1.84 M	5.3	2.2	1.65 M	4.1	1.0
$j^1 : \lvert\eta\rvert < 2.5$	1.89 M	10.4	5.2	1.77 M	8.9	3.8	1.59 M	8.0	4.0
$j^2 : p_T 100\,\mathrm{GeV}$	1.81 M	14.5	4.6	1.67 M	14.1	5.7	1.53 M	11.0	3.3
$H_T > 350\,\mathrm{GeV}$	(309 ± 1) k	85.4	82.9	(286 ± 1) k	85.3	82.9	(255 ± 1) k	85.2	83.4
$\alpha_T > 0.55$	0.03 ± 0.02	≥ 99.9	100.0	1.40 ± 1.40	≥ 99.9	100.0	0.16 ± 0.11	≥ 99.9	100.0
Dead ECAL	0.00 ± 0.00	100.0	100.0	1.40 ± 1.40	≥ 99.9	0.0	0.08 ± 0.08	≥ 99.9	50.0
$\not{H}_T / \not{E}_T < 1.25$	0.00 ± 0.00	100.0	-	0.00 ± 0.00	100.0	100.0	0.00 ± 0.00	100.0	100.0

Table 28: Cut flow for $35\,\mathrm{pb}^{-1}$ for $N^j = 2$. Column $a)$ is the number of events passing the cut, column $b)$ is the percentage of events lost of those passing the intial $H_T > 250$ GeV cut (cumulative), and column $c)$ is the percentage lost from the previous cut.

Cut	QCD Pythia 6 (384p3)			QCD Pythia 8 (384p3)		
	a)	b)	c)	a)	b)	c)
Selection	9.87 M	-	-	9.15 M	-	-
$H_T > 250\,\mathrm{GeV}$	2.46 M	0.0	75.0	2.01 M	0.0	78.0
$N^\gamma = 0$	2.46 M	0.2	0.2	2.01 M	0.2	0.2
$N^e = 0$	2.46 M	0.3	0.1	2.00 M	0.3	0.1
Odd μ veto	2.40 M	2.4	2.2	1.96 M	2.3	2.0
$N^\mu = 0$	2.40 M	2.5	0.0	1.96 M	2.3	0.0
Bad μ in j	2.40 M	2.7	0.3	1.96 M	2.6	0.3
Odd j veto	2.35 M	4.6	1.9	1.91 M	4.7	2.2
$j^1 : \lvert\eta\rvert < 2.5$	2.26 M	8.2	3.8	1.84 M	8.4	3.9
$j^2 : p_T 100\,\mathrm{GeV}$	2.16 M	12.1	4.3	1.74 M	13.6	5.7
$H_T > 350\,\mathrm{GeV}$	(390.4 ± 0.5) k	84.2	82.0	(299 ± 1) k	85.1	82.8
$\alpha_T > 0.55$	0.45 ± 0.45	≥ 99.9	100.0	0.00 ± 0.00	100.0	100.0
Dead ECAL	0.45 ± 0.45	≥ 99.9	0.0	0.00 ± 0.00	100.0	-
$\not{H}_T / \not{E}_T < 1.25$	0.00 ± 0.00	100.0	100.0	0.00 ± 0.00	100.0	-

Table 29: Cut flow for $35\,\mathrm{pb}^{-1}$ for $N^j = 2$. Column a) is the number of events passing the cut, column b) is the percentage of events lost of those passing the intial $H_T > 250$ GeV cut (cumulative), and column c) is the percentage lost from the previous cut.

Cut	$W + nj$			$Z + nj$			$Z \to \nu\nu$			$t\bar{t}$		
	a)	b)	c)	a)	b)	c)	a)	b)	c)	a)	b)	c)
Selection	(3.0 ± 0.0) k	-	-	528.3 ± 7.2	-	-	337.6 ± 5.8	-	-	753.0 ± 1.8	-	-
$H_T > 250\,\mathrm{GeV}$	974.0 ± 10.3	0.0	67.6	118.9 ± 3.4	0.0	77.5	157.9 ± 4.0	0.0	53.2	141.0 ± 0.8	0.0	81.3
$N^\gamma = 0$	804.1 ± 9.4	17.4	17.4	84.8 ± 2.9	28.7	28.7	157.9 ± 4.0	0.0	0.0	114.0 ± 0.7	19.1	19.1
$N^e = 0$	739.4 ± 9.0	24.1	8.1	76.4 ± 2.7	35.7	9.9	157.8 ± 4.0	0.1	0.1	101.1 ± 0.7	28.3	11.3
Odd μ veto	708.7 ± 8.8	27.2	4.2	72.4 ± 2.7	39.1	5.3	153.0 ± 3.9	3.1	3.0	96.8 ± 0.6	31.3	4.3
$N^\mu = 0$	474.9 ± 7.2	51.2	33.0	39.1 ± 2.0	67.1	45.9	152.9 ± 3.9	3.2	0.1	65.2 ± 0.5	53.8	32.7
Bad μ in j	469.3 ± 7.2	51.8	1.2	38.8 ± 2.0	67.3	0.8	152.2 ± 3.9	3.6	0.5	64.6 ± 0.5	54.2	1.0
Odd j veto	458.7 ± 7.1	52.9	2.3	37.7 ± 1.9	68.3	3.0	151.0 ± 3.9	4.3	0.8	62.9 ± 0.5	55.4	2.5
$j^1 : \lvert\eta\rvert < 2.5$	445.4 ± 7.0	54.3	2.9	35.4 ± 1.9	70.2	6.0	148.2 ± 3.8	6.1	1.8	62.7 ± 0.5	55.6	0.4
$j^2 : p_T 100\,\mathrm{GeV}$	344.2 ± 6.1	64.7	22.7	30.8 ± 1.7	74.1	13.1	101.5 ± 3.2	35.7	31.5	53.6 ± 0.5	62.0	14.5
$H_T > 350\,\mathrm{GeV}$	96.8 ± 3.3	90.1	71.9	5.11 ± 0.71	95.7	83.4	35.3 ± 1.9	77.6	65.2	11.0 ± 0.2	92.2	79.5
$\alpha_T > 0.55$	1.09 ± 0.35	99.9	98.9	0.00 ± 0.00	100.0	100.0	1.79 ± 0.42	98.9	94.9	0.06 ± 0.02	≥ 99.9	99.5
Dead ECAL	0.98 ± 0.33	99.9	10.0	0.00 ± 0.00	100.0	-	1.79 ± 0.42	98.9	0.0	0.05 ± 0.01	≥ 99.9	14.3
$\not{H}_T / \not{E}_T < 1.25$	0.98 ± 0.33	99.9	0.0	0.00 ± 0.00	100.0	-	1.79 ± 0.42	98.9	0.0	0.04 ± 0.01	≥ 99.9	25.0

Table 30: Cut flow for $35\,\mathrm{pb}^{-1}$ for $N^j = 2$. Column $a)$ is the number of events passing the cut, column $b)$ is the percentage of events lost of those passing the intial $H_T > 250$ GeV cut (cumulative), and column $c)$ is the percentage lost from the previous cut.

Cut	$\gamma + j$ Pythia 6			$\gamma + j$ MadGraph		
	a)	b)	c)	a)	b)	c)
Selection	(6.7 ± 0.0) k	-	-	(18.2 ± 0.0) k	-	-
$H_T > 250\,\mathrm{GeV}$	(1.1 ± 0.0) k	0.0	82.8	(4.4 ± 0.0) k	0.0	75.9
$N^\gamma = 0$	873.0 ± 14.1	23.8	23.8	(2.4 ± 0.0) k	44.9	44.9
$N^e = 0$	868.9 ± 14.1	24.1	0.5	(2.3 ± 0.0) k	47.9	5.5
Odd μ veto	858.5 ± 14.1	25.0	1.2	(2.2 ± 0.0) k	49.1	2.3
$N^\mu = 0$	858.5 ± 14.1	25.0	0.0	(2.2 ± 0.0) k	49.1	0.0
Bad μ in j	856.1 ± 14.1	25.2	0.3	(2.2 ± 0.0) k	49.2	0.3
Odd j veto	840.9 ± 14.1	26.6	1.8	(2.2 ± 0.0) k	49.7	1.0
$j^1 : \lvert\eta\rvert < 2.5$	630.1 ± 13.9	45.0	25.1	(2.2 ± 0.0) k	50.6	1.7
$j^2 : p_T 100\,\mathrm{GeV}$	596.9 ± 13.9	47.9	5.3	(2.1 ± 0.0) k	52.8	4.5
$H_T > 350\,\mathrm{GeV}$	130.6 ± 9.6	88.6	78.1	499.5 ± 3.7	88.6	75.8
$\alpha_T > 0.55$	0.04 ± 0.00	≥ 99.9	100.0	0.02 ± 0.02	≥ 99.9	100.0
Dead ECAL	0.03 ± 0.00	≥ 99.9	28.0	0.00 ± 0.00	100.0	100.0
$\not{H}_T / \not{E}_T < 1.25$	0.03 ± 0.00	≥ 99.9	0.2	0.00 ± 0.00	100.0	-

Table 31: Cut flow for $35\,\mathrm{pb}^{-1}$ for $N^j = 2$. Column a) is the number of events passing the cut, column b) is the percentage of events lost of those passing the intial $H_T > 250$ GeV cut (cumulative), and column c) is the percentage lost from the previous cut.

Cut	LM0			LM1			LM2			LM3		
	a)	b)	c)	a)	b)	c)	a)	b)	c)	a)	b)	c)
Selection	237.3 ± 1.2	-	-	47.9 ± 0.2	-	-	4.92 ± 0.02	-	-	15.1 ± 0.1	-	-
$H_T > 250\,\mathrm{GeV}$	172.8 ± 1.1	0.0	27.2	44.6 ± 0.2	0.0	6.9	4.67 ± 0.02	0.0	5.1	13.1 ± 0.1	0.0	13.4
$N^\gamma = 0$	156.6 ± 1.0	9.4	9.4	41.2 ± 0.2	7.6	7.6	4.35 ± 0.02	6.9	6.9	11.7 ± 0.1	10.7	10.7
$N^e = 0$	147.0 ± 1.0	14.9	6.1	38.2 ± 0.2	14.3	7.3	4.11 ± 0.02	12.1	5.6	11.0 ± 0.1	15.8	5.7
Odd μ veto	137.7 ± 1.0	20.3	6.3	34.9 ± 0.2	21.8	8.7	3.60 ± 0.02	22.9	12.3	9.95 ± 0.07	23.8	9.4
$N^\mu = 0$	116.9 ± 0.9	32.3	15.1	29.9 ± 0.2	33.0	14.3	3.26 ± 0.02	30.3	9.6	8.55 ± 0.07	34.5	14.1
Bad μ in j	116.3 ± 0.9	32.7	0.5	29.7 ± 0.2	33.3	0.5	3.24 ± 0.02	30.6	0.5	8.51 ± 0.07	34.8	0.5
Odd j veto	114.6 ± 0.9	33.7	1.5	29.3 ± 0.2	34.3	1.5	3.19 ± 0.02	31.8	1.7	8.40 ± 0.07	35.6	1.3
$j^1 : \lvert\eta\rvert < 2.5$	114.1 ± 0.9	33.9	0.4	29.3 ± 0.2	34.4	0.1	3.18 ± 0.02	31.8	0.1	8.39 ± 0.07	35.7	0.1
$j^2 : p_T 100\,\mathrm{GeV}$	83.9 ± 0.7	51.4	26.5	24.0 ± 0.1	46.2	18.0	2.72 ± 0.02	41.7	14.5	6.83 ± 0.06	47.7	18.6
$H_T > 350\,\mathrm{GeV}$	57.8 ± 0.6	66.6	31.2	21.2 ± 0.1	52.4	11.4	2.59 ± 0.02	44.6	4.9	6.09 ± 0.06	53.3	10.8
$\alpha_T > 0.55$	12.4 ± 0.3	92.8	78.5	7.37 ± 0.08	83.5	65.3	1.00 ± 0.01	78.6	61.4	2.05 ± 0.03	84.3	66.3
Dead ECAL	11.9 ± 0.3	93.1	4.0	7.20 ± 0.08	83.9	2.2	0.98 ± 0.01	79.0	2.0	2.01 ± 0.03	84.6	2.0
$\not{H}_T / \not{E}_T < 1.25$	11.3 ± 0.3	93.5	5.0	7.13 ± 0.08	84.0	1.1	0.98 ± 0.01	79.1	0.3	1.99 ± 0.03	84.8	1.3

B.2 Cutflow for n $\geq$ 3 jets

Table 32: Cut flow for 35 pb^{-1} for $N^j \geq 3$. Column *a*) is the number of events passing the cut, column *b*) is the percentage of events lost of those passing the intial $H_T > 250$ GeV cut (cumulative), and column *c*) is the percentage lost from the previous cut. Pythia samples produced with CMSSW_3_6_X.

Cut	SM (Pythia 6 QCD)			SM (Pythia 8 QCD)			SM (MadGraph)			Data		
	a)	b)	c)	a)	b)	c)	a)	b)	c)	a)	b)	c)
Selection	4.61 M	-	-	5.65 M	-	-	2.53 M	-	-	3.50 M	-	-
$H_T > 250\,\mathrm{GeV}$	2.92 M	0.0	36.7	3.53 M	0.0	37.4	1.63 M	0.0	35.5	2.44 M	0.0	30.2
$N^\gamma = 0$	2.91 M	0.2	0.2	3.53 M	0.2	0.2	1.63 M	0.2	0.2	2.44 M	0.2	0.2
$N^e = 0$	2.91 M	0.2	0.1	3.52 M	0.3	0.1	1.63 M	0.2	0.1	2.44 M	0.3	0.1
Odd μ veto	2.85 M	2.2	1.9	3.45 M	2.3	2.0	1.59 M	2.3	2.1	2.37 M	3.0	2.7
$N^\mu = 0$	2.85 M	2.2	0.0	3.45 M	2.3	0.0	1.59 M	2.3	0.0	2.37 M	3.0	0.0
Bad μ in j	2.84 M	2.7	0.5	3.44 M	2.7	0.3	1.58 M	2.8	0.5	2.36 M	3.4	0.4
Odd j veto	2.79 M	4.4	1.8	3.37 M	4.8	2.2	1.57 M	3.9	1.1	2.33 M	4.7	1.4
$j^1 : \lvert\eta\rvert < 2.5$	2.67 M	8.6	4.4	3.21 M	9.1	4.5	1.49 M	8.4	4.7	2.24 M	8.4	3.8
$j^2 : p_T 100\,\mathrm{GeV}$	1.01 M	65.5	62.2	1.28 M	63.9	60.2	(611 ± 1) k	62.5	59.1	(929 ± 1) k	61.9	58.5
$H_T > 350\,\mathrm{GeV}$	(580 ± 2) k	80.1	42.4	(775 ± 3) k	78.1	39.4	(358 ± 1) k	78.0	41.3	(557 ± 1) k	77.2	40.1
$\alpha_T > 0.55$	11.0 ± 1.1	≥ 99.9	≥ 99.9	59.3 ± 41.5	≥ 99.9	≥ 99.9	38.0 ± 28.4	≥ 99.9	≥ 99.9	30.0 ± 5.5	≥ 99.9	≥ 99.9
Dead ECAL	9.74 ± 1.07	≥ 99.9	11.2	54.4 ± 41.5	≥ 99.9	8.3	8.34 ± 0.78	≥ 99.9	78.0	25.0 ± 5.0	≥ 99.9	16.7
$\not{H}_T / \not{E}_T < 1.25$	6.51 ± 0.70	≥ 99.9	33.1	6.69 ± 0.75	≥ 99.9	87.7	6.64 ± 0.71	≥ 99.9	20.4	9.00 ± 3.00	≥ 99.9	64.0

Table 33: Cut flow for 35 pb^{-1} for $N^j \geq 3$. Column a) is the number of events passing the cut, column b) is the percentage of events lost of those passing the intial $H_T > 250$ GeV cut (cumulative), and column c) is the percentage lost from the previous cut. Pythia samples produced with CMSSW_3_8_X.

Cut	SM (Pythia 6 QCD)			SM (Pythia 8 QCD)			SM (MadGraph)			Data		
	a)	b)	c)	a)	b)	c)	a)	b)	c)	a)	b)	c)
Selection	5.11 M	-	-	5.85 M	-	-	2.53 M	-	-	3.50 M	-	-
$H_T > 250$ GeV	3.30 M	0.0	35.4	3.69 M	0.0	36.9	1.63 M	0.0	35.5	2.44 M	0.0	30.2
$N^\gamma = 0$	3.29 M	0.2	0.2	3.68 M	0.2	0.2	1.63 M	0.2	0.2	2.44 M	0.2	0.2
$N^e = 0$	3.29 M	0.2	0.1	3.68 M	0.3	0.1	1.63 M	0.2	0.1	2.44 M	0.3	0.1
Odd μ veto	3.24 M	1.9	1.6	3.62 M	1.9	1.6	1.59 M	2.3	2.1	2.37 M	3.0	2.7
$N^\mu = 0$	3.24 M	1.9	0.0	3.62 M	1.9	0.0	1.59 M	2.3	0.0	2.37 M	3.0	0.0
Bad μ in j	3.23 M	2.2	0.3	3.61 M	2.2	0.3	1.58 M	2.8	0.5	2.36 M	3.4	0.4
Odd j veto	3.17 M	4.0	1.8	3.52 M	4.5	2.3	1.57 M	3.9	1.1	2.33 M	4.7	1.4
$j^1 : \lvert\eta\rvert < 2.5$	3.04 M	8.0	4.2	3.36 M	8.9	4.6	1.49 M	8.4	4.7	2.24 M	8.4	3.8
$j^2 : p_T 100$ GeV	1.22 M	63.0	59.8	1.34 M	63.7	60.2	(611 ± 1) k	62.5	59.1	(929 ± 1) k	61.9	58.5
$H_T > 350$ GeV	(724 ± 1) k	78.0	40.7	(820 ± 2) k	77.8	38.7	(358 ± 1) k	78.0	41.3	(557 ± 1) k	77.2	40.1
$\alpha_T > 0.55$	27.0 ± 4.7	≥ 99.9	≥ 99.9	32.4 ± 9.2	≥ 99.9	≥ 99.9	38.0 ± 28.4	≥ 99.9	≥ 99.9	30.0 ± 5.5	≥ 99.9	≥ 99.9
Dead ECAL	21.2 ± 4.2	≥ 99.9	21.5	23.6 ± 7.9	≥ 99.9	27.0	8.34 ± 0.78	≥ 99.9	78.0	25.0 ± 5.0	≥ 99.9	16.7
$\not{H}_T / \not{E}_T < 1.25$	6.42 ± 0.70	≥ 99.9	69.7	6.40 ± 0.70	≥ 99.9	72.9	6.64 ± 0.71	≥ 99.9	20.4	9.00 ± 3.00	≥ 99.9	64.0

Table 34: Cut flow for $35\,\text{pb}^{-1}$ for $N^j \geq 3$. Column a) is the number of events passing the cut, column b) is the percentage of events lost of those passing the intial $H_T > 250$ GeV cut (cumulative), and column c) is the percentage lost from the previous cut.

Cut	QCD Pythia 6 (361p4)			QCD Pythia 8 (361p4)			QCD MadGraph		
	a)	b)	c)	a)	b)	c)	a)	b)	c)
Selection	4.60 M	-	-	5.64 M	-	-	2.52 M	-	-
$H_T > 250\,\text{GeV}$	2.91 M	0.0	36.7	3.53 M	0.0	37.4	1.62 M	0.0	35.6
$N^\gamma = 0$	2.91 M	0.2	0.2	3.52 M	0.2	0.2	1.62 M	0.1	0.1
$N^e = 0$	2.91 M	0.2	0.1	3.52 M	0.3	0.1	1.62 M	0.1	0.1
Odd μ veto	2.85 M	2.1	1.9	3.45 M	2.3	2.0	1.59 M	2.2	2.1
$N^\mu = 0$	2.85 M	2.1	0.0	3.45 M	2.3	0.0	1.59 M	2.2	0.0
Bad μ in j	2.84 M	2.6	0.5	3.44 M	2.6	0.3	1.58 M	2.7	0.5
Odd j veto	2.79 M	4.3	1.8	3.36 M	4.8	2.2	1.56 M	3.7	1.1
$j^1 : \lvert\eta\rvert < 2.5$	2.66 M	8.6	4.4	3.21 M	9.1	4.5	1.49 M	8.3	4.7
$j^2 : p_T 100\,\text{GeV}$	1.01 M	65.5	62.2	1.28 M	63.9	60.3	(608 ± 1) k	62.5	59.1
$H_T > 350\,\text{GeV}$	(579 ± 2) k	80.1	42.5	(774 ± 3) k	78.1	39.4	(357 ± 1) k	78.0	41.4
$\alpha_T > 0.55$	2.97 ± 0.83	≥ 99.9	100.0	51.3 ± 41.5	≥ 99.9	100.0	30.0 ± 28.4	≥ 99.9	100.0
Dead ECAL	2.36 ± 0.78	≥ 99.9	20.8	47.0 ± 41.5	≥ 99.9	8.3	0.94 ± 0.27	≥ 99.9	96.9
$\not{H}_T / \not{E}_T < 1.25$	0.12 ± 0.04	≥ 99.9	94.9	0.29 ± 0.29	≥ 99.9	99.4	0.23 ± 0.14	≥ 99.9	75.0

Table 35: Cut flow for $35\,\mathrm{pb}^{-1}$ for $N^j \geq 3$. Column $a)$ is the number of events passing the cut, column $b)$ is the percentage of events lost of those passing the intial $H_T > 250$ GeV cut (cumulative), and column $c)$ is the percentage lost from the previous cut.

Cut	QCD Pythia 6 (384p3)			QCD Pythia 8 (384p3)		
	a)	b)	c)	a)	b)	c)
Selection	5.10 M	-	-	5.84 M	-	-
$H_T > 250\,\mathrm{GeV}$	3.29 M	0.0	35.4	3.68 M	0.0	36.9
$N^\gamma = 0$	3.29 M	0.2	0.2	3.68 M	0.2	0.2
$N^e = 0$	3.29 M	0.2	0.1	3.67 M	0.3	0.1
Odd μ veto	3.23 M	1.8	1.6	3.62 M	1.9	1.6
$N^\mu = 0$	3.23 M	1.9	0.0	3.61 M	1.9	0.0
Bad μ in j	3.22 M	2.1	0.3	3.60 M	2.2	0.3
Odd j veto	3.17 M	3.9	1.8	3.52 M	4.5	2.3
$j^1 : \lvert\eta\rvert < 2.5$	3.03 M	7.9	4.2	3.36 M	8.8	4.6
$j^2 : p_T 100\,\mathrm{GeV}$	1.22 M	63.0	59.8	1.34 M	63.7	60.2
$H_T > 350\,\mathrm{GeV}$	(723 ± 1) k	78.0	40.7	(819 ± 2) k	77.8	38.7
$\alpha_T > 0.55$	19.0 ± 4.6	≥ 99.9	100.0	24.4 ± 9.2	≥ 99.9	100.0
Dead ECAL	13.8 ± 4.1	≥ 99.9	27.3	16.2 ± 7.9	≥ 99.9	33.4
$\not{H}_T / \not{E}_T < 1.25$	0.03 ± 0.02	≥ 99.9	99.8	0.01 ± 0.00	≥ 99.9	100.0

Table 36: Cut flow for $35\,\mathrm{pb}^{-1}$ for $N^j \geq 3$. Column a) is the number of events passing the cut, column b) is the percentage of events lost of those passing the intial $H_T > 250$ GeV cut (cumulative), and column c) is the percentage lost from the previous cut.

Cut	$W+nj$			$Z+nj$			$Z \to \nu\nu$			$t\bar{t}$		
	a)	b)	c)	a)	b)	c)	a)	b)	c)	a)	b)	c)
Selection	(1.3 ± 0.0) k	-	-	230.4 ± 4.8	-	-	154.0 ± 3.9	-	-	(3.0 ± 0.0) k	-	-
$H_T > 250\,\mathrm{GeV}$	979.9 ± 10.3	0.0	25.6	160.3 ± 4.0	0.0	30.4	127.4 ± 3.6	0.0	17.2	(2.4 ± 0.0) k	0.0	19.8
$N^\gamma = 0$	858.5 ± 9.7	12.4	12.4	127.1 ± 3.5	20.7	20.7	127.4 ± 3.6	0.0	0.0	(2.2 ± 0.0) k	7.3	7.3
$N^e = 0$	809.1 ± 9.4	17.4	5.7	117.1 ± 3.4	26.9	7.9	127.4 ± 3.6	0.0	0.0	(2.1 ± 0.0) k	10.8	3.8
Odd μ veto	781.5 ± 9.2	20.2	3.4	112.8 ± 3.3	29.6	3.7	122.9 ± 3.5	3.6	3.6	(2.0 ± 0.0) k	13.7	3.3
$N^\mu = 0$	602.2 ± 8.1	38.5	22.9	82.4 ± 2.8	48.6	26.9	122.9 ± 3.5	3.6	0.0	(1.8 ± 0.0) k	23.8	11.7
Bad μ in j	583.6 ± 8.0	40.4	3.1	81.0 ± 2.8	49.4	1.7	121.8 ± 3.5	4.4	0.9	(1.8 ± 0.0) k	25.1	1.6
Odd j veto	574.7 ± 7.9	41.4	1.5	78.8 ± 2.8	50.9	2.8	121.1 ± 3.5	5.0	0.6	(1.7 ± 0.0) k	26.6	2.0
$j^1 : \lvert\eta\rvert < 2.5$	552.6 ± 7.8	43.6	3.8	74.5 ± 2.7	53.5	5.4	118.7 ± 3.4	6.9	2.0	(1.7 ± 0.0) k	27.4	1.2
$j^2 : p_T 100\,\mathrm{GeV}$	266.2 ± 5.4	72.8	51.8	34.2 ± 1.8	78.7	54.1	59.0 ± 2.4	53.7	50.3	779.2 ± 1.8	67.1	54.6
$H_T > 350\,\mathrm{GeV}$	184.8 ± 4.5	81.1	30.6	22.6 ± 1.5	85.9	33.9	43.8 ± 2.1	65.7	25.8	639.1 ± 1.7	73.0	18.0
$\alpha_T > 0.55$	2.84 ± 0.56	99.7	98.5	0.00 ± 0.00	100.0	100.0	2.39 ± 0.49	98.1	94.5	2.71 ± 0.11	99.9	99.6
Dead ECAL	2.62 ± 0.54	99.7	7.7	0.00 ± 0.00	100.0	-	2.39 ± 0.49	98.1	0.0	2.34 ± 0.10	≥ 99.9	13.5
$H_T / \not{E}_T < 1.25$	2.29 ± 0.50	99.8	12.5	0.00 ± 0.00	100.0	-	2.29 ± 0.48	98.2	4.2	1.78 ± 0.09	≥ 99.9	23.9

Table 37: Cut flow for 35 pb^{-1} for $N^j \geq 3$. Column a) is the number of events passing the cut, column b) is the percentage of events lost of those passing the intial $H_T > 250$ GeV cut (cumulative), and column c) is the percentage lost from the previous cut.

Cut	$\gamma + j$ Pythia 6			$\gamma + j$ MadGraph		
	a)	b)	c)	a)	b)	c)
Selection	(1.2 ± 0.0) k	-	-	(5.6 ± 0.0) k	-	-
$H_T > 250\,\text{GeV}$	708.0 ± 11.0	0.0	40.8	(3.9 ± 0.0) k	0.0	30.9
$N^\gamma = 0$	570.3 ± 10.5	19.4	19.4	(2.7 ± 0.0) k	30.0	30.0
$N^e = 0$	567.6 ± 10.5	19.8	0.5	(2.6 ± 0.0) k	32.0	2.8
Odd μ veto	560.8 ± 10.5	20.8	1.2	(2.6 ± 0.0) k	33.5	2.2
$N^\mu = 0$	560.8 ± 10.5	20.8	0.0	(2.6 ± 0.0) k	33.5	0.0
Bad μ in j	557.4 ± 10.4	21.3	0.6	(2.6 ± 0.0) k	33.7	0.4
Odd j veto	549.3 ± 10.3	22.4	1.5	(2.5 ± 0.0) k	34.2	0.8
$j^1 : \lvert\eta\rvert < 2.5$	408.5 ± 9.2	42.3	25.6	(2.5 ± 0.0) k	36.0	2.7
$j^2 : p_T 100\,\text{GeV}$	191.9 ± 3.6	72.9	53.0	(1.3 ± 0.0) k	66.9	48.3
$H_T > 350\,\text{GeV}$	117.0 ± 1.8	83.5	39.1	822.4 ± 4.1	78.7	35.6
$\alpha_T > 0.55$	0.06 ± 0.01	≥ 99.9	99.9	0.07 ± 0.04	≥ 99.9	100.0
Dead ECAL	0.03 ± 0.00	≥ 99.9	48.9	0.06 ± 0.03	≥ 99.9	25.0
$\not{H}_T / \not{E}_T < 1.25$	0.03 ± 0.00	≥ 99.9	11.0	0.04 ± 0.03	≥ 99.9	33.3

Table 38: Cut flow for $35\,\mathrm{pb}^{-1}$ for $N^j \geq 3$. Column a) is the number of events passing the cut, column b) is the percentage of events lost of those passing the intial $H_T > 250$ GeV cut (cumulative), and column c) is the percentage lost from the previous cut.

Cut	LM0			LM1			LM2			LM3		
	a)	b)	c)	a)	b)	c)	a)	b)	c)	a)	b)	c)
Selection	810.9 ± 2.3	-	-	84.3 ± 0.3	-	-	10.6 ± 0.0	-	-	78.5 ± 0.2	-	-
$H_T > 250\,\mathrm{GeV}$	781.3 ± 2.3	0.0	3.6	83.7 ± 0.3	0.0	0.7	10.6 ± 0.0	0.0	0.5	77.6 ± 0.2	0.0	1.1
$N^\gamma = 0$	721.7 ± 2.2	7.6	7.6	77.8 ± 0.3	7.0	7.0	9.79 ± 0.03	7.3	7.3	70.9 ± 0.2	8.6	8.6
$N^e = 0$	677.9 ± 2.1	13.2	6.1	72.2 ± 0.2	13.7	7.2	9.17 ± 0.03	13.2	6.3	67.1 ± 0.2	13.5	5.4
Odd μ veto	636.7 ± 2.0	18.5	6.1	65.6 ± 0.2	21.5	9.1	8.06 ± 0.03	23.7	12.1	61.1 ± 0.2	21.3	9.1
$N^\mu = 0$	548.0 ± 1.9	29.9	13.9	56.2 ± 0.2	32.8	14.4	7.17 ± 0.03	32.2	11.1	53.0 ± 0.2	31.7	13.2
Bad μ in j	537.0 ± 1.9	31.3	2.0	55.5 ± 0.2	33.7	1.3	7.06 ± 0.03	33.2	1.5	51.9 ± 0.2	33.1	2.0
Odd j veto	528.0 ± 1.9	32.4	1.7	54.6 ± 0.2	34.8	1.7	6.94 ± 0.03	34.3	1.7	51.1 ± 0.2	34.2	1.6
$j^1 : \lvert\eta\rvert < 2.5$	524.4 ± 1.9	32.9	0.7	54.4 ± 0.2	35.0	0.2	6.93 ± 0.03	34.4	0.1	51.0 ± 0.2	34.3	0.2
$j^2 : p_T 100\,\mathrm{GeV}$	380.5 ± 1.6	51.3	27.5	47.5 ± 0.2	43.2	12.7	6.41 ± 0.03	39.3	7.5	45.0 ± 0.2	42.0	11.7
$H_T > 350\,\mathrm{GeV}$	362.4 ± 1.5	53.6	4.7	46.6 ± 0.2	44.3	1.9	6.37 ± 0.03	39.7	0.7	44.5 ± 0.2	42.6	1.0
$\alpha_T > 0.55$	43.3 ± 0.5	94.5	88.0	13.5 ± 0.1	83.9	71.1	2.05 ± 0.02	80.6	67.9	7.39 ± 0.06	90.5	83.4
Dead ECAL	39.7 ± 0.5	94.9	8.3	12.7 ± 0.1	84.9	5.9	1.91 ± 0.01	81.9	6.5	6.76 ± 0.06	91.3	8.6
$\not{H}_T / \not{E}_T < 1.25$	35.8 ± 0.5	95.4	10.0	12.4 ± 0.1	85.2	2.2	1.89 ± 0.01	82.1	1.1	6.46 ± 0.06	91.7	4.4

C Details on W prediction

We present here the details of the estimate of the W+jets events in the hadronic channel, given the number of reconstructed W+jets events with W $\to \mu\nu$.

The first step is to unfold the number of measured W-Bosons (W^{μ}_{data}) events to the total number of W $\to \mu\nu$ events, W^{μ}_{total}, without detector effects, just like in a cross-section measurement:

$$W^{\mu}_{total} = W^{\mu}_{data}\frac{W^{\mu}_{MC;total}}{W^{\mu}_{MC}} = W^{\mu}_{data}\left(f_W\frac{1}{a_W\times\epsilon_W} + f_{tt}\frac{1}{a_{tt}\times\epsilon_{tt}}\right)P$$

where:

- $W^{\mu}_{MC;total}$ is the (Monte Carlo) total number of W $\to \mu\nu$ events and W^{μ}_{MC} is the actual number of (Monte Carlo) events expected after the selection requirements.
- W^{μ}_{data} is the number of events in the μ control sample in data.
- f_W and f_{tt}, are the fractions of W+jet and $t\bar{t}$ events in the boosted W sample
- P is the purity of the muon control sample: $\frac{N(W+jet)+N(t\bar{t})}{\text{allevents}}$
- $a\times\epsilon$ is the product of the acceptance times the efficiency for muons in W+jet or $t\bar{t}$ events

Using the number of boosted W (W^{μ}_{total}) in the relevant phase-space, we next include the probability that the W boson decays leptonically, i.e. to either $e\nu, \mu\nu, \tau\nu$, and no muon passing the selection cuts is reconstructed. Depending on whether the α_{T} cut is applied, the efficiency of the α_{T} cut needs to be taken into account. The number of boosted W-Bosons (W^{had}_{data}) events in the hadronic signal region is then given by:

$$W^{had}_{data} = W^{\mu}_{total}\frac{W^{had}_{MC}}{W^{true}_{MC}} = W^{\mu}_{total}\times\left(f_W p_h^W \epsilon(\alpha_T)^W + f_{tt}p_h^{tt}\epsilon(\alpha_T)^{tt}\right)$$

where:

- W^{had}_{MC} number of events expected in the hadronic signal region.
- p_h^W and p_h^{tt} are the probabilities that the charged lepton was not identifies as such
- $\epsilon(\alpha_{\mathrm{T}})$ is the efficiency of the α_{T} cut (given the control sample without the α_{T} cut)

Replacing W^{μ}_{total} in the above formula, we obtain:

$$W^{had}_{data} = W^{\mu}_{data}\frac{W^{had}_{MC}}{W^{total}_{MC}}\frac{W^{\mu}_{MC;total}}{W^{\mu}_{MC}} = W^{\mu}_{data}\left(f_W\frac{1}{a_W\times\epsilon_W} + f_{tt}\frac{1}{a_{tt}\times\epsilon_{tt}}\right)\times\left(f_W p_h^W\epsilon(\alpha_T)^W + f_{tt}p_h^{tt}\epsilon(\alpha_T)^{tt}\right)\times P$$

From MC we know that:

$$\frac{p_h^W\epsilon(\alpha_T)^W}{a_W\times\epsilon_W} = 0.19 \sim \frac{p_h^{tt}\epsilon(\alpha_T)^{tt}}{a_{tt}\times\epsilon_{tt}} = 0.18$$

This means that after the H_T^{miss} and H_T cuts the $\frac{p_h\epsilon(\alpha_T)}{a\times e}$ does not depend much on the origin of the boosted W-Boson. Therefore, even though occurring quadratically, the fraction of $t\bar{t}$ and W+jets events does not effect the prediction significantly. The estimate is linear in all the other parameters, allowing a simple error propagation of the uncetainties.

subsectionUncertainties on W decay modeling

Table 39: Fraction of backgrounds from boosted W-Bosons. Unless stated otherwise there was on a single W-Boson in the MC.

W to τ hadronic	W to μ or e out of accep.	W to μ or e not vetoed	$t\bar{t}$ fully leptonic
37%	35%	24%	5%

To discuss the uncertainties on the modeling the boosted W-Boson decay and thus p_h^W and p_h^{tt} (as defined in C) we use three classification of the boosted W-Boson decays. The dominant class is the hadronic tau decay, followed events where electron or muons are out of the acceptance of the detector. Muons and electrons within acceptance, but where the veto failed are the smallest categories (Table 39). For each category different uncertainties are applied:

- The electron and muons out of acceptance: The kinematic properties of W have been shown to be properly modeled (e.g. [23]). We assign a uncertainty of 10%. It was also tested that the NLO POWHEG (used in [23]) and the used W+jet madgraph sample did not significantly differe for the accepetance corrections.
- The electron ID and are counted as jets. The modeling of the electron ID was tested in [23] (Table page 51). With $3pb^{-1}$ of integrated luminosity the efficiency was measured in a tag and probe procedure with Zs. The efficiency in the barrel was found to be 92.6% $\pm$ stat 1.6% $\pm$ syst. 1.5% in the data and 94.9 in MC in the barrel region. It was 86.9% $\pm$ stat 2.0% $\pm$ syst. 1.5% in the data and 90.5 in MC in the endcap region. The inefficiency was in both region about 30% underestimated in data. We also tested in the muon control sample if the combined isolation changed between the first $15pb^{-1}$ and the last t $13pb^{-1}$ and if it is described by MC(Figure 34). Especially the isolation would be different due to the extra pileup, further for this HT and MHT region the could be especially badly modeled in MC. Figure 34 show only very few events in data that exceed the 0.15 isolation used.
  The muons reconstruction efficiencies for Standalone muon, tracker muons and the isolation for data and MC shown in Table 5 of [23] as obtained with tag and probe from Z$\rightarrow \mu\mu$ events. The modeling shows generally good agreement with a very slight trend of underestimating the inefficiencies.
  Given the above shown data MC comparison in the relevant variables, and the isolation agreement we assign conservatively a 100% uncertainty on the modelling of the vetos, which is well above the measured discrepancies.
- The tau decay hadronic: We did change the tau-jet response by 10% up and down. Which is an conservative estimate, given that the jet-energy scale uncertainty of jets is 5% [15]. The effect of the final number of hadronic tau decay candidated in the MC did change by 7%. Given that the tau spectra of the selected events in the hadronic search reason looks is similat for W+jet and $t\bar{t}$, we used the large statistics sample of $t\bar{t}$ in order to perform this test. We therefore assign an uncertainty of $\pm$ 7%.
- Fully leptonic $t\bar{t}$ decay is dominated by two τ decays. The expected contribution is marginal (only 5% of the W background), it not expected to have drastically different uncertainties than the single W case. We assign a 50% uncertainty, given that the veto inefficiencies and the tau response modeling and the the acceptance are all of relavance.

averaging these uncertainties with the weights of derived from Table 39 leads to an uncertainty of 33%.

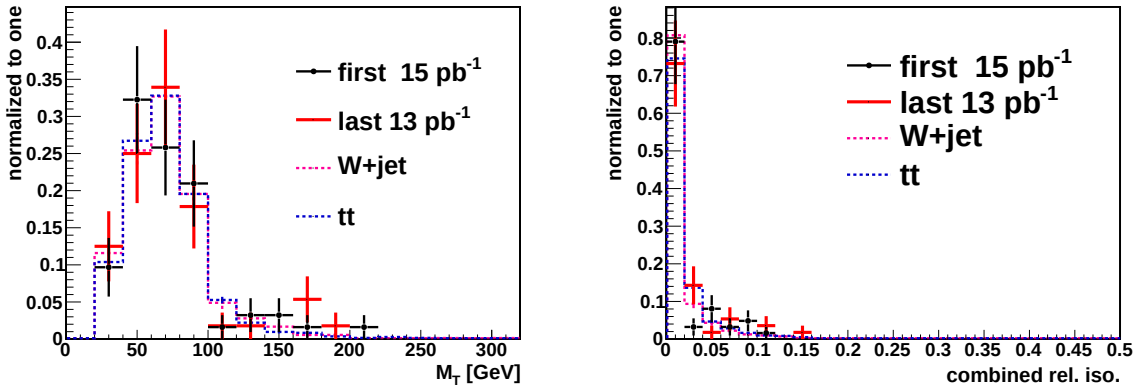

Figure 34: Left: transverse mass of W candidate with relaxed combined isolation criteria (combined relative isolation < 0.5). Right: Combined realative isolation distributions (electron veto cut used <0.15).

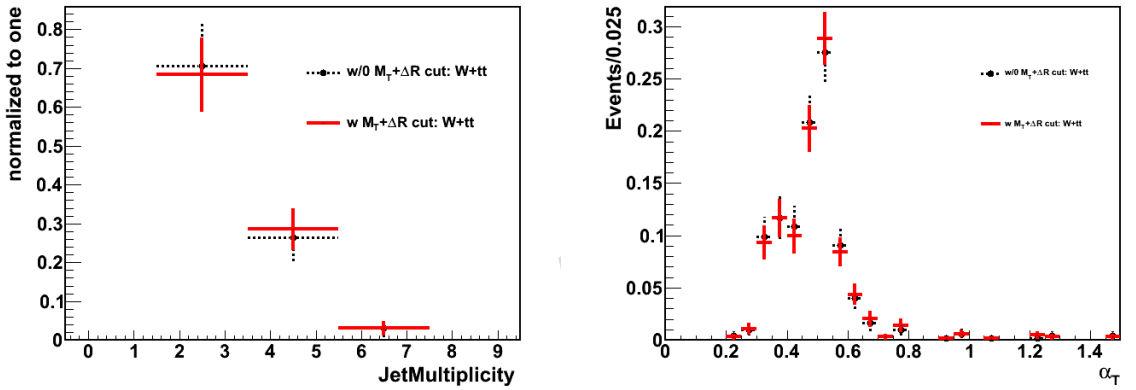

Figure 35: Distributions normalized to one from MC with and without ΔR(jet,μ)>0.5 and $M_T > 30$ GeV cut. Left: jet multiplicity, Right: α_T

subsectionImpact of ΔR(jet,μ)>0.5 and $M_T > 30$ GeV on Kinematics The muon control sample selection was modified by lifting the following cuts: ΔR(jet,μ)>0.5 and $M_T > 30$ GeV. Figure 35 shows the distributions of jet multiplicity and α_T normalized to unity for the MC. Both distributions are significantly changed.

D Further studies of cMSSM exclusion limits

Figure 36 compares the measured limit obtained if signal contamination in the control samples is taken into account to the one obtained if this contamination is neglected. The excluded area would appear slightly larger in the second case.

Figure 37 presents the exclusion limit in case that systematic uncertainties on signal acceptance times efficiency and background predictions are not taken into account. The impact of the systematic uncertainties is small compared to that of statistic fluctuations, which lead to the difference between expected and measured limit.

The exclusion limit obtained if dijet events and events with more than two jets are treated seperately is presented in figure 38. The improvement in reach is still small compared to statistical

fluctuations. An in detail discussion of the change in background estimation procedures necessary for this splitting in jet mulitplicities is therefore not presented in this document. It will be part of a later analysis with more available data.

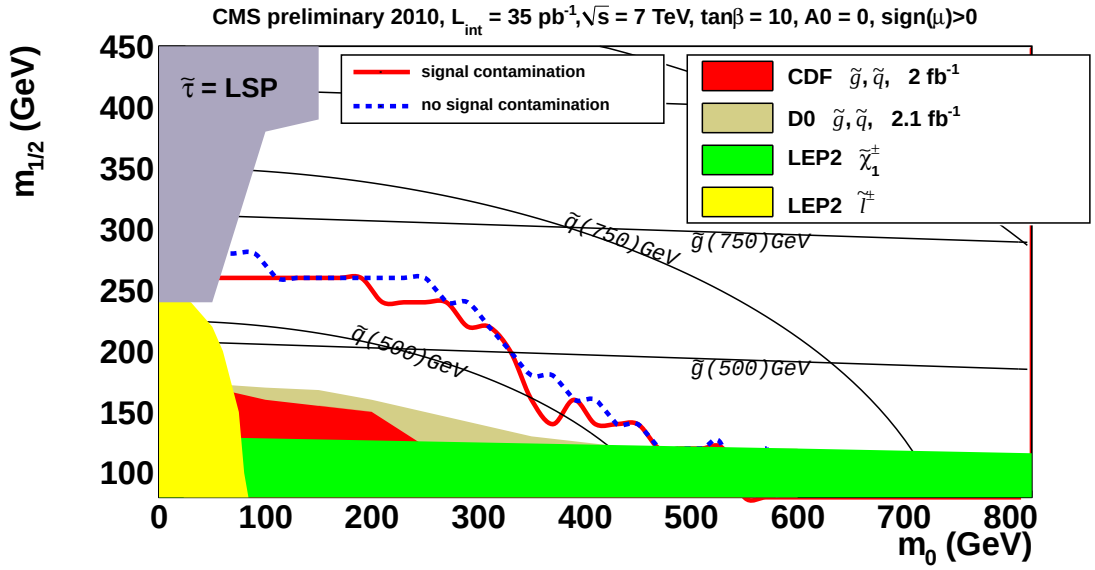

Figure 36: Measured 95% CL exclusion contours in the cMSSM $m_0 - m_{1/2}$ plane ($\tan\beta = 10$, $A_0 = 0$, $\text{sign}(\mu) > 0$), once in the case that a possible signal contamination in the control samples is taken into account and once in the case that this contamination is neglected.

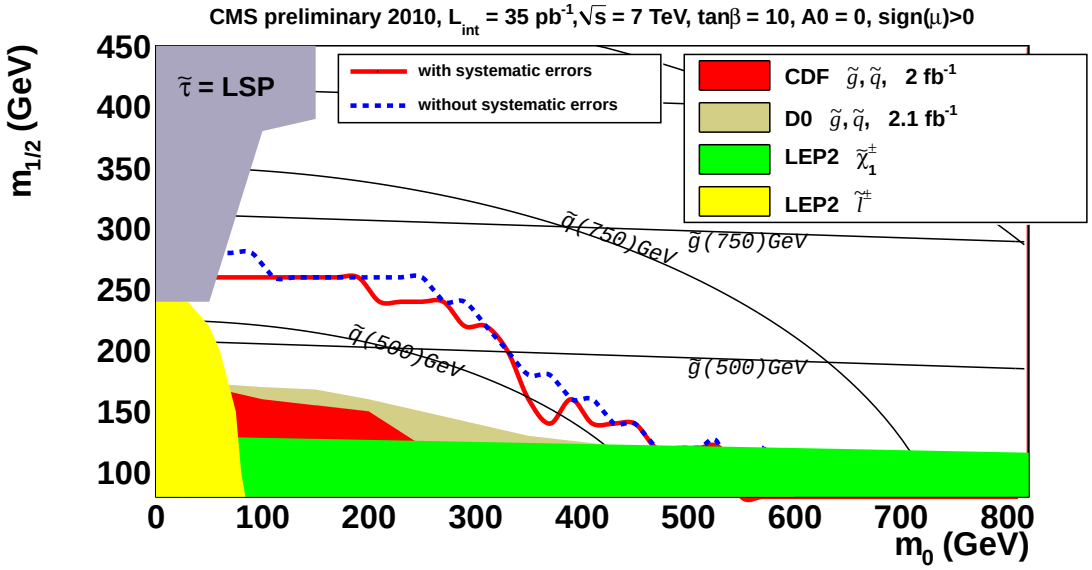

Figure 37: Measured 95% CL exclusion contours in the cMSSM $m_0 - m_{1/2}$ plane ($\tan\beta = 10$, $A_0 = 0$, $\text{sign}(\mu) > 0$), once in the case that systematic uncertainties on the signal acceptance times efficiency and the background predictions are taken into account and once in the case that these uncertainties are neglected.

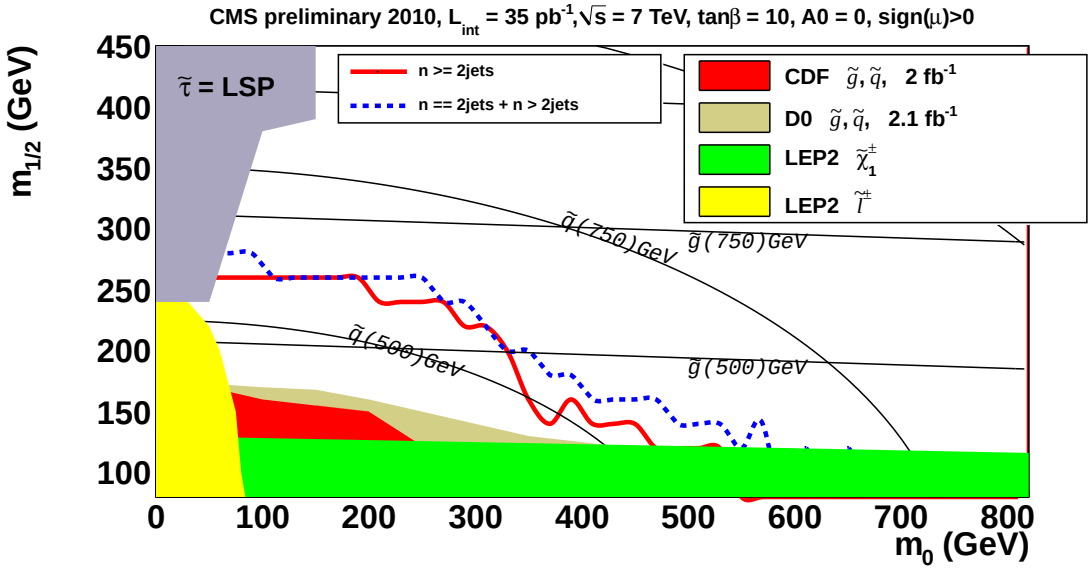

Figure 38: Measured 95% CL exclusion contours in the cMSSM $m_0 - m_{1/2}$ plane ($\tan\beta = 10$, $A_0 = 0$, $\text{sign}(\mu) > 0$), once in the case that dijet events and events are analyzed separately and their probability density functions are multiplied at the end and once in the case that no separation is made between events with different jet multiplicities.